Ministry of Higher Education and Scientific Research
University of Babylon
College of Science
Department of Physics

A Simulation Process of Tunable Open Path Diode Laser Spectrometer to Measure a Gases Concentration

A Thesis Submitted to the Council of Physics Department, College of Science, University of Babylon in Partial Fulfilment of the Requirements for the Degree of Master of Science in Physics

By

Ruaa Qahtan Mohammed Mazloom

B.Sc. in Physics /2011

Supervised by

Assis. Prof. Dr. **Samira Adnan Mehdi**

1442A.H. **2021A.D.**

بسم الله الرحمن الرحيم

﴿وَالرَّاسِخُونَ فِي الْعِلْمِ يَقُولُونَ آمَنَّا بِهِ كُلٌّ مِنْ عِنْدِ رَبِّنَا﴾

صدق الله العظيم

سورة ال عمران، الآية ﴿7﴾

Supervisors Certification

I certify that this thesis is titled **(A Simulation Process of Tunable Open Path Diode Laser Spectrometer to Measure A Gases Concentration)** will be prepared by **(Ruaa Qahtan Mohammed Mazloom)** under my supervisions at Department of Physics, College of Science, University of Babylon, as a partial fulfillment of the requirements for practical work of Physics Master thesis in (Laser Physics).

Signature:

Supervisor: Dr. Samira Mehdi

Title: Assis. Professor
Address: Department of physics - College of Science - University of Babylon
Date: / / 2021

Certification of the Head of the Department

In view of the available recommendations, I forward latter thesis for debate by the examination committee.

Signature:

Name: Dr. Abdulazeez O. Mousa
Title: Professor
Address: Head of Physics Department /College of Science /University of Babylon
Date: / /2021

Dedication

To the one lying under the dust, to his pure spirit that did not leave me throughout my life after his departure, my deceased father. To the one who gives me determination, to the person who lights my life, to the one who illuminates my path, my mom god prolong her life. To the most beautiful thing in my life, to my companion, to the one who endured life with me, to the one who will accompany me in my path, my husband. To those who set me on the path of life, made me calm, and took care of me until I became old, my daughter. To the loveliest persons to my heart who helped me with everything they could offer, my brother and my sister

RUAA

Acknowledgments

I should thank my Almighty (Allah) for helping me in completing my thesis.

I would like to express my deep thanks and gratitude to my supervisors,

***Assis. Prof. Dr. Samira Mehdi** for remarkable notes during the whole work of mine.*

Many thanks to College of Education for Pure Sciences and Department of Physics for offering me the opportunity to complete my thesis and College of Science, Department of Physics, University of Babylon.

RUAA

Summary

In this work the simulation process of TDLS has been demonstrated to enhance the sensitivity of the spectrometer by modulating the wavelength of a DFB tunable laser diode using a sinusoid signal. The drive current of the laser has been tuned, therefore the wavelength of the laser diode will be change in tuning limits reach about 0.02 nm in Near Infrared Region (NIR) and Mid Infrared Region (MIR) regions. That was done using three types of a toxic Methane CH_4, Ammonia NH_3, and Carbon monoxide CO.

The evaluation of TDLS sensitivity was carried out at a constant concentration value 0.5 ppb and a constant length of the open path (the distant between the laser source and retroreflector) 100 m. A MATLAB code has been written to tune the accurate wavelength in the NIR region and MIR, then the frequency domain measurements have been carried out to extract the second harmonic as an indicator of gas presence. The results show the accurate value of wavelength for methane gas in NIR region is 1653.48 nm and the accurate wavelength for methane gas in MIR region is 3290.987 nm. while, ammonia gas the result shows the accurate wavelength in NIR region is 1543.027 nm and the accurate wavelength for ammonia gas in MIR region is 2399.977 nm. whereas, carbon monoxide gas the result shows the accurate wavelength in NIR region is 1584.877 nm and the accurate wavelength for ammonia gas in MIR region is 4650.463 nm. Note that the measurements have been demonstrate at L = 100 m, the gas concentration was N = 0.05 to 0.5 ppb in 0.2 step for all gas types measurement.

Abbreviation	
TDLAS	Tunable Diode Laser Absorption Spectroscopy
DFB	Distributed Feedback
LD	Laser Diode
NIR	Near Infrared Region
MIR	Mid Infrared Region
ppm	Parts-Per-Million
ppb	Parts-Per-Billion
PD	Photo Diode
DA	Direct Absorption
TDL	Tunable Diode Laser
TDLS	Tunable Diode Laser Spectrometer
WMS	Wavelength Modulation Spectroscopy
FFT	Fast Fourier Transformation
WM	Wavelength Modulation
FMS	Frequency Modulation Spectroscopy
TTFMS	Two-Tone Frequency Modulation Spectroscopy
LOD	Limit Of Detection
$\mathbf{I_{ih}}$	Threshold Current
DAC	Data Acquisition Converter System

$\mathbf{f_o}$	Modulation Frequency
δ	Differential Efficiency
γ	Modulation Factor
W_p	Peak Value of The Absorption Spectrum
W_o	The Initial Value of The Scanning Wavelength
a	Amplitude of The Sine Wave
ω	Angular Frequency
DSP	Digital Signal Processing
FEF	Frequency Exponent Factor

CHAPTER ONE
INTRODUCTION

1.1- Introduction

Sensors based on Tunable Diode Laser Absorption Spectroscopy (TDLAS) have the advantages of high sensitivity, high stability, high selectivity and fast response, and have been widely applied in atmospheric environmental monitoring [1–3], medical health [4], industrial production [5,6], military surveying [7,8] and other fields. Given that the absorption spectrum is primarily determined by the atomic and molecular composition of the measured sample, it is a useful tool to determine the presence of a particular substance in a sample [9–12]. Nevertheless, the performance of TDLAS systems can be limited by many factors [13,14], especially, the measurement signal incorporates numerous contributions from optical components (interference fringe) and electronic components [15,16].

Background errors, which are caused by background extraction, also limit the detection precision of the system. Therefore, signal preprocessing is necessary to improve the accuracy of TDLAS-based analytical instruments.

In the development of TDLAS, many methods have been proposed to improve system accuracy and to measure resolution [17–22], which can be divided into two classes: software processing and hardware-based processing.

Some hardware-based approaches such as multi-pass cells, differential, and wavelength modulation techniques have been proved to ameliorate signal quality effectively [23–26]. Besides, with the continuous evolution of data processing technology, many data analysis algorithms have emerged in some fields [27,28]. Some of these methods have been introduced and applied in TDLAS systems to enhance the accuracy and resolution performance.

Current work focuses more on software-based methods, some algorithms have also been proposed to address pertinent issues in TDLAS signals. The applicability of these algorithms has been experimentally demonstrated [29].

1.2- Internal Circuit of TDL

Figure 1.1 shows the internal structure of this package. The main device is an InGaAsP commercial Distribution Feed Back (DFB) butterfly (NLK1655STG) Laser Diode (LD), with 1m pigtail fiber optics. The central wavelength is 1653.7 nm 3291.6 nm for methane gas ,1584.6 nm ,4650.8 nm for carbon monoxide gas and 1543.4 nm, 2399.9 nm for ammonia gas in near and mid infrared region respectively, the fiber optic output power is 26.8 mW.

They lase by applying forward current exceeding threshold values $I_{th} = 17$ mA, $T = 22$ C°. The internal circuit of the butterfly DFB also has An InGaAs PIN monitoring Photo Diode (PD). In this work, this PD is called the internal photodiode and it is monitored to measure the 1/f noise spectrum that is generated by the laser light. The PD is mounted with a tin-lead solder at around 400 picometer from the rear facet of the laser with an angle of 30" to prevent optical feedback in the laser cavity.

The temperature of the diode laser is monitored with a thermistor in the butterfly package. A Peltier cooler is used to control the temperature of the laser. All these components are housed in a 14 pin Package.

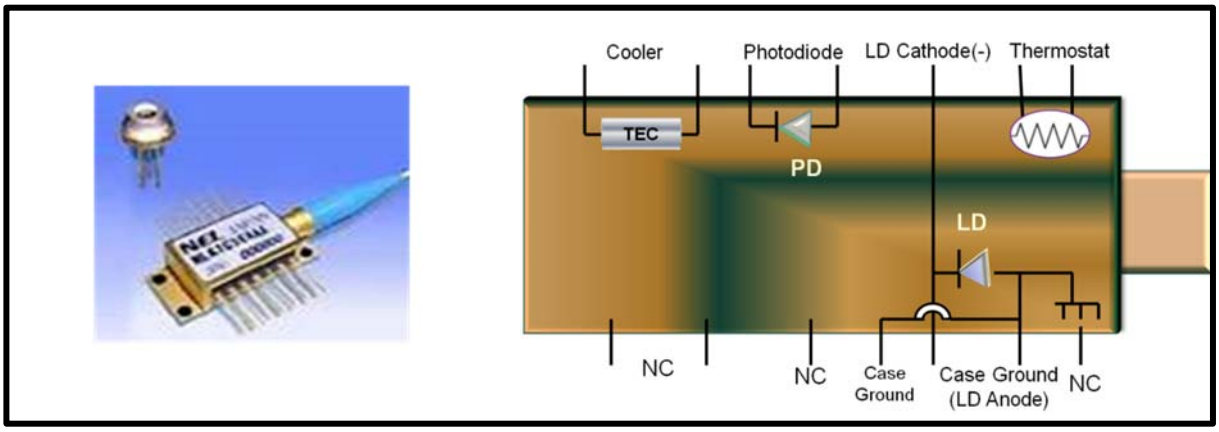

Figure 1.1: Near-infrared tunable diode laser: package picture of TDL (left), internal circuit of TDL (NLK1655STG) (right).

1.3- Tunable Infrared Laser Source

The majority of current semiconductor lasers are constructed from n- and p-type layers of different semiconductor materials in Groups 13 and 15 of the periodic table. As research and development have progressed, many complicated lattice matched structures such as AlGaAs, InGaAs, GaAlAs and GaAlAsP have evolved. To date the best monolithic diode laser sources are those with Distributed Feedback (DFB) structures [6].

The product of 1.3 and 1.5 μm DFB lasers that appears in Figure 1.2 have several characteristics such as, pure single frequency emission at high modulation frequencies, continuous wavelength tuning, a lifetime in excess of 10 years, and can operate at room-temperature. The output power of these near- infrared Distributed-Feedback (DFB) lasers at levels up to 25mW. Therefore, they have been developed for communications and the gas detection measurement field [7].

Near-IR lasers are compact and have high electro-optical conversion efficiency. Of special interest for spectroscopic applications is the fast tunability of the laser emission wavelength and the high spectral resolution. Together with sophisticated noise suppression schemes, they allow highly sensitive spectroscopic gas analysis. The availability of single-mode diode lasers will lead to many applications based on molecular spectroscopy. Also, inexpensive auxiliary equipment such as thermo-electric coolers, collimating lenses, optical Isolators, low noise current drivers and detectors makes them more valuable devices [19].

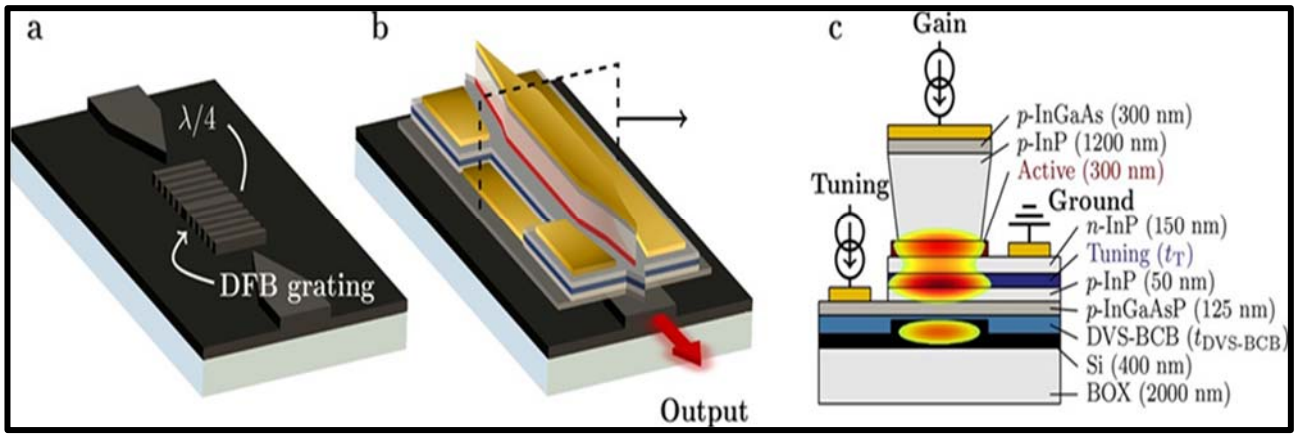

Figure 1.2: Electronically tunable DFB laser structure. A: 3D schematic of the SOI waveguide circuit; b: 3D schematic of the full laser structure; c: cross- sectional view in the middle of the laser structure with indication of the different layers and metal contacts [30].

One significant drawback of these devices is that they exhibit a large component of 1/f noise at low frequency spectrum. Another drawback of near-IR diodes is that only a limited number of molecular species have absorption features in the spectral region covered by these lasers. Furthermore, the near-IR absorptions are overtone or combination bands that are typically one to several orders of magnitude weaker than the IR fundamental band [7].

Nevertheless, many molecules of interest have near-IR absorption bands that are strong enough for detection at parts-per-million (ppm) and, in some cases, even parts-per-billion (ppb) levels. For example: lasers that operate in the near-IR spectral region has been used to detect, ammonia (NH_3) at 1543.4[31], and 2399.9 nm [32], carbon monoxide (CO) at 1584.2 [33] and 4650.8 [34], methane (CH_4) detects with a center wavelength at 1653.7 nm [35] and at 3291.6 nm [36].

1.4- Tunable Diode Laser Spectrometer (TDLS)

The TDLS works by sweeping a narrow bandwidth beam of laser light through an absorption peak for a particular gas. If the gas is present, there will be a lowering in the intensity of the received light. Because the technique requires

measuring a small decrease in a large background signal, frequency domain techniques are usually used to detect the gas absorption signal. There are several kinds of TDLS depending on the method of gas measurements. The following are examples of TDLS systems [21].

1.4.1- Multiple- Reflection Cell Spectrometer

A multi-reflection absorption cell was implemented in the detection absorption signal process in order to obtain more sensitive atmospheric measurements. The most commonly used multi-reflection cell is the White cell as shown in figure 1.3 [37-39].

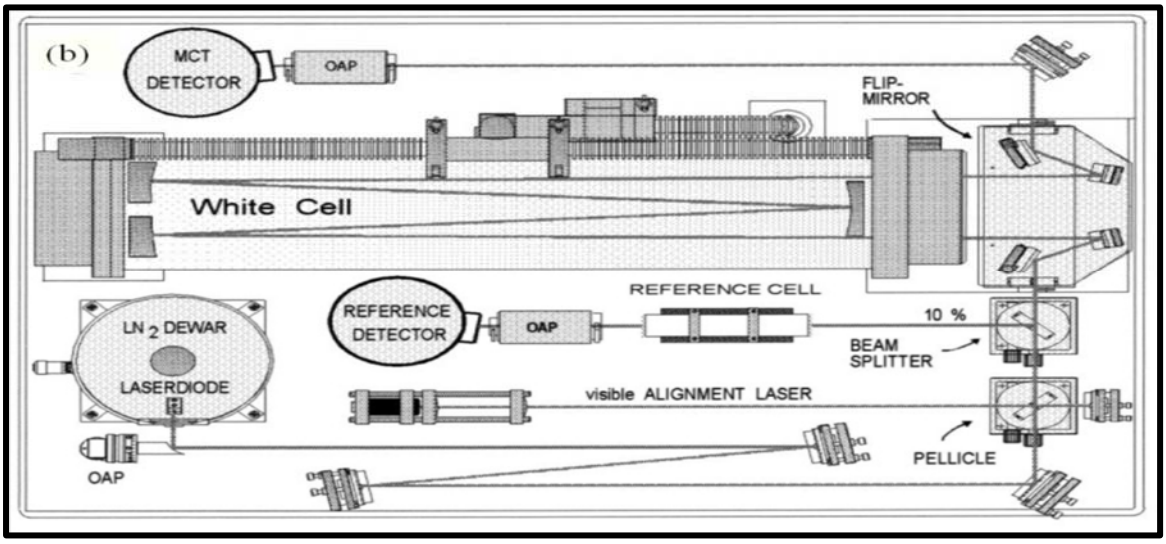

Figure 1.3: Multi-reflection cell (white cell) spectrometer design [37].

It has three spherical mirrors separated by a close distance, between which the laser beam is multiply reflected. Employing three mirrors makes this design somewhat bulky, limited by reducing the intensity of light, and limited by overlapping the light spots on the surface of the mirrors. The multi-reflection process causes interference fringes due to the optical oscillation between the mirrors as shown in Figure 1.4a.

The other kind of multi-reflection cell is the Herriott cell [40,41]. It consists of two concave mirrors with the same radius of curvature separated by a distance d which, closely equals the radius of curvature of the mirror as shown in Figure 1.4b.

However, these cells are not especially compact, because achieving a long and re-entrant path requires large mirrors. In addition, because the light pattern on the spherical mirrors consists of a circular ring of spots, the light fills only a small fraction of the cell's volume. In this sense these cells are not space efficient. More dense patterns can be produced with astigmatic mirrors [26].

Variation in the Herriott cell that spread the light spots over the mirror surfaces, greatly increasing the number of spots achievable without overlapping spots [42]. However, this requires customized mirrors with extraordinarily well-defined focal lengths. These cells were developed to achieve a multi-pass cell with folded optical paths of 100 m or even more [43- 46].

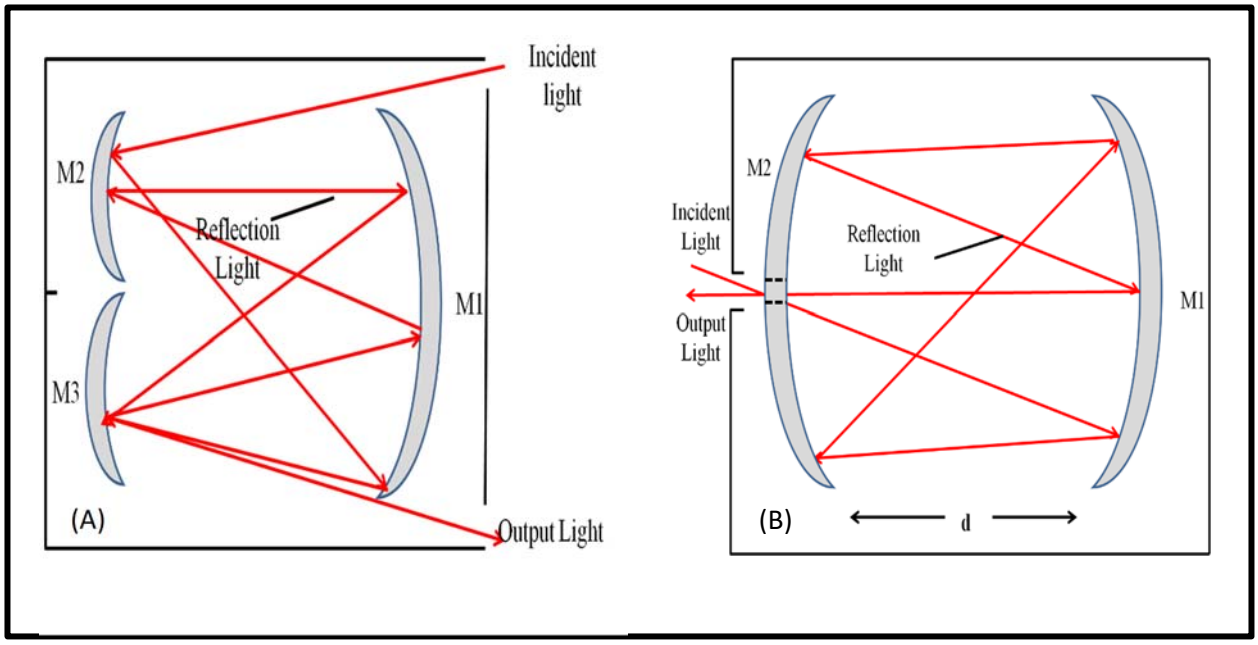

Figure 1.4: Illustrate multi-reflection process in multi-reflection cell spectrometer, A: white cell; B: Herriott cell [40].

1.4.2- Open-path Tunable Spectrometer

Compared with the compact multiple-reflection cell system, the long open-path system can accurately measure gas concentrations over a large spatial area, particularly in poorly mixed atmospheres [47, 48].

It can also directly provide accurate, simultaneous measurements of the average concentration of a number of trace gases over long open-paths. Moreover, the long open-path system can monitor changes in gas concentration in time over a long distance, so it can be used to monitor gas emission flux [49]. Also, it has been used to measure the air quality and the amount of pollutant that emission from on-road vehicles [50-52].

In addition, it simply consists of tunable diode laser, photodetector, hardware devices to manipulate the absorption signal for a specific gas concentration, retro-reflector, and sometimes a telescope is needed to collect the absorption signal that comes from a remote target as shown in Figure 1.5 [53,54].

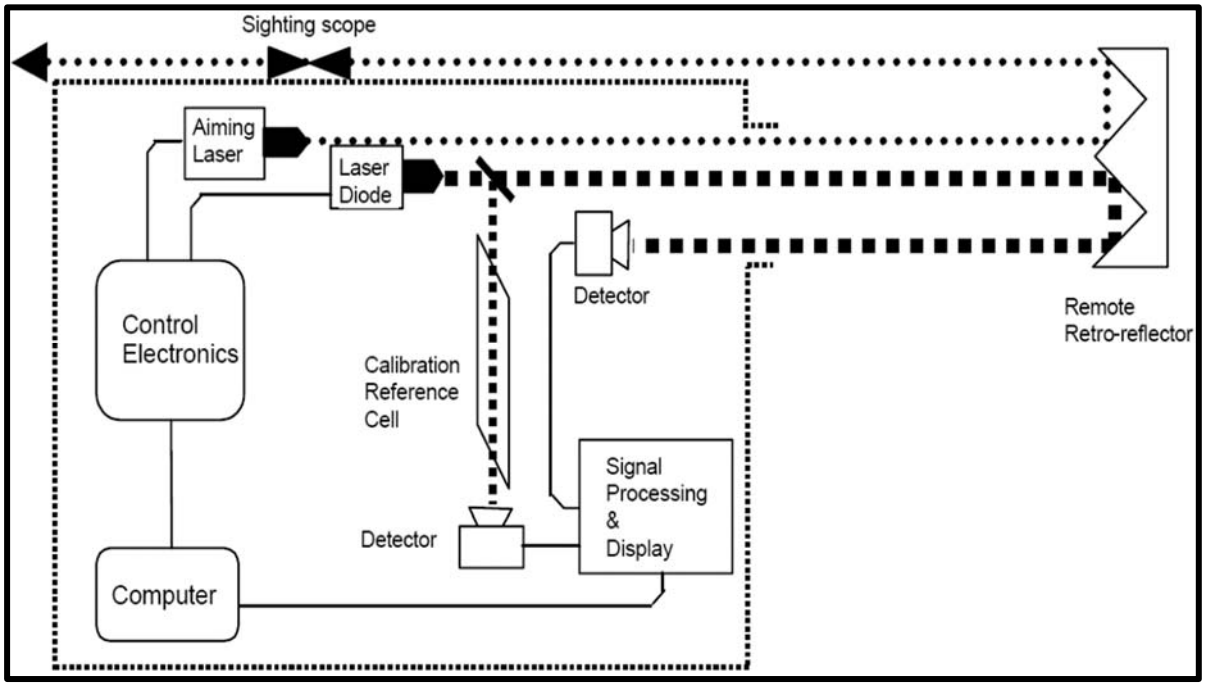

Figure 1.5: Scheme of open path gas monitoring with a retro reflector. Path lengths between 1 and 1000 m are possible [53].

The open-path spectrometer hardware is much simpler than that for long-path spectrometers, which include a multi-reflection cell, diode laser, photodetector, several mirrors to align the laser light through the spectrometer, pumping system, and hardware system to manipulate the absorption signal (lock-amplifier, frequency generator, power supply, computer.

The current on-going system is designed for gas detection on Mars. The TDLS is designed to be placed on a mobile robot, which moves around in order to take measurements of gas concentration in the Martian atmosphere at distances as small as 20 meters to as long as 2 Km as shown in Figure 1.6 [55]. Therefore, the spectrometer should be robust and have simple, light, small-scale equipment, unlike most of the high-resolution spectrometers that use reference gas cells and high frequency operation.

Figure 1.6: Robotic system searching for biogenic gases [55].

1.5- Wavelength Modulation Technique

Wavelength modulation spectroscopy (WMS) has been widely employed in the majority of atmospheric chemistry investigations. It has been used to achieve a high absorbance sensitivity using a tunable diode laser sources since the early 1970s [56- 66]. In this technique, the diode laser injection current is modulated with a sinusoidal current, $I = a\sin(2\pi f_o)$, that produces a repetitive sinusoidal wavelength spectrum in the laser's output and as shown in figure 1.7.

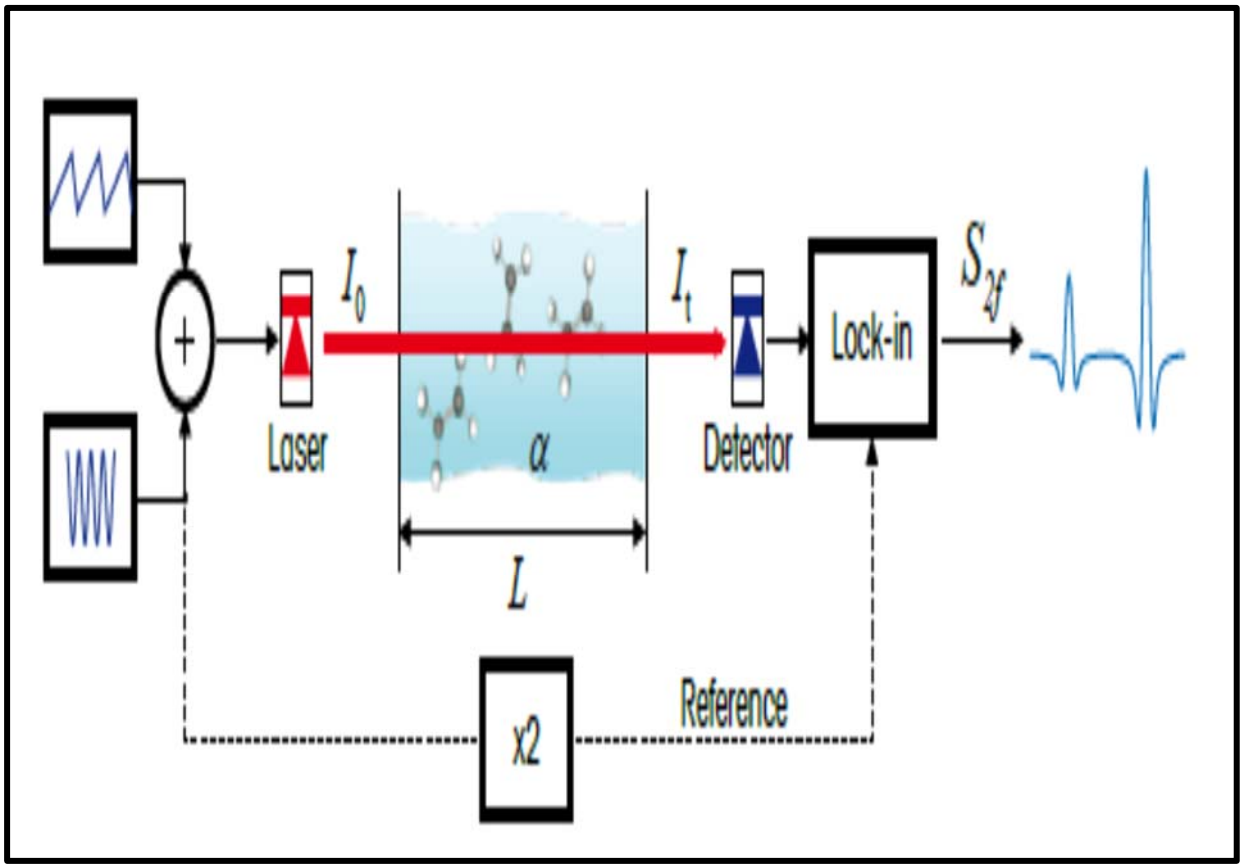

Figure 1.7. Schematic setup for wavelength modulation spectroscopy [67].

In this way, the laser's wavelength can be tuned through an absorption line of the gas species of interest. The absorption signal appears twice per period. Or at the 2nd harmonic of sinusoidal modulation frequency if the absorption spectrum occurs in middle of sine wave. Therefore, the second harmonic signal can be

measured with lock-in amplifier and is proportional to the gas concentration [68]. Figure 1.8 shows how the first four harmonics looks as the laser is scanned over the absorption line. It is most common to use the second harmonic since it does not have a DC-component and it gives a maximum at the line center an important advantage of this technique is to shift detection to higher frequencies where the laser flicker noise (1/f noise) is reduced [70].

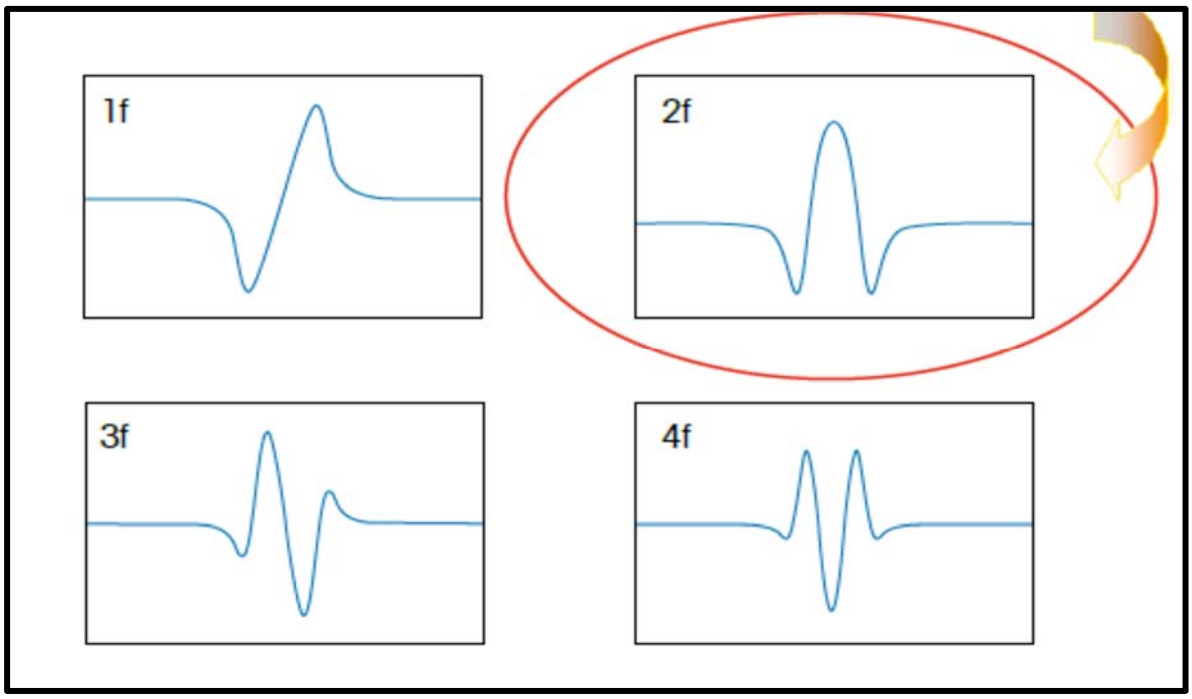

Figure 1.8: View of the detector signal for the first four harmonics of the Fourier expansion as the laser is scanned over the absorption line [69].

The proposed work has employed WMS technique using a sinusoidal waveform, a sawtooth with superimposed sine wave, and a step with superimpose sine waveform. However, the Fast Fourier Transformation (FFT) technique was demonstrated on the time domain signal to extract the useful harmonic (nf), for example (2f, 3f… etc.) to represent the strength of the absorption signal.

1.6- Absorption Line Broadening

Absorption lines are widened by Doppler broadening at low pressure. Therefore, a Gaussian line shape was used to describe the absorption line of the gas molecules. At higher gas pressures, collision broadening which is often referred to as pressure broadening dominates. In this case, a Lorentzian line-shape can be used to describe the absorption line-shape of the gas molecule [71]. In addition, a third absorption line-shape is a combination between the Gaussian and Lorentzian line-shape which called Voigt line-shape, Figure 1.9 illustrates the different line shapes discussed.

.

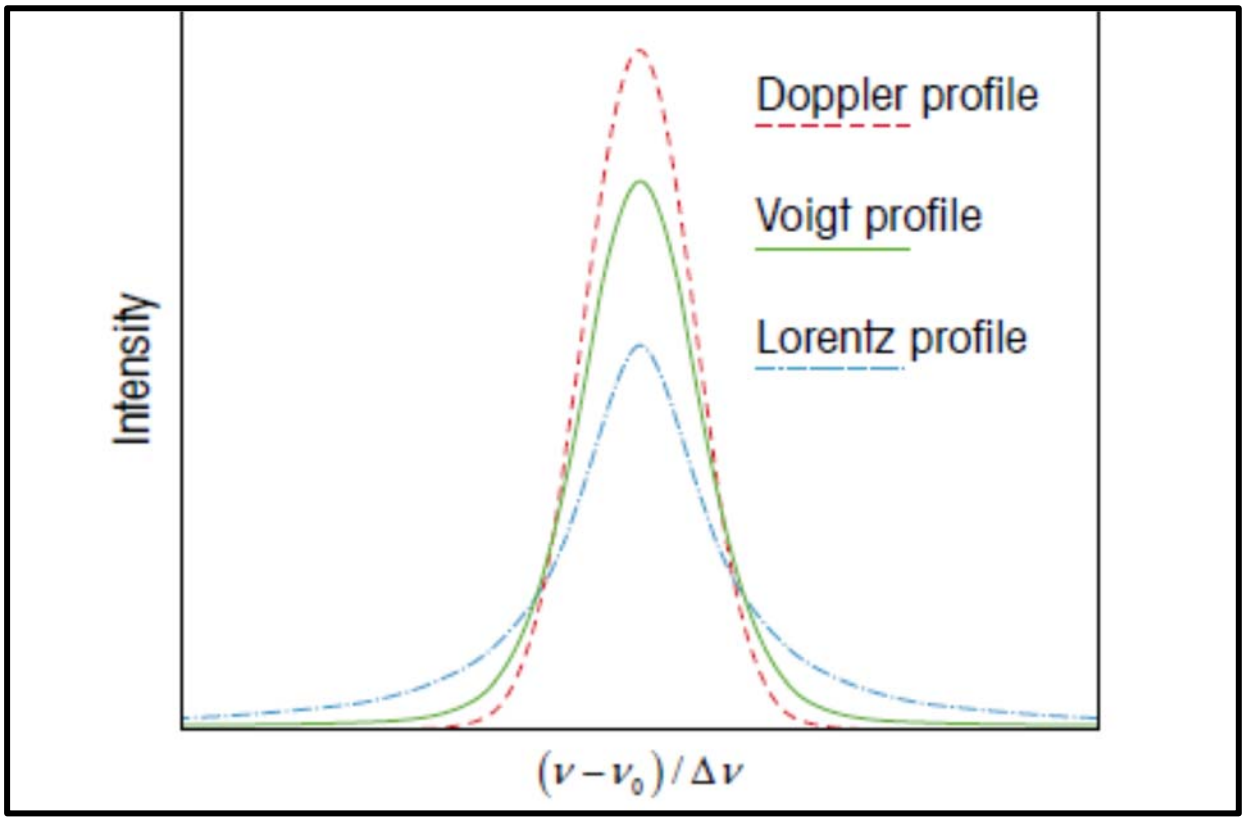

Figure 1.9: Comparison between the Doppler, Voigt and Lorentz line shapes [72]

1.7- Doppler Broadening

The atoms (or gas molecules) are constantly moving during the evacuation process. The motion and direction of the atoms (or gas molecules) are random, and depends on their mass and the temperature of the gas. Due to this motion the light passing through the gas and detected is Doppler shifted, the normalized line-shape function takes the form of a Gaussian function [73, 74]. As the atom speed is small compared to the speed of light, the Doppler shift is small, but is enough to be detected. A range of frequencies can be produced because different atoms have different speeds and the Doppler shift varies from atom to atom as shown in figure1.10 [72].

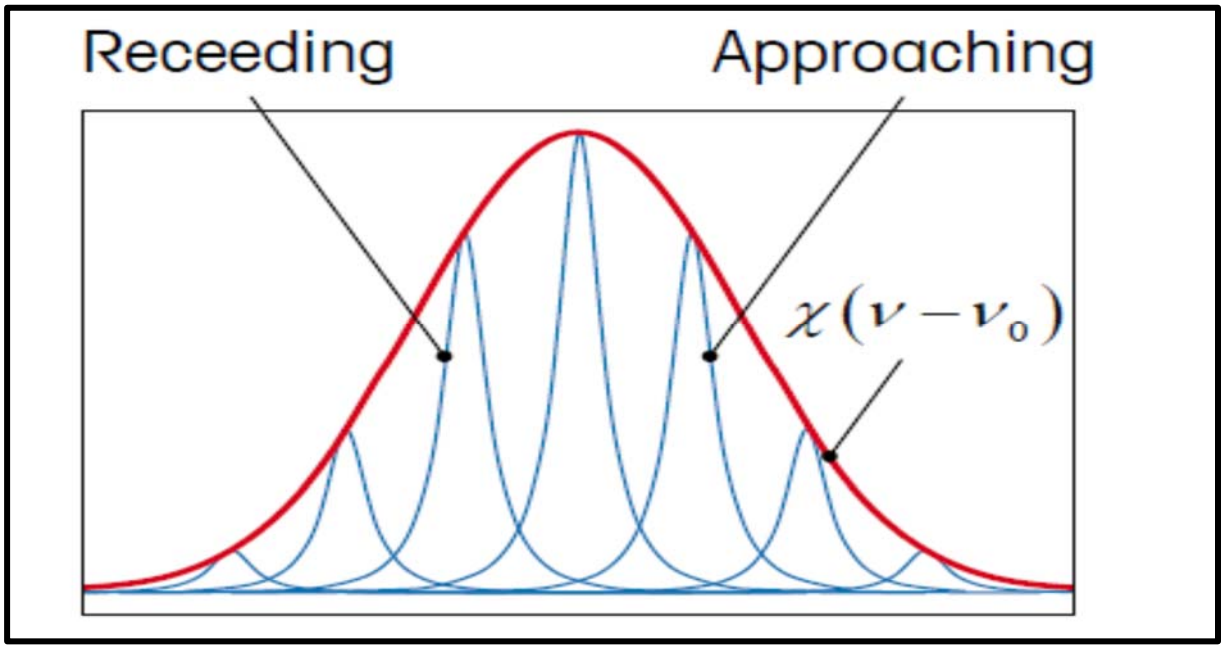

Figure 1.10: illustration of the inhomogeneous broadening due to the Doppler effect [72].

From statistical thermodynamics [75], the Maxwell-Boltzmann distribution has been used to set an expression of the intensity of the absorption line as a function of frequency for the case of Doppler broadening. The probability function of finding an atom in three dimensions with components of velocity (vx, vy, vz) is:

$$\frac{dV(v_x, v_y, v_z)}{n} = Ae^{-m\frac{v^2}{2KT}} = \left(\frac{m}{2\pi KT}\right)^{3/2} e^{-m\frac{(v_x+v_y+v_z)^2}{2KT}} dv_x\, dv_y dv_z \qquad (1\text{-}1)$$

where, n is the total number of atoms, m is the atom mass, v is the velocity of an atom, K is Boltzmann constant, T is the temperature. Now, assume the x-direction is the direction of light detection, any motion in a direction perpendicular to the x-direction does not produce a Doppler shift, and so does not contribute to line broadening. The Doppler shift amplitude is proportional to the velocity of the atom in the x-direction [76]

$$(\nu - \nu_o) = \nu_o \frac{v_x}{c} \rightarrow dv_x = \frac{c\, d\nu}{\nu_o} \qquad (1\text{-}2)$$

Where, c is the light velocity, ν_o is the central frequency of the absorption line, and ν is the absorbed frequency. The combination of equation (1-1) and equation (1-2) will generate.

$$\frac{dV(\nu)}{n} = \frac{c}{\nu_o}\left(\frac{m}{2\pi KT}\right)^{1/2} e^{-\frac{mc^2(\nu-\nu_o)^2}{2\nu_o{}^2 KT}} d\nu \qquad (1\text{-}3)$$

The resultant curve is known as a Gaussian. After taking the normalization condition for the distribution function $\int_0^\infty \emptyset_\nu\, d\nu = 1$, the Doppler width is defined as.

$$\Delta\nu_D = \frac{\nu_o}{c}\left(\frac{2KT}{m}\right)^{1/2} \qquad (1\text{-}4)$$

After those assumptions the distribution function can be defined

$$\emptyset_\nu = \frac{1}{\Delta\nu_D \sqrt{\pi}} e^{-\frac{(\nu-\nu_o)^2}{\Delta\nu_D{}^2}} \qquad (1\text{-}5)$$

1.8- Ammonia Gas Spectrum

Lundsberg-Nielsen et al. reported that ammonia absorption lines have (1710) [77], where (381) lines referred to rotational–vibrational transitions in the combination band and the overtone band. Webber et al. [78] examined these lines for interferences and pointed out the best lines for monitoring purposes. From their report, one of the lines at 1531.7 nm (6528.8 cm^{-1}) was chosen as the operating wavelength for the NH_3 sensor. Moreover, in the near-IR region, especially in the spectrum range 1450 to 1560 nm (6400–6900 cm^{-1}) ammonia has many spectral lines [79-83].

In the MIR region, the earliest and recent investigations on NH_3 were mostly focused in the study of the rotational-vibrational transition bands in the wavelength range of 1.5 μm to 3 μm by using high-resolution spectroscopic analysis techniques [77, 84–88]. More recently, the highly sensitive detection of part per billion of the ν2 fundamental vibrational band of NH_3 around 10.3 μm was reported [89–92]. Although the absorption lines of NH_3 are very strong in the wavelength region centered at 10 μm, this region is affected substantially by the interference of CO_2 absorption lines. Therefore, there is a need to explore another wavelength region over which the absorption lines of NH_3 present stronger absorption than in the 10 μm region. Interestingly, the region centered at 6.6 μm has strong absorption lines which are additionally free of the interference of CO_2. Unfortunately, in this region, water absorbs strongly, making the region less explored.

As shown in figure 1.11, high resolution and high-sensitive spectroscopic analysis of NH_3 centered at 6.2 μm [93]. Therefore, further work is needed in the wavelength ranges between 5 and 7 μm where strong absorption lines of fundamental and combinational vibrational bands of ν4 and ν2 are located.

Exploring these absorption bands allows alternative measurements as well as spectroscopic studies with excellent performance and higher sensitivity [94,95]

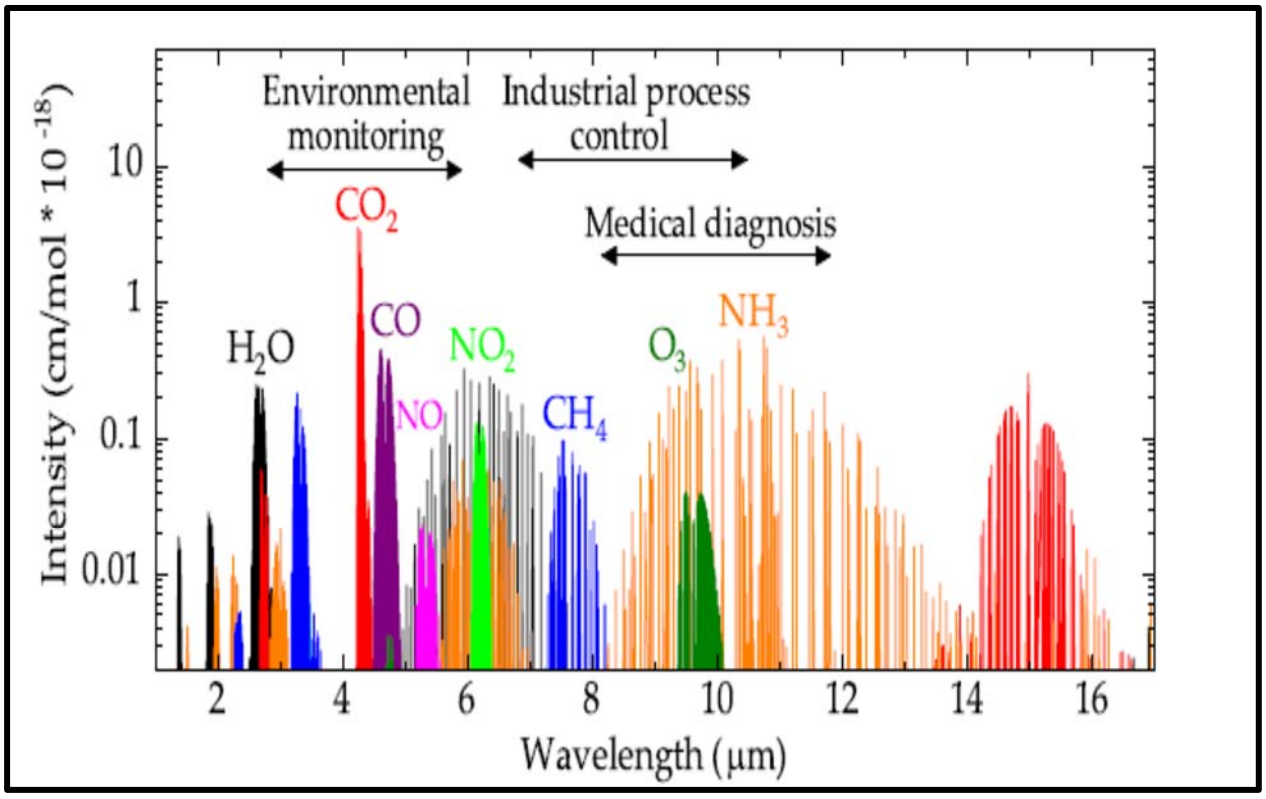

Figure 1.11: Mid-infrared absorption spectra of selected molecules with their relative intensities. H_2O: water; CO_2: carbon dioxide; CO: carbon monoxide; NO: nitric oxide; NO_2; nitrogen dioxide; CH_4: methane; O_3: oxygen; NH_3: ammonia. Source: HITRAN [94].

1.9- Methane Gas Spectrum

In several research papers methane is used as the gas to study methods to increase the sensitivity of TDLS systems [70, 96]. In this study, a long-path cell technique was used to improve the sensitivity of the methane gas measurement under a low pressure 3.6 mtorr. A tunable diode laser spectrometer (TDLS) was employed and Wavelength Modulation (WM) was implemented at a low frequency of modulation 500 Hz. A sine wave was fed to the tunable diode laser to sweep its wavelength through the desired absorption band of the methane gas.

Methane has three absorption lines which are in the wavelength range of 1653.72 ± 0.01 nm, which often look like a single line. Within 0.5 nm of this

wavelength there are not any strong absorption lines from other gases (such as water vapor, nitrogen, carbon dioxide, etc.) In fact, the intensity of the methane absorption line is more 6500 times than the intensity of other gas absorption lines in the same scope. Therefore, the absorption line not only achieve a lower detection limit but also avoid interference of other gases. So, the tunable diode laser which central wavelength is 1653.72 nm is selected in the system [97].

The CH_4 molecule has a spherical top and is part of the tetrahedral point family. It has four basic modes of vibration: $\upsilon 1 = 2913\ cm^{-1}$, $\upsilon 2 = 1533.3\ cm^{-1}$, $\upsilon 3 = 3018.9\ cm^{-1}$ and $\upsilon 4 = 1305.9\ cm^{-1}$ [98]. Of these, the two bending vibrations are $\upsilon 2$ (asymmetric) and $\upsilon 4$ (symmetric), while $\upsilon 1$ (symmetric) and $\upsilon 3$ (asymmetric) are the two stretching vibrations [99]. The successive resonance spacing is about $1500\ cm^{-1}$ [100]. In the near-infrared region (1100–1800 nm), the $2\upsilon 3$ band near 1670 nm and the $\upsilon 2 + 2\upsilon 3$ band near 1300 nm are primary overtone rotational-vibrational combination bands.

According to differences in measurement area and monitoring technique, different frequency bands involving methane transitions from near infrared to mid infrared have been applied [101]. With the development of near-infrared light sources and fiber technology, the corresponding test system in the near infrared region is more mature [102–104]. the absorption strengths of the $2\upsilon 3$ band were suitable for providing high sensitivity for ground-based high-resolution spectrometry in the near-infrared spectrum [105].

The absorption intensity of CH_4 in the $2\upsilon 3$ band is more than four orders of magnitude stronger than that of H_2O and CO_2, which can be safely neglected [106]. The related spectroscopic parameters of $2\upsilon 3$ band, including line positions, line intensities, line widths, line shifts, and line couplings are certain, as described in reference [107–111].

Also, for methane (CH_4), three well isolated lines are available in 1647 – 1655 nm range. But unlike CO and CO_2 absorption lines, CH_4 lines are blended by closely packed secondary peaks. For example, the primary transition line at 1650.961 nm has three secondary peaks at 1650.958 nm, 1650.955 nm, and 1650.948 nm respectively and as shown in figure 1.12 [35].

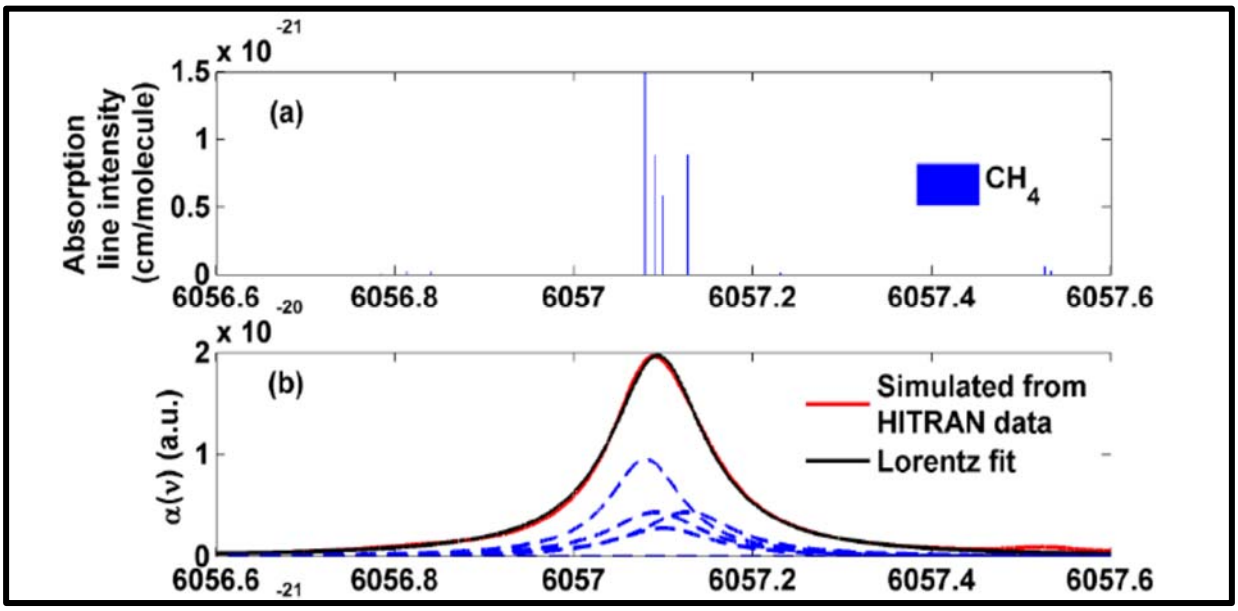

Figure 1.12: Methane absorption line transitions, a: near 1651 nm, b: Methane absorption profile simulated at 100 kPa and 296 K using HITRAN data with Lorentz fit to verify its symmetry [112].

Also, lasers that operate in the mid-IR spectral region has been used to detect, methane gas with a center wavelength of 3291 nm for methane detection. An interference-free methane line located at 3038.5 cm^{-1} was selected as the target line to perform methane detection in ambient air [36]

1.10- Carbon Monoxide Spectrum

The strong fundamental absorption band of CO near 4.7 μm offers potential for very sensitive species detection, even at short path-lengths (< 10 cm). However, until recent years, laser technology in the mid-infrared (> 3 μm) has typically required cryogenic cooling systems that render the lasers impractical for most sensing applications beyond the laboratory. Due to readily available room-

temperature diode lasers and optical hardware in the near-infrared wavelength domain (1–3 μm), most previous CO absorption-based sensors have been designed to probe the overtone vibrational bands near 1.55 μm [113–116] and 2.3 μm [117-119], which unfortunately are more than four and two orders of magnitude weaker, respectively, than the fundamental band Weak absorption strength, combined with spectral interference from carbon dioxide and water, renders the near-infrared CO sensors insufficient for most short path-length combustion systems.

In Figure 1.13 the absorption lines for carbon monoxide (CO) and carbon dioxide (CO_2) are shown overlapped for a wavelength range of 1560 nm to 1600 nm. The distinction between their absorption lines is quite clear [33].

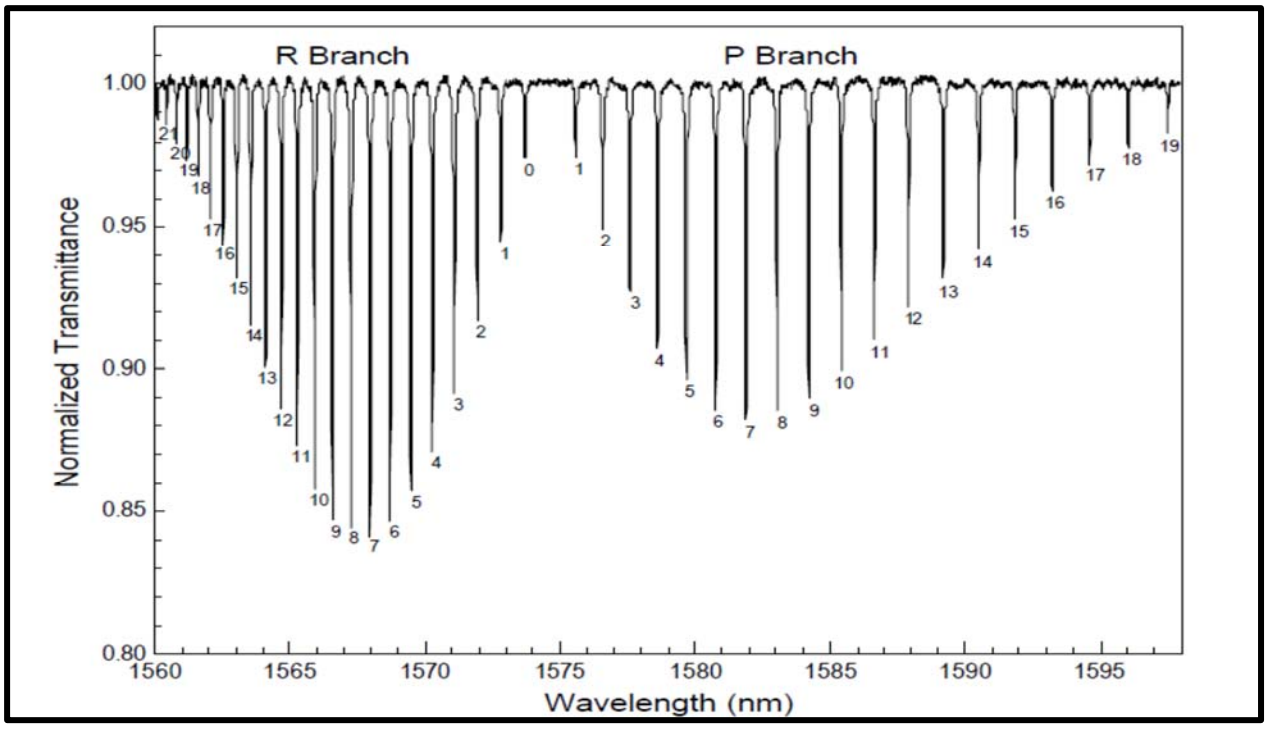

Figure 1-13: Absorption line intensity for carbon monoxide (CO) in the near infrared range (1560 nm ~ 1600 nm) [33]

1.11- Literature Survey

This section includes previous studies by researchers and the results of their work:

In (2021) H. Chuantao et al., [120]. In this study the development of an effective, portable, real-time, and high-precision remote sensing system of ammonia (NH_3) is of great importance to protect the environment and the health of citizens.

They developed a NH_3 remote sensing system based on diode laser absorption spectroscopy (TDLAS) technology to measure NH_3 leakage. In order to eliminate water interference Vapor detection in NH_3, spectroscopy technique for closed wavelength modulation by wavelength Certified to stabilize the output wavelength of the laser at 6612.7cm^{-1} And which significantly Increase the sampling frequency of the sensor system. To solve the problem in that light. The intensity received by the detector is constantly changing, 2f / 1f signal processing technology is adopted. The practical application results proved that the 2f / 1f signal processing technique was satisfactory. The effect of suppression on signal oscillation caused by a change of distance.

In (2020) So, Sunghyun, *et al*., [121] In this study, a combustion system of a partially premixed flamed burner was designed to control the equivalence ratio for fuel-rich conditions. CO concentration was measured using a distributed feedback laser with a wavenumber of 4300.7 cm^{-1} in the mid-infrared region. The results showed that the CO concentration measured at an equivalence ratio of 1.15 to 1.50 was 0.495% to 6.139%. The detection limit in the combustion environment was analyzed at a path length of 190 cm and an internal temperature of 733 K.

The ranges of the peak absorbance were derived as 0.064 and 0.787, because in LPG/Air Flame Flue Gas a combustion reaction of hydrocarbon fuel, carbon monoxide (CO) is a gas species that is closely related to air pollution generation and combustion efficiency. Therefore, it is essential to measure CO concentration in order to optimize the combustion condition. it is difficult to measure the CO concentration in a combustion furnace in real-time because of the harsh

environment in the furnace. Tunable diode laser absorption spectroscopy, which has the advantages of non-invasiveness, fast response, and in situ measurement-based optical measurement, is highly attractive for measuring the concentration of a certain gas species in a combustion environment.

In (2020) X. Chunlei, *et al.,* [122] Spectroscopic measurement of methane gas concentrations using absorption lines in the near infrared (the 1.67 μm region) has been demonstrated by several research teams. this paper, a methane telemetry system based on tunable diode laser absorption spectroscopy (TDLAS) is proposed and demonstrated. The center wavelength of the laser is locked to the methane absorption peak and the second harmonic detection technology is used to realize the real time monitoring of the methane gas concentration.

In (2019) F. Wang, *et al.,* [124], In this review, methane absorption characteristics mainly in the near-infrared region and typical types of currently available semiconductor lasers are described. Wavelength modulation spectroscopy (WMS), frequency modulation spectroscopy (FMS), and two-tone frequency modulation spectroscopy (TTFMS), as major techniques in modulation spectroscopy, are presented in combination with the application of methane detection.

In (2019) Z. Xiaorui, *et al*., [124] This paper referred to demonstrate accurate CO_2 concentration measurement using tunable diode laser absorption spectroscopy (TDLAS). Temperature variations of flue gas have an effect on carbon dioxide (CO_2) emissions monitoring. A distributed feedback diode laser at 1579 nm was chosen as the laser source for CO_2 measurements. A modeled flue gas was made referring to CO_2 concentrations of 10–20% and temperatures of 298–338 K in the exhaust of a power plant. Two temperature compensation methods based on direct absorption (DA) and wavelength modulation (WMS) are presented to improve the accuracy of the concentration measurement. The relative standard deviations of

DA and WMS measurements of concentration were reduced from 0.84% and 0.35% to 0.42% and 0.31%, respectively.

In (2018) T. Zhang, et *al*., [125] a studied tunable diode laser absorption spectroscopy technology (TDLAS) has been widely applied in gaseous component analysis based on gas molecular absorption spectroscopy. When dealing with molecular absorption signals, the desired signal is usually interfered by various noises from electronic components and optical paths. This paper introduces TDLAS-specific signal processing issues and summarizes effective algorithms so solve these.

In (2018) J. Sebastian *et al.,* [126] in this study uses a tunable diode laser-based sensor is reported to monitor carbon monoxide (CO) concentration under conditions similar to those of laboratory-scale tests used to characterize the behavior of heavy crude oil during in situ combustion (ISC).

The sensor uses a DFB diode laser operating over the spectral range of the rotational transition R (11) of the first overtone, wherein simulations of spectral absorption bands for CO, CO_2, and H_2O showed minimal spectral interference. The absorption spectra were calculated using the HITRAN 2008 database at temperatures varying between 150°C and 800°C, pressures from 1 to 5 atm, and the typical concentration of major species in ISC characterization experiments.

The measurements of CO concentration were conducted at ambient temperature and pressure in a static glass cell of borosilicate, with a path length of 3.81 cm, to validate the CO sensor architecture under controlled laboratory environments. The calibration curve for CO obtained by quantifying the optical density at the line center of R (11) for a molar-concentration range between 0.7% and 3.4% demonstrated a linear response (coefficient of determination of 0.9986).

In (2018) L. Bin *et al*., [127] a studied a wavelength modulation spectroscopy-(WMS-) based gas sensing system was established to measure concentration of

carbon monoxide (CO) in the range 0–100%. The CO absorption line at 1563.06 nm was scanned with a tunable distributed feedback (DFB) laser, and two InGaAs photodiodes were applied to perform optic-electric conversion. The gas cell deployed in the system was fiber coupled with a total effective optical path length of 50 cm.

The second-order harmonic signal was extracted, and experiments of gas detection were carried out to investigate the performance of the sensor, including detection repeatability, detection accuracy, response time, and limit of detection (LOD). Experiment results show that the sensor is reliable and has acceptable probing performance.

In (2017) Cui, Xiaojuan, *et al.*, [128] in this paper due to the fact of global warming, air quality deterioration and health concern over the past few decades, great demands and tremendous efforts for new technology to detect hazard gases such as CH_4, CO_2, CO, H_2S, and HONO have been performed. Tunable diode laser absorption spectroscopy (TDLAS) is a kind of technology with advantages of high sensitivity, high selectivity, and fast responsivity. It has been widely used in the applications of greenhouse gas measurements, industrial process control, combustion gas measurements, medicine, and so on.

In (2016) Cai. *et al.,* [129] a studied reported –wavelength 2.33 μm multi-mode diode laser for simultaneous measurement of the concentrations of CH_4 and CO in the ambient air. The signals identification and quantitative analysis are performed using correlation spectroscopy. A Herriot cell and the wavelength modulation spectroscopy technique with second harmonic detection are also utilized to improve the detection sensitivity of the system. The detection limits of the system are estimated to be about 81 ppb and 31 ppb for CH_4 and CO, respectively. The accuracy, sensitivity, precision, and stability are also analyzed to confirm the potential of the system.

In (2016) Amiya Behera, and A. Wang. [130] a study in This paper offers a simple, practical strategy to implement wavelength modulation spectroscopy (WMS) with a tunable diode laser. It eliminates the need to pre-characterize the laser intensity parameters or make any design changes to a conventional WMS system. Consequently, sensitivity and signal strength remain the same as what can be obtained from a traditional WMS setup at low modulation amplitude. and also discussed uncertainties and noises associated with the estimated absolute line shape function and the applicability of this new method to detect several gases in the near infrared region. We used measurements of the 1650.96 nm absorption line for 1% and 8% methane concentration in the 60–100 kPa pressure range to validate the efficacy of this new RAM recovery technique and demonstrated a calibration-free system.

In (2013) J Qiang Huanga *et al.,* [131] this paper studied a portable near-infrared (NIR) CH_4 detection sensor based on a distributed feedback (DFB) laser modulated at 1.654 μm is experimentally demonstrated. Intelligent temperature controller with an accuracy of −0.07 to +0.09 °C as well as a scan and modulation module generating saw-wave and cosine-wave signals are developed to drive the DFB laser, and a cost-effective lock-in amplifier used to extract the second harmonic signal is integrated.

Thorough experiments are carried out to obtain detection performances, including detection range, accuracy, Measurement results show that the absolute detection error relative to the standard value is less than 7% within the range of 0–100%, under an absorption length of 0.2 m and a noise level of 2 mVpp. Twenty-four hours monitoring on two gas samples (0.1% and 20%) indicates that the absolute errors are less than 7% and 2.5%, respectively, suggesting good long-term stability.

The sensor reveals competitive characteristics compared with other reported portable or handheld sensors. The developed sensor can also be used for the detection of other gases by adopting other DFB lasers with different center-wavelength using the same hardware and slightly modified software.

1.12- Aim of The Work

In this study, we try to find a method for detecting and measuring atmospheric gases by using adjustable diode laser absorption spectroscopy (TDLAS) to determine and measure the concentration of two types of gases, which are carbon monoxide (CO)and methane (CH_4), as these two gases are air pollutants. In this paper, a system based on signal processing will be constructed to measure gas concentration and the percentage of pollution in the air. Fourier transforms will also be used and then the second harmonic will be chosen, which is a major indicator of the presence of the gas, and the standard relationship between gas concentration and the second harmonic will also be demonstrated.

The aims of this study are:

1- Simulate the TDLS work using MATLAB code based on signal processing technique.
2- Improve the sensitivity of TDLS using wavelength modulation technique and search the desired and exact absorption wavelength of the specific gas.
3- Modulate the tuned signal of the laser diode using a sine wave.
4- Find the calibration curve between the measured gases concentration such as carbon mono oxide CO, methane CH_4 and ammonia NH_3 and the second harmonic.

CHAPTER TWO
THEORETICAL PART

2.1- Introduction

This chapter covers a general description of the theoretical parts measurements; Prototype of the open-path TDLS, this chapter gives a theoretical review including all the relations, scientific explanations, and the equations which are used in this thesis as shown in works scheme which illustrated the main steps of this work as shown in figure 2.1.

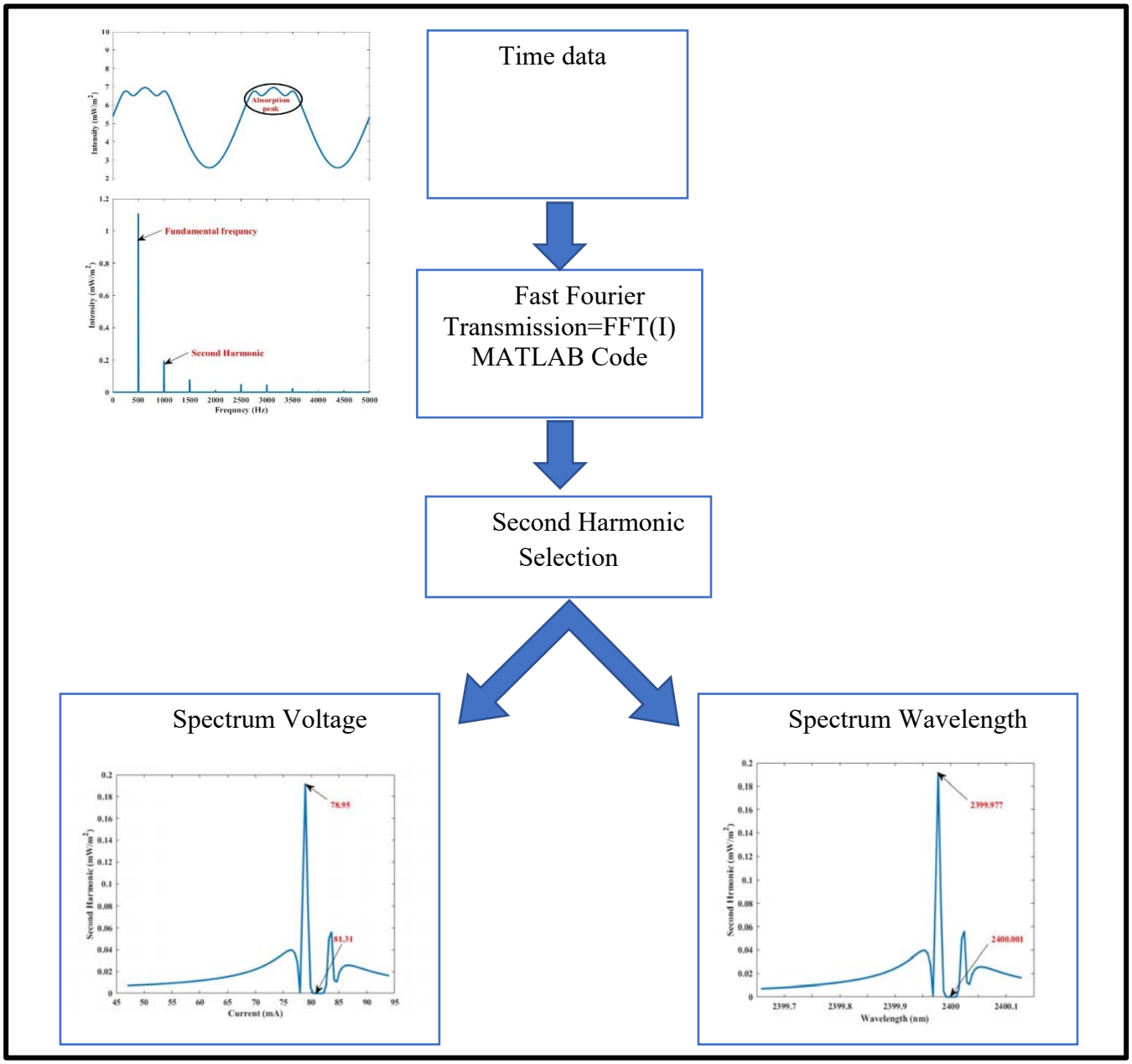

Figure 2.1: The experimental procedure as a block diagram of the main steps in this work.

2.2- Prototype of The Open-Path TDLS

In an open-path TDLAS system, the laser beam propagates in the open atmosphere over a sufficient absorption path length and it reflects back to a photodetector by using an appropriate retro-reflector. The laser light will be absorbed in situ by the molecules of interest. The absorption of laser energy is related to the molecular absorption based on the Beer-Lambert law. Figure 2.2 presents the architecture of the TDLS.

The main device is an InGaAsP commercial Distribution Feed Back (DFB) butterfly (NLK1655STG) Laser Diode (LD), with a pigtail fiber-optic. The central wavelength is 1543.4 nm and 2399.9 nm for NH_3, 1653.7 nm and 3291.6 nm for CH_4, 1584.2 nm and 4650.8 nm for CO and the output power at the fiber-optic is 26.8 mW. The diode lasers by applying a forward current exceeding the threshold value of $I_{th} = 19$ mA with $T = 22$ °C. The internal circuit of the butterfly DFB consists of an InGaAs PIN monitoring photodiode (internal PD) mounted at the rear facet of the laser.

The butterfly package also contains a thermistor to monitor the laser temperature. An internal Peltier cooler can be used to control the temperature of the chip carrier. A telescope (MEADE ETX125-AT***)*** was employed to collect the reflected light from a remote corner-cube retro-reflector.

To simplify the alignment process of the laser light towards the retro-reflector the movements of the telescope (right-left, and up-down) were controlled using software. The laser diode was held on the front face of the telescope to send the light signal, and the photodiode was mounted on the rear face of the telescope to receive the reflected light signal.

The Data Acquisition Converter system (DAC) device has 16-bit analog inputs and outputs and a 250K Sample/Sec maximum sampling rate. A retro-reflector with

multiple small corner cube prisms was designed to reflect the laser beam back to the detector over long distances.

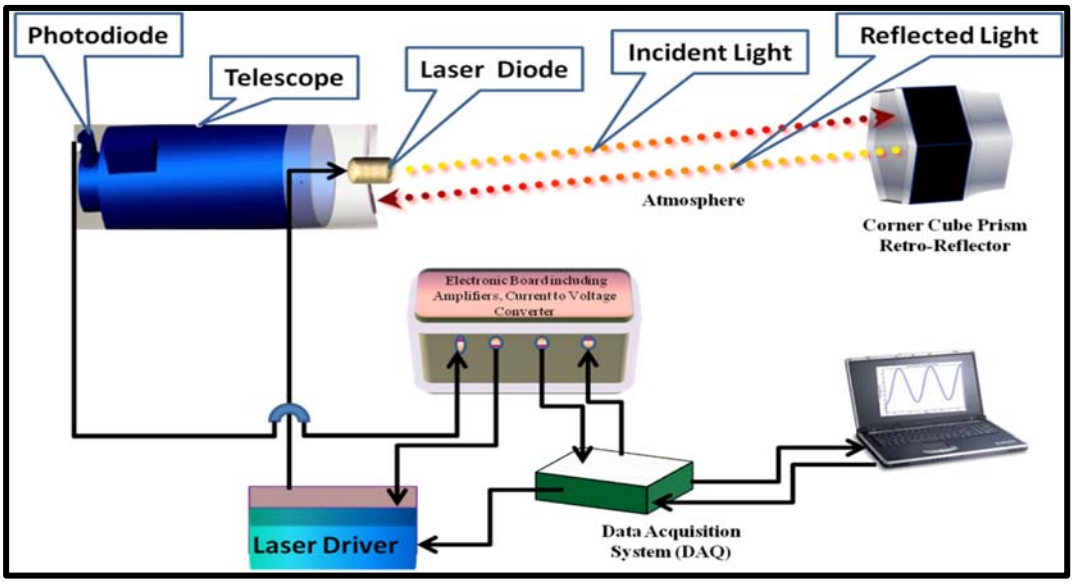

Figure 2.2: TDLS Setup.

2.3- Theory (Simulations)

The simulations of the light absorption by gases are based on the Beer-Lambert law [132]:

$$I = I_o e^{-\beta\sigma NL} \ldots\ldots\ldots\ldots\ldots\ldots \text{(2-1)}$$

where Io is the fundamental incident intensity of IR laser light received by the photodiode when no gas is present. The incident intensity was modulated using sinusoidal waveform as shown in equation (2-2).

$$I_o = [(i_{offset} - i_{th}) + a \sin\ (2\pi f_o\, t)]\frac{\delta}{area} \ldots\ldots\ldots\ldots \text{(2-2)}$$

where $i_{offset} = 99$ mA is the DC offset; $i_{th} = 19$ mA is the threshold current; $a = 42$ mA is the amplitude of the sine wave; $f_o = 500$ Hz is the modulation frequency; $\delta = 0.2055$ mW/mA is the differential efficiency (the direct relation constant that convert the laser current to the laser power); $area = 3.1$ mm^2 is the active area of the photodiode. A narrow bandwidth beam of the laser light

was generated and swept through the absorption peak of methane, carbon monoxide gases.

Depending on the weather conditions in the Martian atmosphere, the pressure is only a few millibars, with a mean pressure of roughly 730 Pa = 7. 3 millibar [132]. Doppler broadening dominates and the line-shape of the absorption cross-section σ becomes Gaussian, as shown in equation (2-3).

$$\sigma = C\, e^{-\frac{(w_o + a\,\gamma \sin\,(2\pi f_o\, t) - w_p)^2}{2\varepsilon^2}} \quad \ldots\ldots\ldots\ldots\ldots\ldots \text{(2-3)}$$

If we substitute equation (2-2) and Eq. (2-3) in equation (2-1) we get:

$$I = [(i_{offset} - i_{th}) +$$

$$a \sin\,(2\pi f_{mod}\, t)]\, \frac{\delta}{area}\, e^{-\beta NLC\, e^{-\frac{(w_o + a\,\gamma \sin(2\pi f_{mod} t) - w_p)^2}{2\varepsilon^2}}} \quad \ldots\ldots\ldots\ldots\ldots\ldots \text{(2-4)}$$

I_0 and I (mW/mm^2) are the intensity of incident light and transmitted light, respectively; β is a factor to convert the unit from ppm to cm^{-3}.

2.3.1- β Factor Calculation for Methane GAS:

We calculate β factor for Methane gas as follow:

$\beta = 1\ ppm = \frac{1mg}{L} = \frac{10^{-3}\, g}{10^3\, M\, cm^3}$, where M is the molecular weight of methane gas, so $c = \frac{10^{-6}\, g}{\frac{16.043 g}{mol} cm^3} = 0.0624 \times \frac{10^{-6}\, mol}{cm^3} \times N_A$, NA is the Avogadro number (cm-3/ppm), As a result, $\beta = 0.0624 \times \frac{10^{-3}\, mol}{cm^3} \times 6.022 \times 10^{20} \frac{1}{mol} = 0.365 \times \frac{10^{-3}}{cm^3} \times 10^{20} = 0.365\text{E}17$, and; N (parts per million) is the gas concentration; and $L = 100$ m is the light path length through the gas. In equation (2-4), C = 1E-20 cm^2 is the cross-section area of the absorption peak of methane gas and its variance $\varepsilon = 0.1$ nm over the wavelength range which appears in the term of $(w_o + a\,\gamma \sin(2\pi f_o\, t) - w_p)$. $w_o = 1653$ nm in NIR $w_o = 3290$ nm in mid IR is the

initial value of the scanning wavelength of the diode laser; a $\gamma \sin(2\pi f_o t)$ is the AC current waveform used to adjust the wavelength of emitted light from the laser, with $a = 42$ mA is the amplitude of the sine wave; $\gamma = 0.01$ nm/mA is a modulation factor; f_o = 500 Hz is the modulation frequency; t is time in seconds; FWHM = 0.06 nm in NIR [35]; FWHM= 0.07 in MIR [134] is a full width half maximum; and $w_p = 1653.7$ nm [35] $w_p = 3291.6$ nm [36]is the peak value of the absorption spectrum of methane gas in NIR and MIR regions, respectively.

2.3.2- β Factor Calculation for Carbon Monoxide Gas:

We calculate β factor for carbon monoxide gas as follow:

$\beta = 1\ ppm = \frac{1mg}{L} = \frac{10^{-3}\ g}{10^3\ M\ cm^3}$, where M is the molecular weight of Carbon Monoxide gas, so $c = \frac{10^{-6}\ g}{\frac{28.01g}{mol} cm^3} = 0.0357 \times \frac{10^{-6}\ mol}{cm^3} \times N_A$, NA is the Avogadro number (cm^{-3}/ppm), As a result, $\beta = 0.0357 \times \frac{10^{-3}\ mol}{cm^3} \times 6.022 \times 10^{20} \frac{1}{mol} = 0.214 \times \frac{10^{-3}}{cm^3} \times 10^{20} = 0.214E17$, and; N (parts per million) is the gas concentration; and $L = 100$ m is the light path length through the gas. In equation (2-4), C = 1E-20 cm^2 is the cross-section area of the absorption peak of ammonia gas and its variance $\varepsilon = 0.1$ nm over the wavelength range which appears in the term of $(w_o + a\,\gamma \sin(2\pi f_o t) - w_p)$. $w_o = 1584.$nm in NIR $w_o = 4650$ nm in mid IR is the initial value of the scanning wavelength of the diode laser; a $\gamma \sin(2\pi f_o t)$ is the AC current waveform used to adjust the wavelength of emitted light from the laser, with $a = 42$ mA is the amplitude of the sine wave; $\gamma = 0.01$ nm/mA is a modulation factor; f_o = 500 Hz is the modulation frequency; t is time in seconds; FWHM = 0.37 nm in NIR [33]; FWHM =0.33 in MIR [34] is a full width half maximum; and $w_p = 1584.6$ nm [33] $w_o = 4650.8$ nm [34] is the peak

value of the absorption spectrum of carbon monoxide gas in near and mid infrared, respectively.

2.3.3- β Factor Calculation for Ammonia Gas:

We calculate β factor for Ammonia gas as follow:

$\beta = 1\ ppm = \frac{1mg}{L} = \frac{10^{-3}\ g}{10^3\ M\ cm^3}$, where M is the molecular weight of ammonia gas, so $c = \frac{10^{-6}\ g}{\frac{17.031g}{mol} cm^3} = 0.059 \times \frac{10^{-6}\ mol}{cm^3} \times N_A$, NA is the Avogadro number (cm^3/ppm), As a result, $\beta = 0.059 \times \frac{10^{-3}\ mol}{cm^3} \times 6.022 \times 10^{20} \frac{1}{mol} = 0.355 \times \frac{10^{-3}}{cm^3} \times 10^{20} = 0.355E17$, and; N (parts per million) is the gas concentration; and $L = 100$ m is the light path length through the gas. In equation (2-4), C = 1E-20 cm^2 is the cross-section area of the absorption peak of ammonia gas and its variance $\varepsilon = 0.1$ nm over the wavelength range which appears in the term of $(w_o + a\,\gamma \sin(2\pi f_o\, t) - w_p)$. $w_o = 1543$ nm in NIR $w_o = 2399$ nm in mid IR is the initial value of the scanning wavelength of the diode laser; a $\gamma \sin(2\pi f_o\, t)$ is the AC current waveform used to adjust the wavelength of emitted light from the laser, with $a = 42$ mA is the amplitude of the sine wave; $\gamma = 0.01$ nm/mA is a modulation factor; f_o = 500 Hz is the modulation frequency; t is time in seconds; FWHM = 0.24 nm [31] in NIR ; FWHM = 0.33 nm [134] in MIR is a full width half maximum; and $w_p = 1543.4$ nm [31] $w_p = 2399.9$ nm [32] is the peak value of the absorption spectrum of ammonia gas in near and mid infrared region; respectively.

2.4- Fast Fourier Transform (FFT)

The Fast Fourier Transform (FFT) is the one of the most important analysis methods used to investigate information that is carried by a signal in the frequency domain. With Fast Fourier transform analysis, it is necessary to sample the input signal with a sampling frequency f_s that is at least twice the bandwidth of the signal,

due to the Nyquist limit [135-137]. A Fourier transform will then produce a spectrum containing all frequencies from zero to $f_s/2$. Fourier transform analysis was implemented in the WMS instrumentation to detect the second harmonic of the injected sinusoidal current. The second harmonic can be shown to be proportional to the size of the absorption peaks, and thus proportional to gas concentration [138-142].

The first FFT layer was used for quick acquisition of code and carrier. It can only give a coarse carrier frequency. The second FFT layer was used for accurate frequency calculation based on the result of the first FFT layer [143].

The mathematical formula for Fast Fourier Transform is given by equations:

Mathematica:

$$Fourier[\{a1, a2, \ldots\ldots, aM\}] \qquad \frac{1}{\sqrt{N}}\sum_{r=1}^{N} a_r \exp\left[\frac{2\pi i(r-1)(s-1)}{N}\right] \ldots\ldots\ldots \text{(2-5)}$$

And the MATLAB formula for Fast Fourier Transform is given by equations:

MATLAB:

$$fft(x)\sum_{j=1}^{N} x\,(j)\exp\left[-2\pi i(j-1)\left(k-\frac{1}{N}\right]\right. \ldots\ldots\ldots\ldots \text{(2-6)}$$

2.5- Harmonic Detection Technique

Harmonic detection technique uses wavelength modulation and second harmonic (2f) signal detection techniques to achieve highly sensitive detection of target gas. The wavelength modulation of absorption spectra can produce a harmonic signal which is proportional to the concentration of trace gases. In theory, this is a zero-background spectrum detection technique [144,145].

With wavelength modulation technique, to produce the harmonic signals, a cosine modulation of angular frequency(ω) is superimposed upon the laser. This results in a time variation of the laser frequency given by the following expression:

$$\nu = \nu_c + a\ \cos(\omega.t) \ldots\ldots\ldots \text{(2-7)}$$

Where ν is the instantaneous frequency of the laser wavelength; ν_c is the center frequency of the laser modulation; a is modulation depth. Wavelength of the laser output is modulated cosine. Then the sign l generated by the laser passing through gas is a periodic even function, which can be expanded in a cosine Fourier series.

$$S = \sum_{n=0}^{\infty} H_n(\nu_c \cos(n\omega.t) \ldots\ldots\ldots \text{(2-8)}$$

where H_n is the nth harmonic component of the modulated absorption coefficient α If the absorption coefficient is sufficiently small, H_n can be approximately expressed as:

$$H_n \propto I_0 \propto LC \ldots\ldots\ldots\ldots \text{(2-9)}$$

It can be seen from the above equation, that the harmonic components are proportional to the gas concentration. As the theory described above, the harmonic can be used to detect gas concentration. Because the amplitude of each harmonic component decreases with the number of harmonics increasing, low harmonics are often chosen to obtain a higher signal to noise ratio. With the harmonic detection technique, harmonic components can be selected by using a lock-in amplifier.

The maximum value of even-order harmonics occurs at the gas absorption line center, and there is a linear relationship between the size of the peak and the detected gas concentration. The peak of the odd harmonics has a shift relative to the center of the absorption lines. Among them, the second harmonic amplitude is greatest in all the even harmonics. Based on the above analysis, usually the second harmonic signal is used for gas concentrations inversion. Corresponding to the position of the absorption peak, the first harmonic component is regarded as a reference of light source intensity [146].

CHAPTER THREE
RESULTS AND DISCUSSION

3.1- Introduction

In this chapter the simulation measurements of the selected gases types will be display in details.

3.2- Methane Gas Absorption Peak in The NIR Spectral Region

The absorption peak of the CH_4 gas in NIR region has been evaluated using Lambert-Beer law see equation (2-1). Throughout modulating process of the tuning wavelength by a sinusoid signal. A MATLAB code has been written to determine the shape and the location of the absorption signal. Note that the concentration of methane gas has been fixed at 0.5 ppb and the length of the open path spectrometer was fixed at 100 m.

Figure 3.1 illustrates the absorption signal of the methane gas at tuning current of laser diode 79.89mA and the wavelength 1653.48 nm. The absorption peak locates exactly at the middle of the sine wave that mean the gas has been absorb the whole energy of the sine wave. because the frequency of the light wave has been matching the vibrational frequencies of the methane gas at this wavelength.

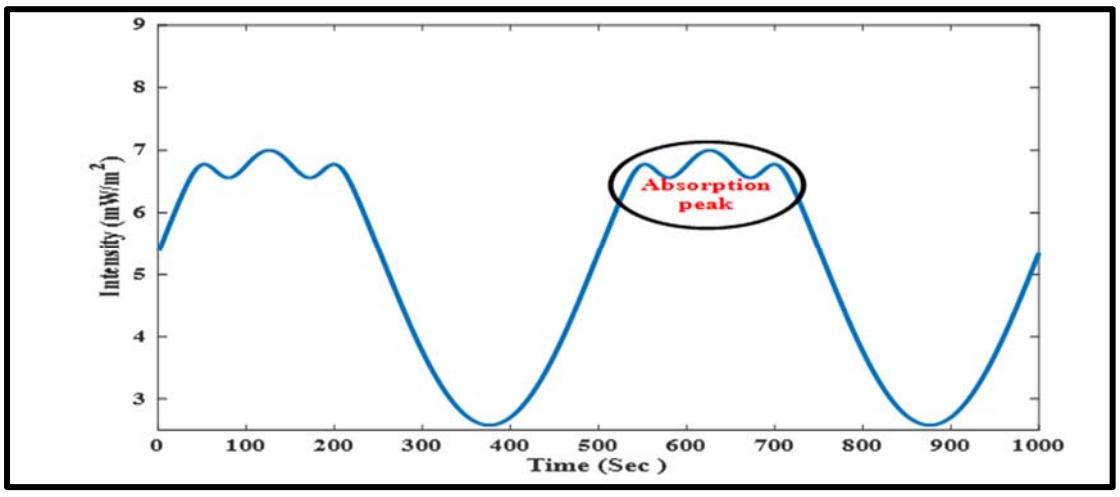

Figure 3.1: The absorption of methane gas in near infrared region peaks at tuning current of laser diode (79.89mA) and the wavelength (1653.48 nm).

Absorption signal in time domain has been plotted as shown in Figure 3.2 It is obvious there is no clear absorption signal as compare as with Figure 3.1. Because the wavelength of the laser passes out the matching point of the vibrational energy states that can be absorb the energy of the light laser beam.

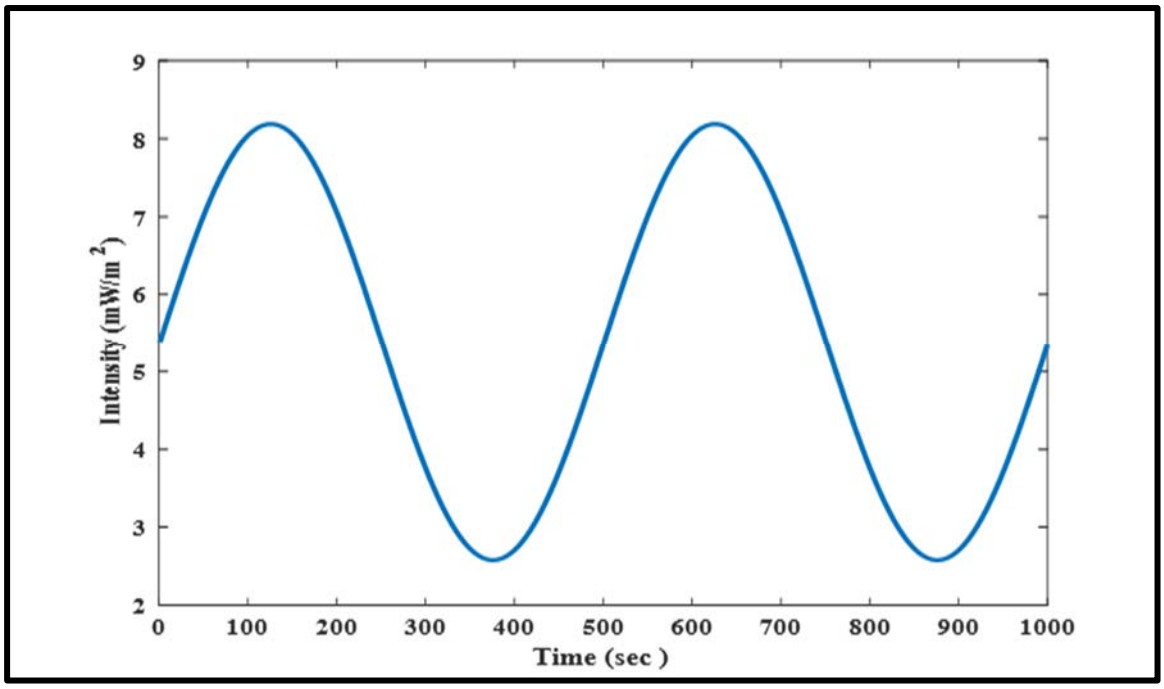

Figure 3.2: Absence of absorption peak of methane gas in near infrared region at tuning current of laser diode (81.31 mA) and wave length (1653.50 nm).

A fast Fourier transformation (FFT) has been implemented to extract the second harmonic as an indicator for the gas presence, that have been done by written a MATLAB code. Figure 3.3 shows the chart of the fast Fourier Transformation (FFT) for the time domain data see Figure 3.1. where the fundamental frequency located at 500 Hz and the second harmonic has been indeed in the 1000 Hz also the value of the second harmonic seems to be significant 0.19 mW/m^2 that mean the energy of light has been mostly absorb.

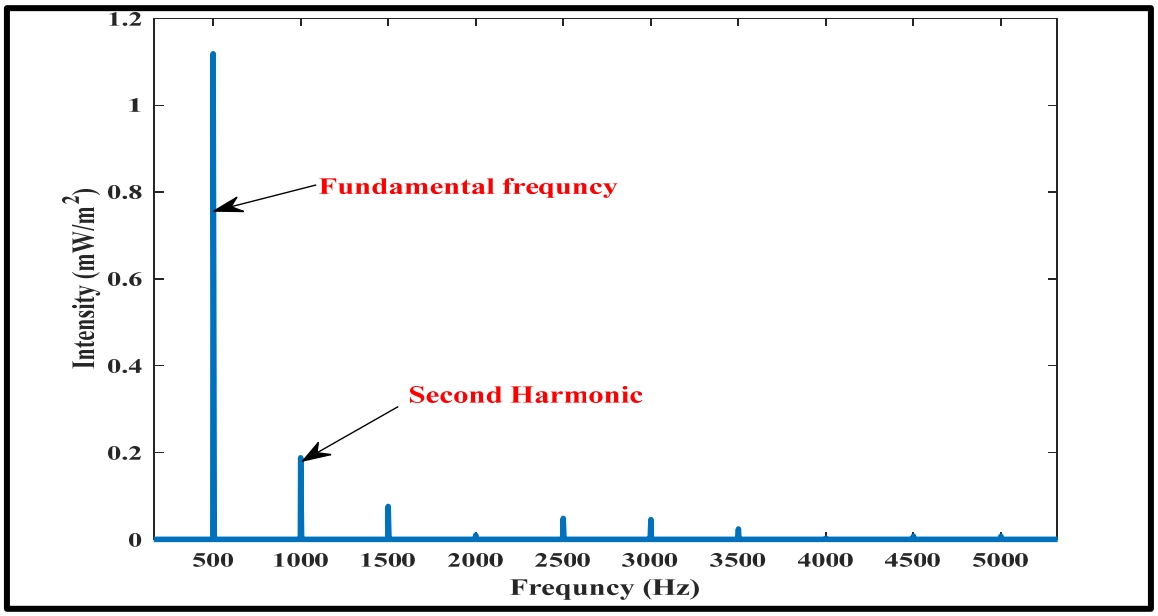

Figure 3.3: The fundamental frequency of methane gas in near infrared region at 500 Hz and the absorption peak at 1000 Hz.

The result in Figure 3.4 exhibits the fundamental frequency and the value of second harmonic, it seems that the second harmonic has been diminished.

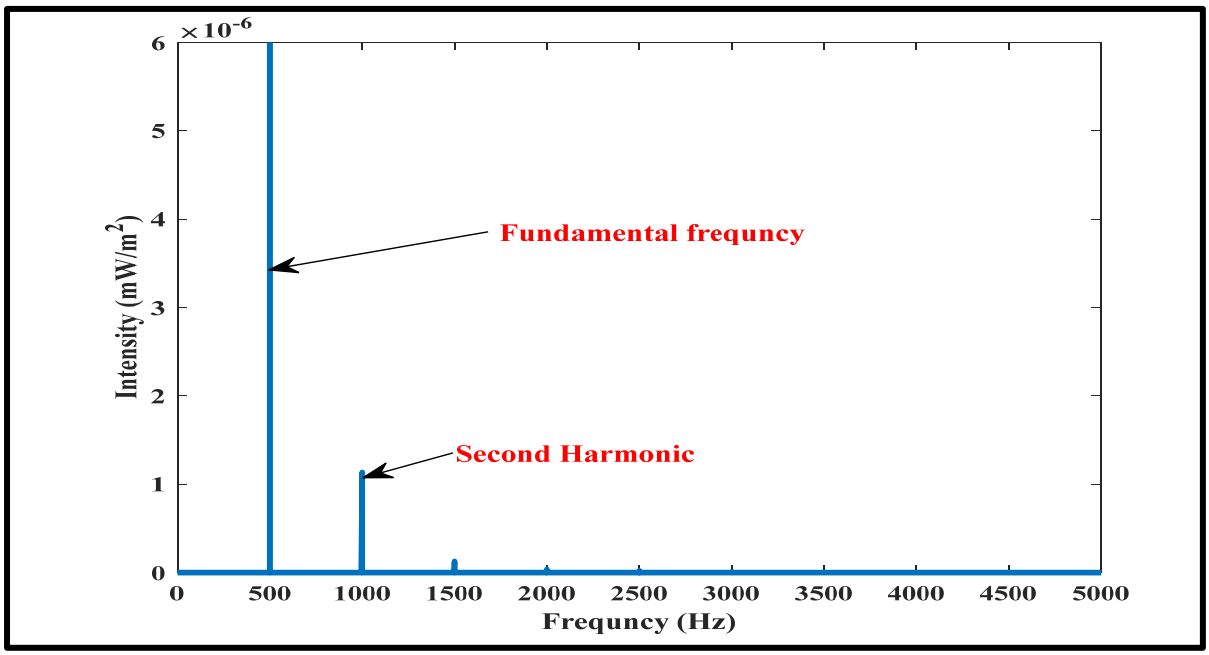

Figure 3.4: The fundamental frequency of methane gas in near infrared region at 500 Hz and the amount of the second harmonic reached about zero at 1000 Hz.

A MATLAB code has been written to evaluate the amount at the operation current of laser diode (LD) that can be give a max second harmonic value and it was found that the relation has max. peak and min. valley at current values 79.89 mA, 81.31mA respectively as shown in figure 3.5.

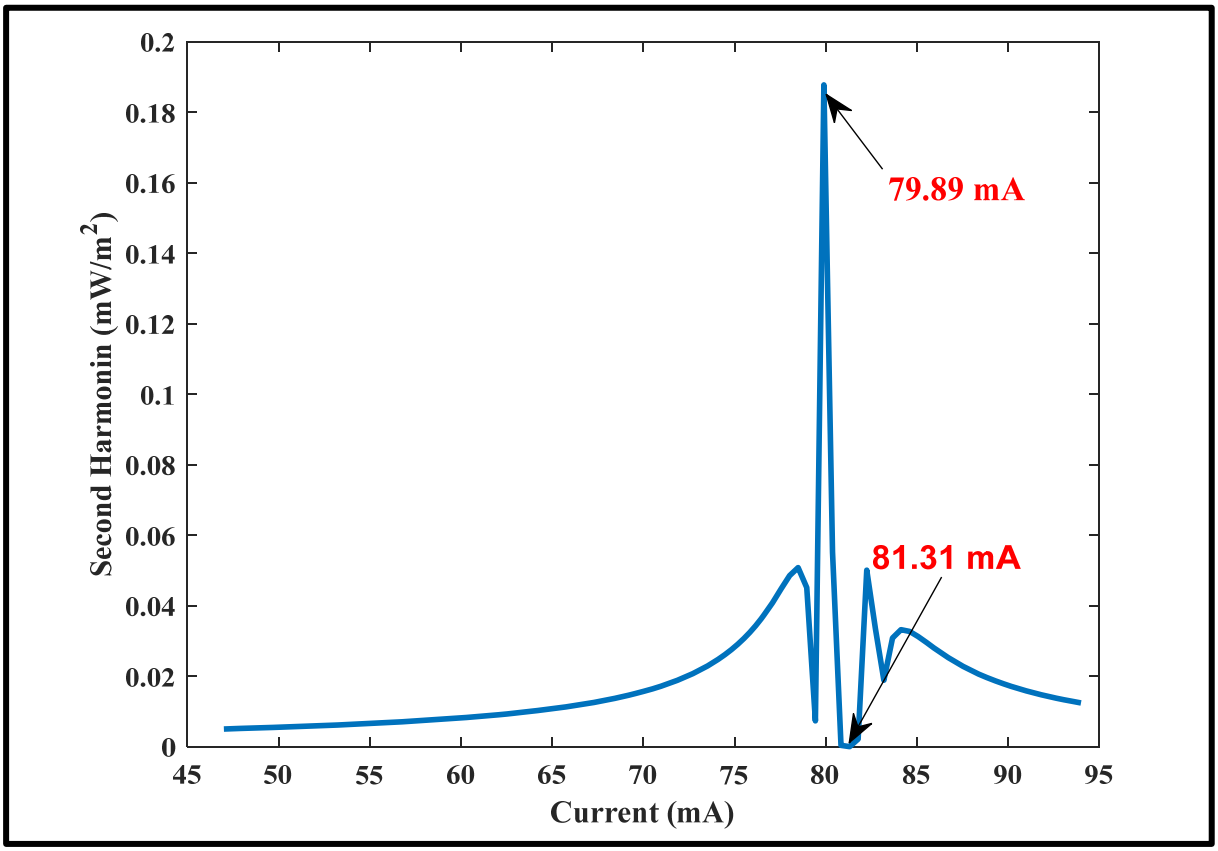

Figure 3.5: The variation of methane gas in near infrared region of the second harmonic with the tuning current.

Then the spectrum wavelength has been tuned around 1nm in 0.02 nm steps to increase the sensitivity of the tunable diode spectrometer (TDLS). And it was the main goal of this work. as illustrate in figure 3.6 and it was found the relation has maximum peak and minimum valley at was wavelength values 1653.48 nm,1653.50 nm respectively in near infrared that was done by MATLAB code.

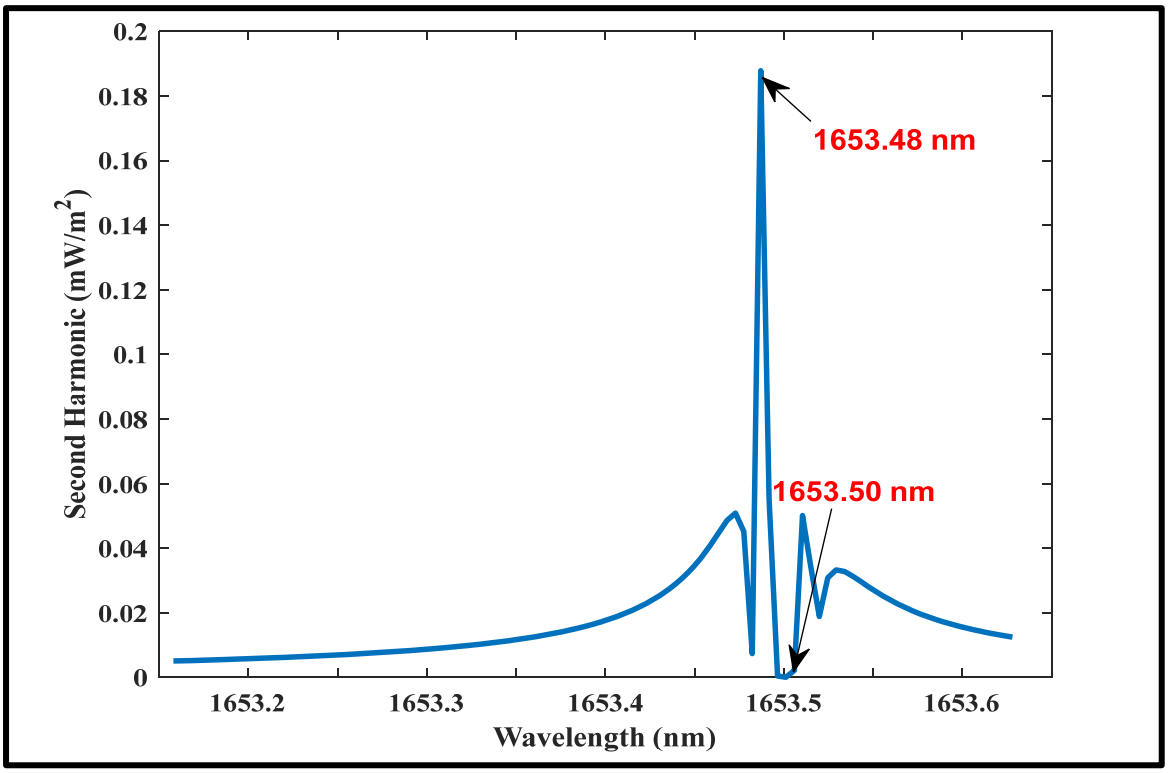

figure 3.6: The wavelength spectrum of methane gas in near infrared has a one peak at (1653.48 nm).

Figure 3.7 shows the relation between the second harmonic and the gas concentration at desired value of the driven current of the laser diode and at exact wavelength the 1653.48 nm the relation seems to be linear and min value of the gas constrainer was 0.05 ppb.

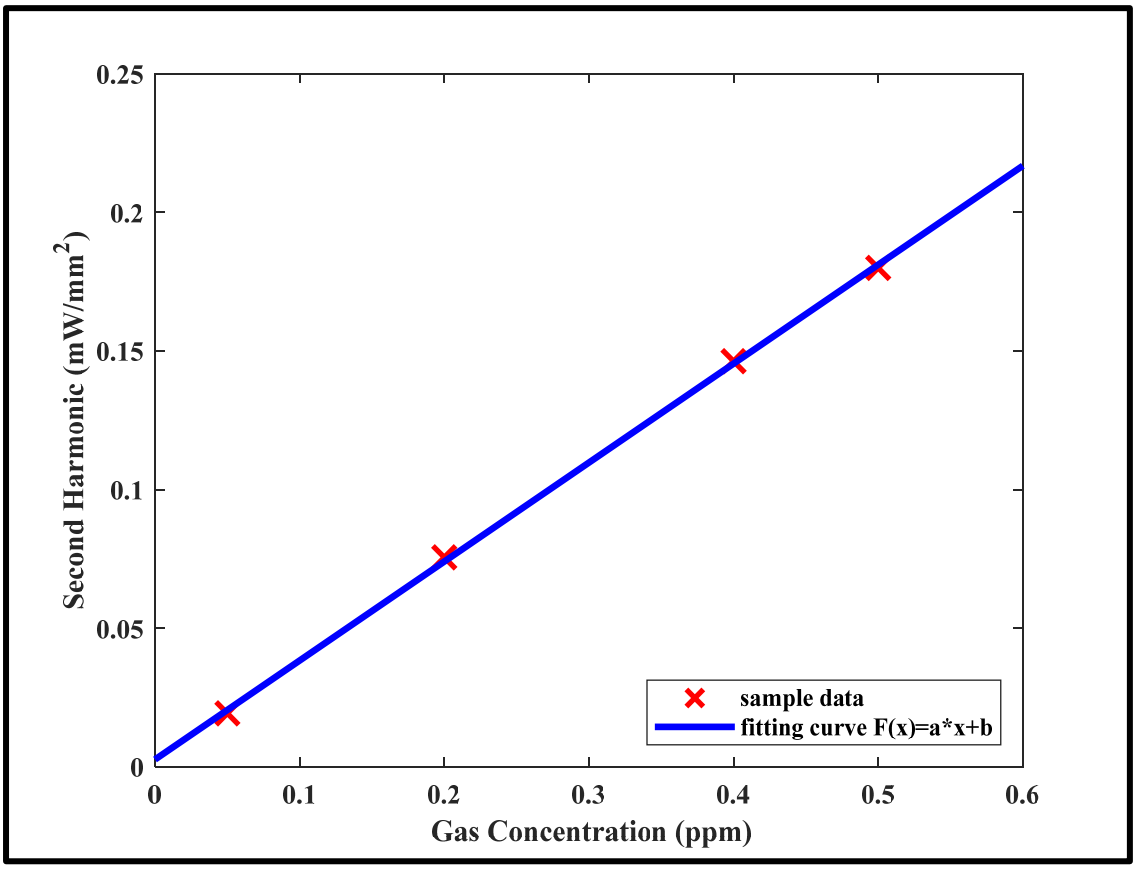

Figure 3.7: Relation between second harmonic and gas concentration of methane gas in near infrared region.

3.3- Methane Gas Absorption Peak in The MIR Spectral Region

The absorption signal of methane gas has been determined at tuning current of laser diode 79.90 mA and wavelength 3290.987 nm are shown in Figure 3.8. Because the frequency of the light wave matches the vibrational frequencies of the methane gas at this wavelength, the absorption peak is located exactly in the center of the sine wave, implying that the gas has absorbed the whole energy of the sine wave. Note that the concentration of methane gas has been fixed at 0.5 ppb and the length of the open path spectrometer was fixed at 100 m.

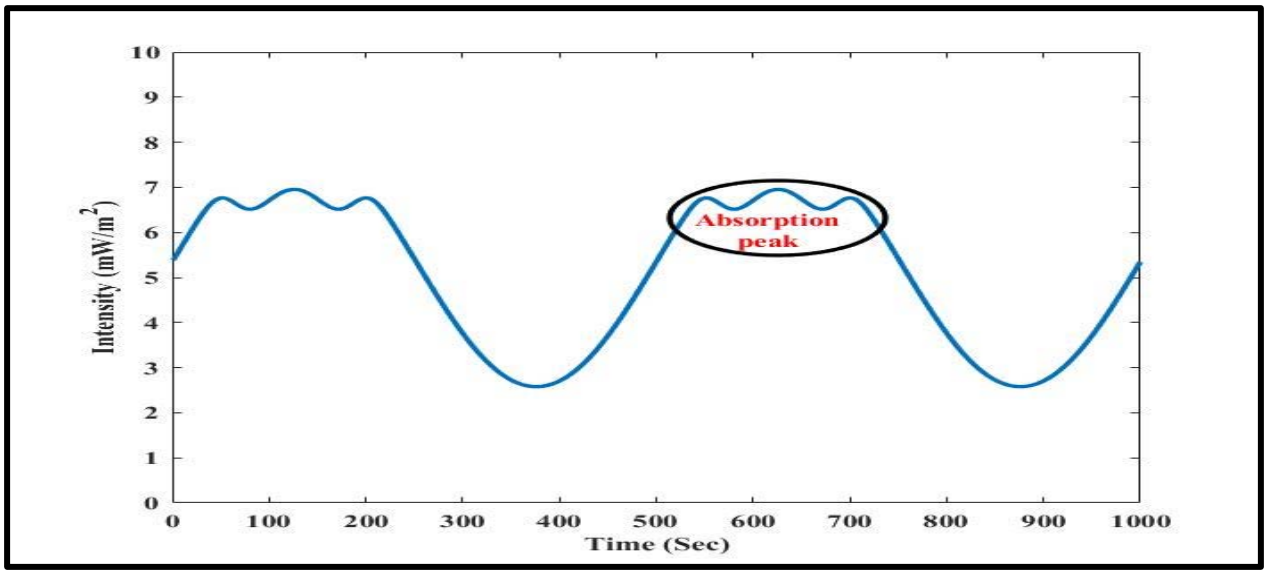

Figure 3.8: The absorption peak of methane gas in mid infrared region at tuning current of laser diode (79.90mA) and the wavelength (3290.987 nm).

Figure 3.9 shows the absorption signal in time domain there is no absorption signal as compare as with Figure 3.8. Because the wavelength of the laser diode isn't matching frequencies of the vibrational energy states that can absorb the laser light energy.

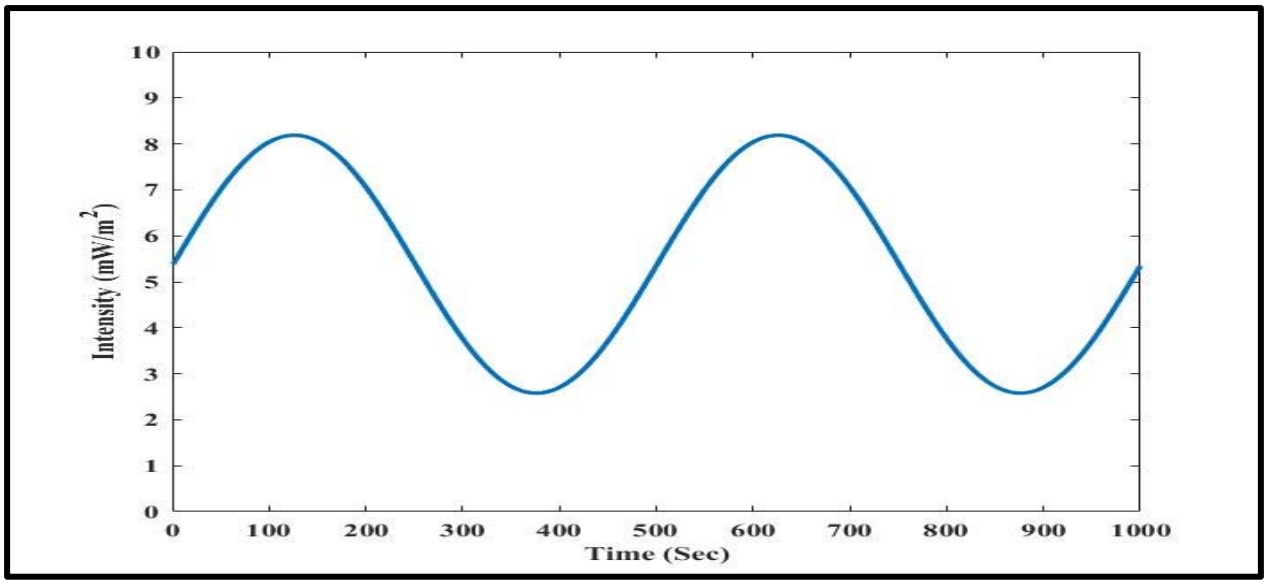

Figure 3.9: Absence of methane gas in mid infrared region absorption peak at tuning current of laser diode (81.31 mA) and wavelength (3291.001 nm).

A fast Fourier transformation (FFT) was used to extract the second harmonic as a gas presence indication, which was done using MATLAB code.

Figure 3.10 displays the fast Fourier Transform (FFT) chart for the time domain data shown in figure 3.8. Where the fundamental frequency is 500 Hz and the second harmonic is in the 1000 Hz, the value of the second harmonic appears to be considerable 0.18 mW/m^2, implying that light energy has been mostly absorbed.

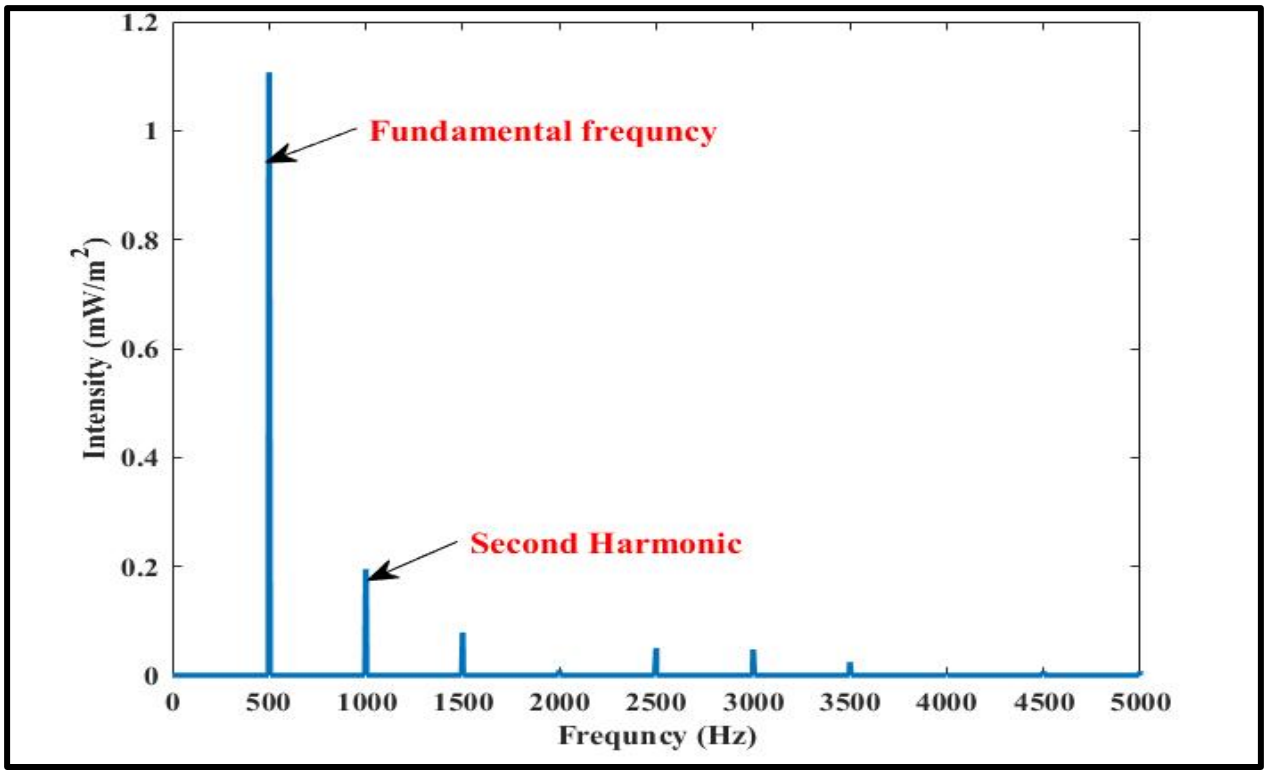

Figure 3.10: Fundamental frequency of methane gas in mid infrared region at 500 Hz and the absorption peak at 1000 Hz.

The fundamental frequency and the value of the second harmonic are shown in figure 3.11. The second harmonic appears to have been reduced (that's mean there is no absorption peak for the methane gas in mid infrared region) when the value of the wavelength little far from the desired wavelength value.

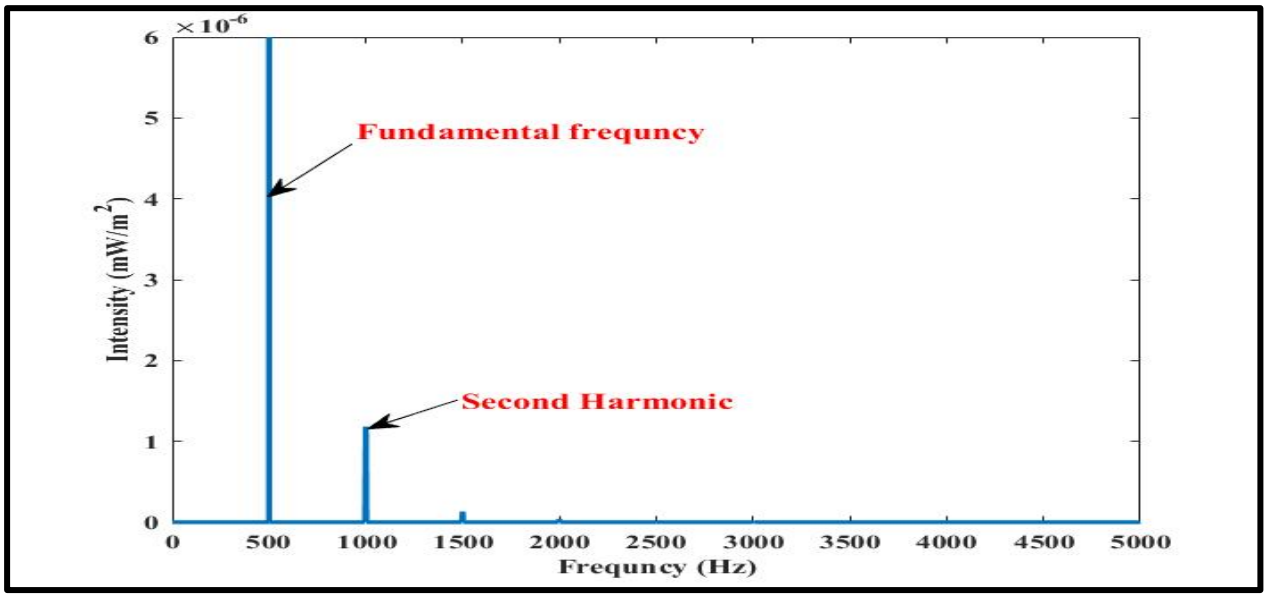

Figure 3.11: fundamental frequency of methane gas in mid infrared region at 500 Hz and the amount of the second harmonic reached about zero at 1000 Hz.

The amount at the operating current of a laser diode (LD) that may generate a max second harmonic value was calculated using a MATLAB code, and it was discovered that the relation has a max. peak and min. valley at current values of 79.90 mA and 81.31 mA, respectively, as shown in figure 3.12.

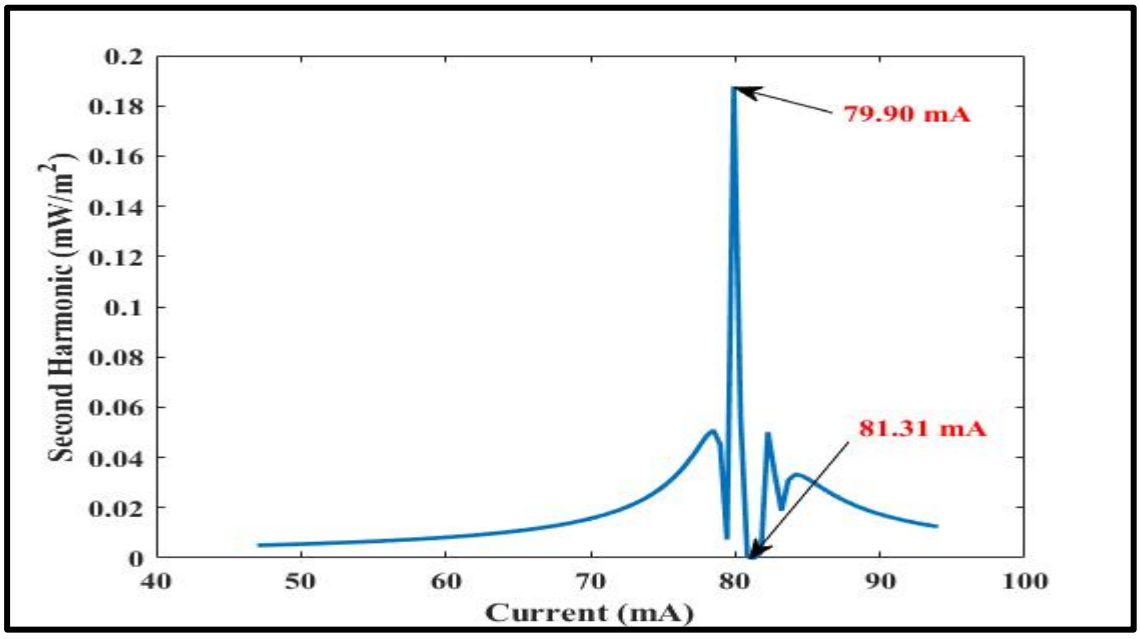

Figure 3.12: The variation of the second harmonic with the tuning current of methane gas in mid infrared region.

The spectrum wavelength was then set about 1nm in 0.02 nm steps to improve the tunable diode spectrometer's sensitivity (TDLS). And that was the primary purpose of this project. As seen in figure 3.13, the relation has a maximum peak and minimum valley at wavelength values of 3290.987 nm and 3291.001 nm in the mid infrared, respectively, as determined by MATLAB code.

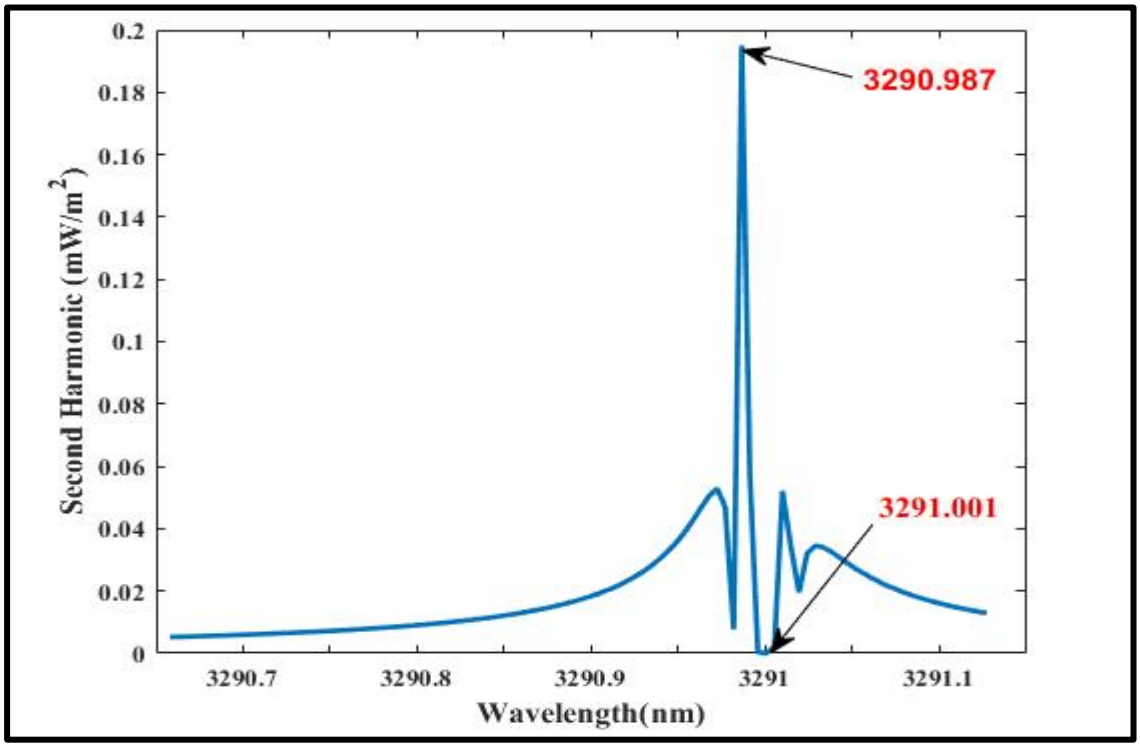

Figure 3.13: The wavelength spectrum of methane gas in mid infrared region has a one peak at (3290.987 nm).

Figure 3.14 depicts the relation between the second harmonic and gas concentration at the required value of the laser diodes driven current and at the correct wavelength 3290.987 nm. The relation seems to be linear, and the gas concentration's minimum value was 0.05 ppb.

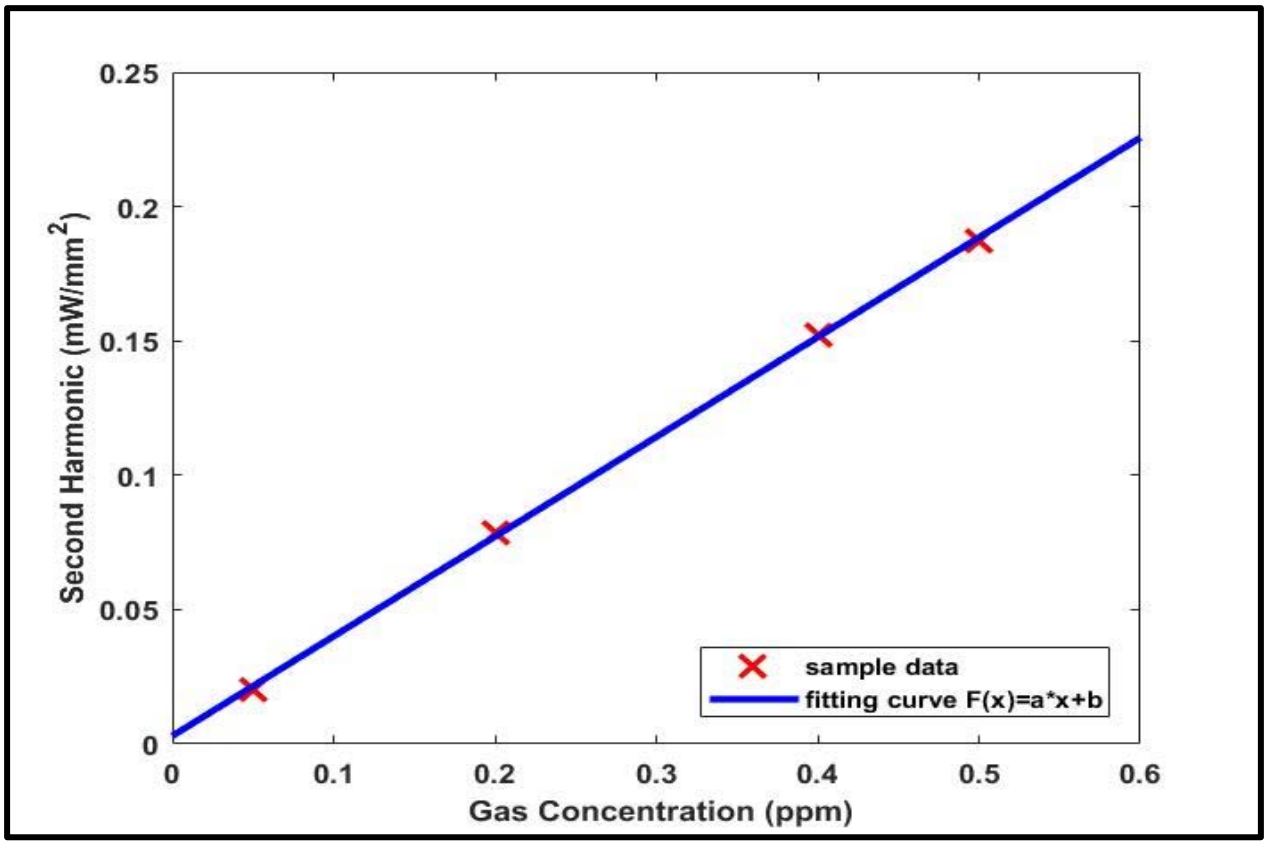

Figure 3.14: Relation between second harmonic and gas concentration of methane gas in mid infrared region.

3.4- Ammonia Gas Absorption Peak in The NIR Spectral Region

Figure 3.15 shows the absorption signal of the ammonia gas at tuning current of laser diode 86.01mA and the wavelength 1543.027 nm. The dip of the absorption peak locates exactly at the middle of the sine wave, and it is a deep and sharp dip. That means there was a highly sense of ammonia gas for that specific wavelength 1543.027 nm, and the frequency of the laser light has been matching vibrational frequencies of the ammonia gas at this wavelength. Note that the concentration of ammonia gas has been fixed at 0.5 ppb and the length of the open path spectrometer was fixed at 100 m.

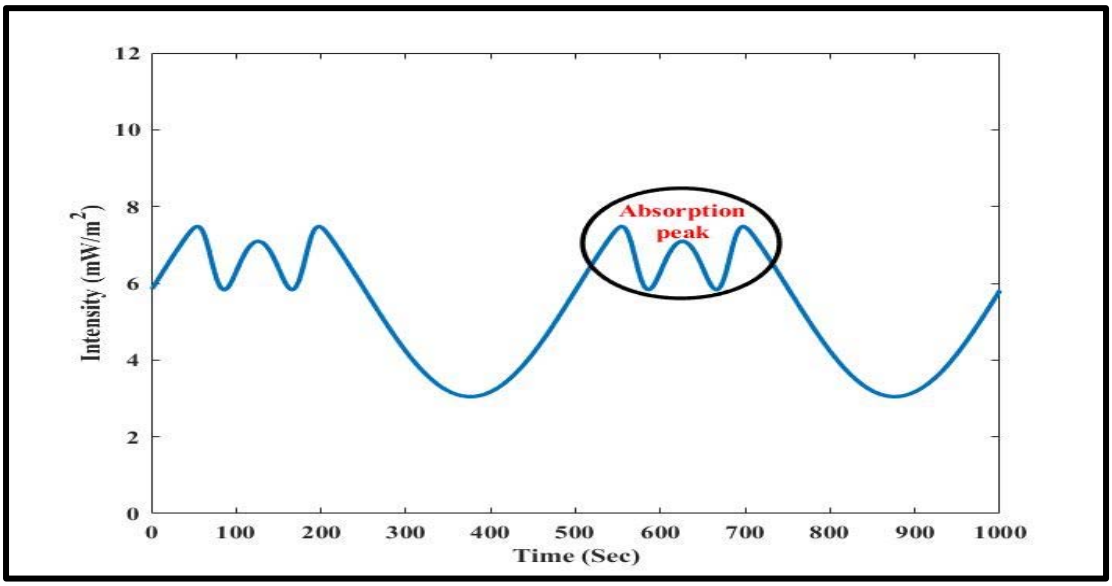

Figure 3.15: Ammonia absorption peak in near infrared region at tuning current of laser diode (86.01mA) and the wavelength (1543.027 nm).

Absorption signal in time domain has been plotted as shown in Figure 3.16. It is obvious there is no clear absorption signal as compare as with Figure 3.15 Because the wavelength of the laser passes out the matching point of the vibrational energy states that can be absorb the energy of the light laser beam.

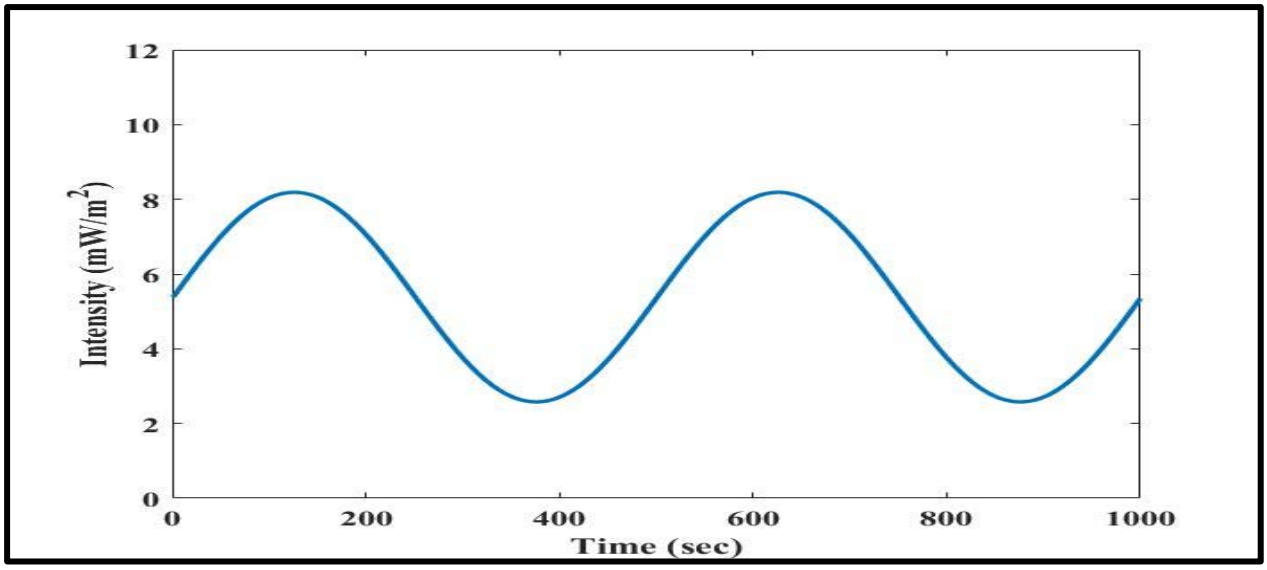

Figure 3.16: Absence of ammonia absorption peak in near infrared region at tuning current of laser diode (88.35 mA) and wave length (1543.051 nm).

A fast Fourier transformation (FFT) has been implemented to extract the second harmonic as an indicator for the gas presence that written done by MATLAB code. Figure 3.17 shows the chart of the fast Fourier Transmission (FFT) for the time domain data that exhibit in figure 3.15 where the fundamental frequency located at 500 Hz and the second harmonic has been indeed in the 1000 Hz also the value of the second harmonic seems to be significant 0. 33 mW/m^2 that mean the energy of light has been mostly absorb.

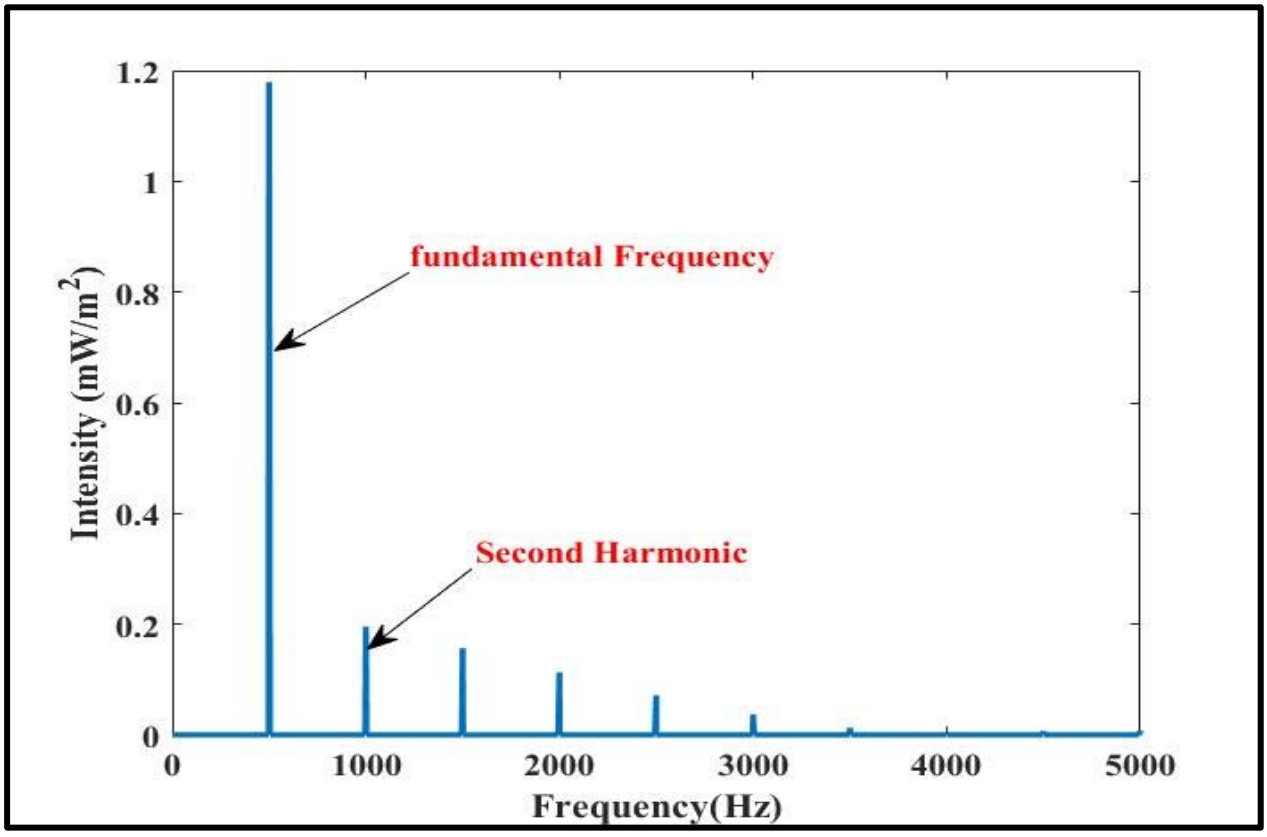

Figure 3.17: Fundamental frequency of ammonia gas in near infrared region at 500 Hz and the absorption peak at 1000 Hz.

The result in figure 3.18 exhibits the fundamental frequency and the value of second harmonic, it seems that the second harmonic has been diminished (there is no absorption peak).

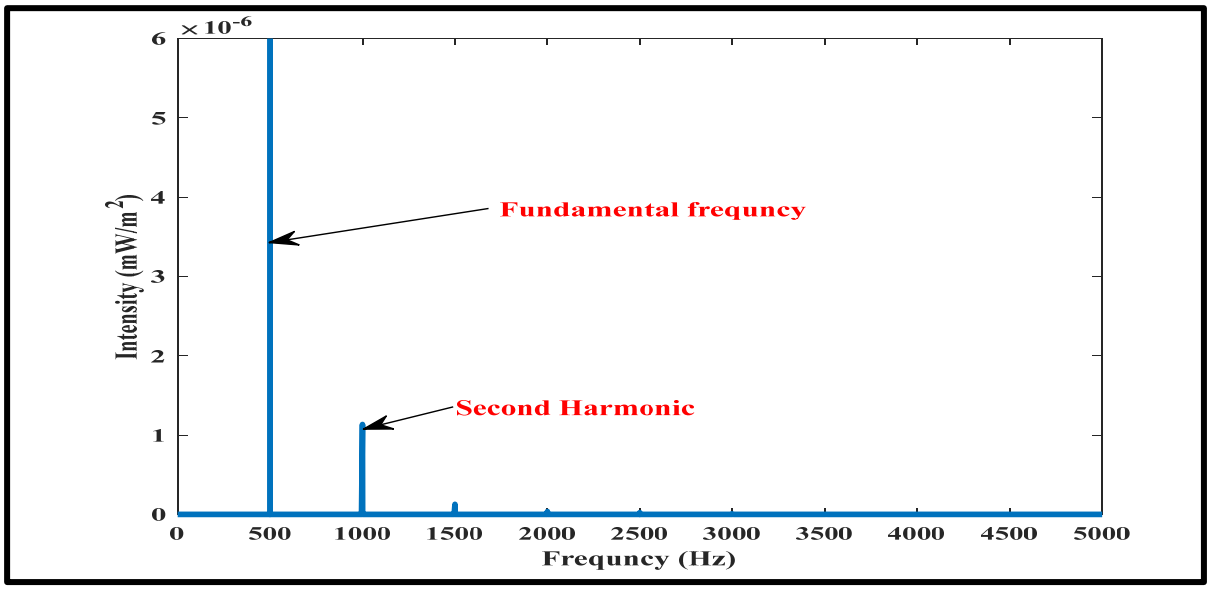

Figure 3.18: Fundamental frequency of ammonia gas in near infrared region at 500 Hz and the amount of the second harmonic reached about zero at1000 Hz.

A MATLAB code has been written to evaluate the amount at the operation current of laser diode (LD) that can be give a max second harmonic value and it was found that the relation has max. peak and min. valley at current values 86.01 mA, 88.35 mA, respectively as shown in figure 3.19.

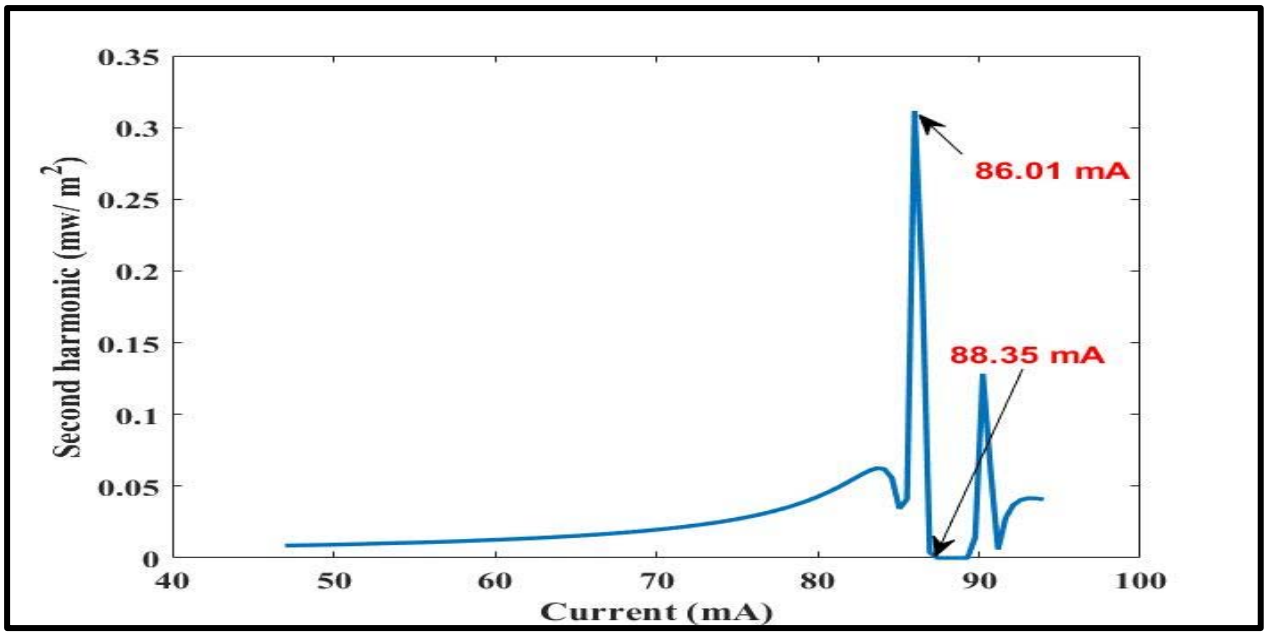

Figure 3.19: Variation of the second harmonic with the tuning current of ammonia gas in near infrared region.

Then the spectrum wavelength has been tuned around 1nm in 0.02 nm steps to increase the sensitivity of the tunable diode spectrometer (TDLS). And it was the main goal of this work. as illustrate in figure 3.20 and it was found the relation has maximum peak and minimum valley at was wavelength values1543.027 nm, 1543.051 nm, respectively in near infrared that was done by MATLAB code.

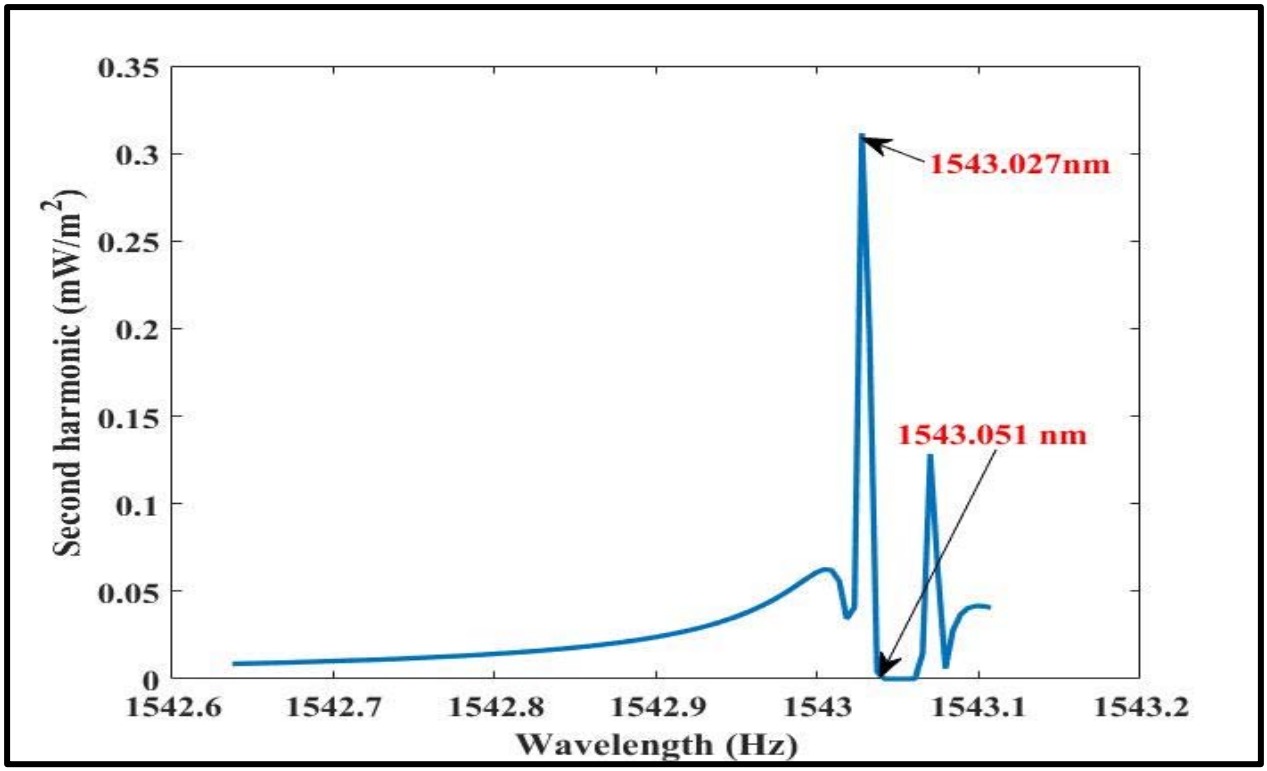

Figure 3.20: The wavelength spectrum of ammonia gas in near infrared region has a one peak at (1543.027 nm).

Figure 3.21 shows the relation between the second harmonic and the gas concentration at desired value of the driven current of the laser diode and at exact wavelength the 1543.027 nm the relation seems to be linear and min. value of the gas constrainer was 0.05 ppb.

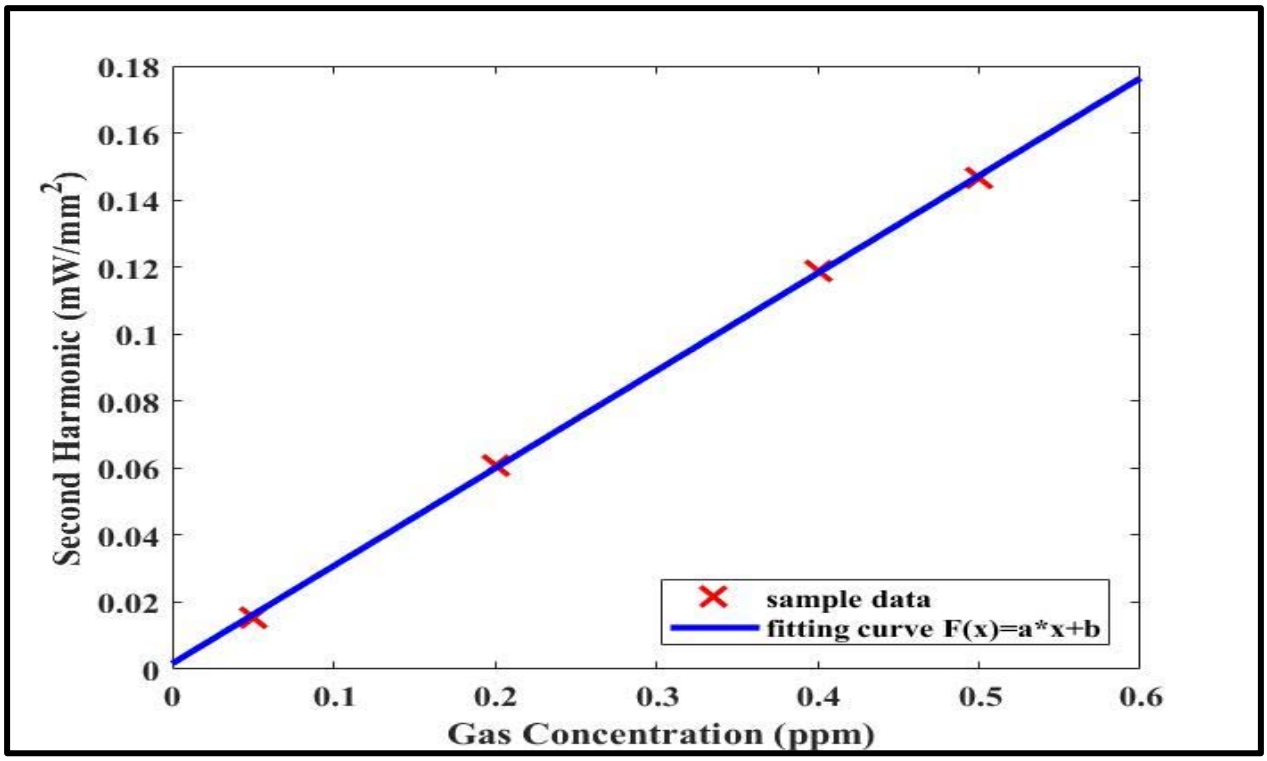

Figure 3.21: Relation between second harmonic and gas concentration of ammonia gas in near infrared region.

3.5- Ammonia Gas Absorption Peak in The MIR Spectral Region

The absorption signal of ammonia gas has been studied in MIR region under tuning current of laser diode 78.95 mA and wavelength 2399.977 nm. Figure 3.22 shows a shallow dip of the absorption signal, this gives that the frequencies of the laser light in MIR region are not favored by ammonia gas. Therefore, the measurements of NH_3 sense should be done in the MIR region see figure 3.22 wavelength, the absorption peak is located exactly in the center of the sine wave, implying that the gas has absorbed the whole energy of the sine wave.

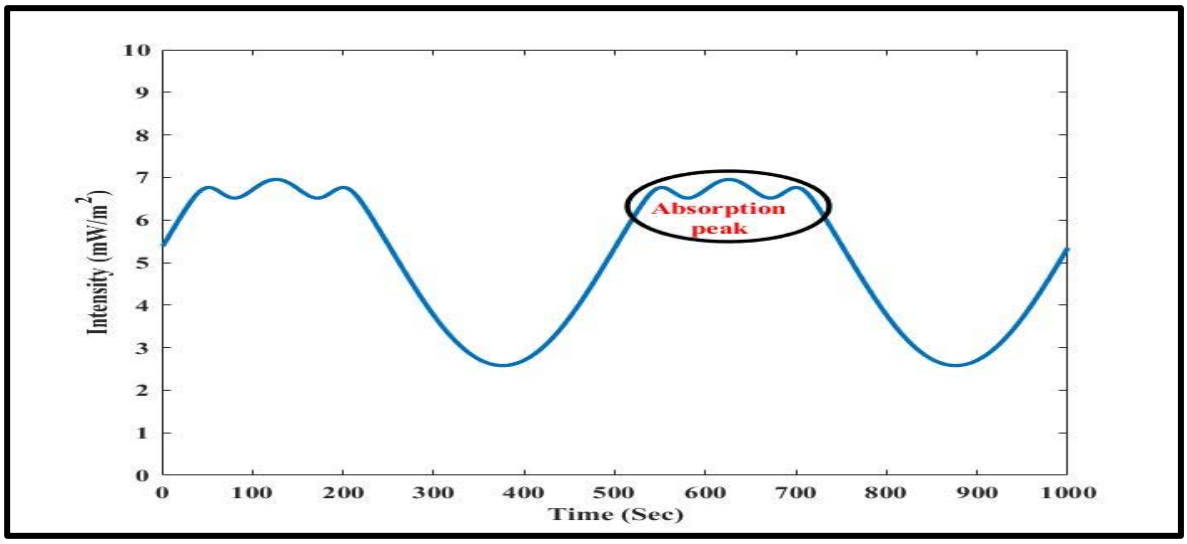

Figure 3.22: The absorption peak of ammonia gas in mid infrared region at tuning current of laser diode (78.95 mA) and the wavelength (2399.977 nm).

Figure 3.23 shows the modulated sine signal in time domain and there is no dip of absorption signal as compare as with Figure 3.22. It is obvious the wavelength 2400 nm has no sense from NH_3 gas. Because it does not touch the min. limits of the vibrational frequencies of ammonia gas.

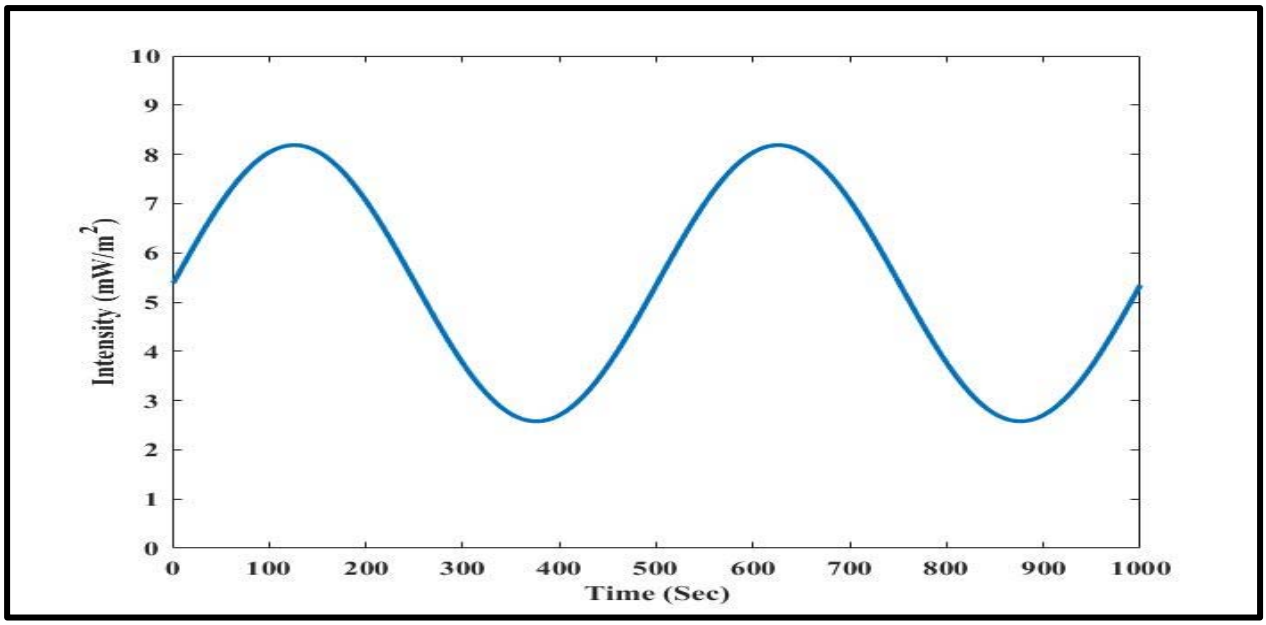

Figure 3.23: Absence of absorption peak of ammonia gas in mid infrared region at tuning current of laser diode (81.31 mA) and wavelength (2400.001 nm).

A signal processing in the frequency domain has been demonstrate using a Fast Fourier Transformation (FFT) to determine the second harmonic as a gas presence indication, that was done using MATLAB code. Figure 3.24 displays the frequency domain measurements of the time domain data shown in figure 3.22. Where the fundamental frequency is 500 Hz and the second harmonic is 1000 Hz, the value of the second harmonic appears to be an acceptable 0.19 mW/m^2 and can be.

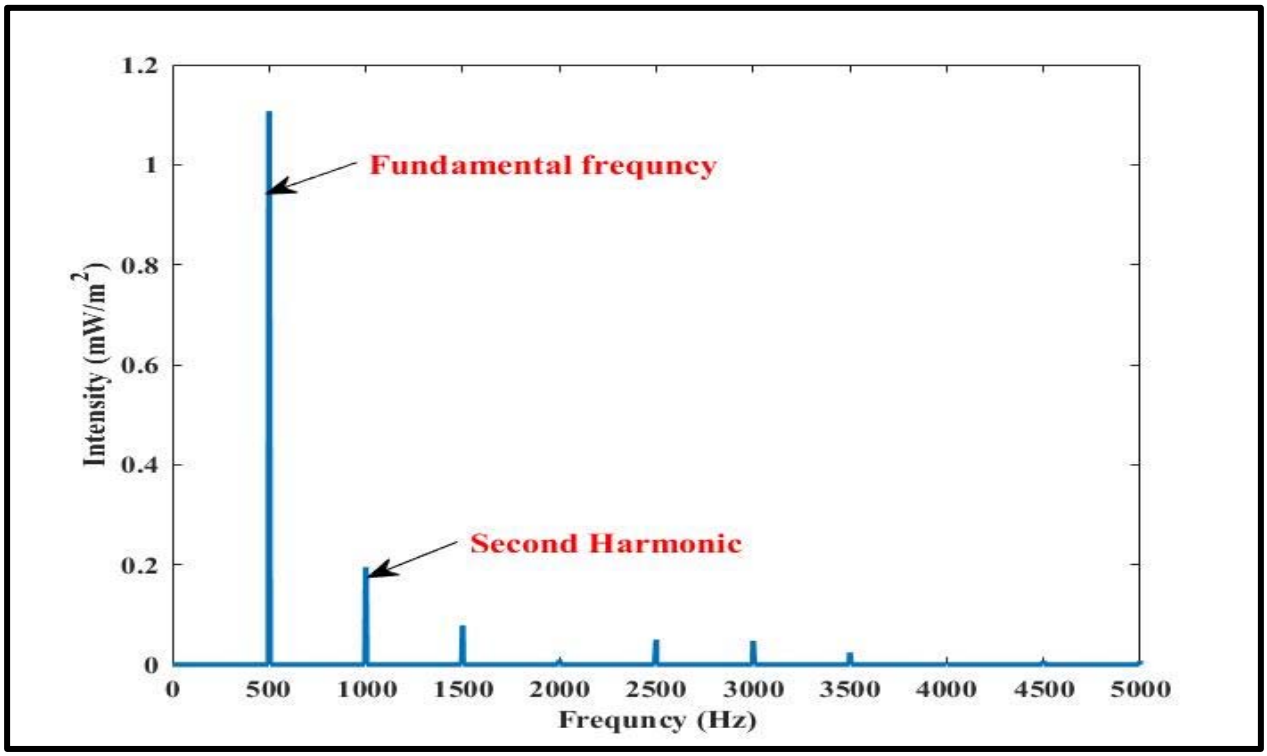

Figure 3.24: The fundamental frequency of ammonia gas in mid infrared region at 500 Hz and the absorption peak at 1000 Hz.

The fundamental frequency and the value of the second harmonic are shown in figure 3.25. The second harmonic have no readable value that can be announces the presence of gas.

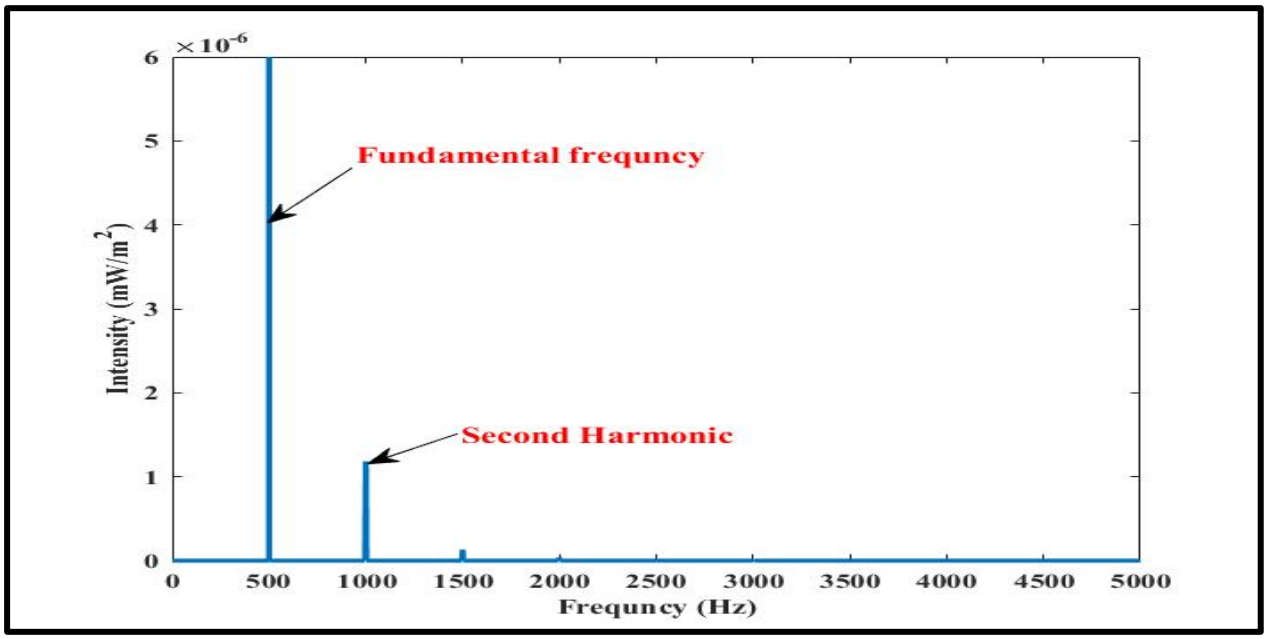

Figure 3.25: The fundamental frequency of ammonia gas in mid infrared region at 500 Hz and the amount of the second harmonic reached about zero at 1000 Hz.

The amount of the operating current of a laser diode (LD) that may generate a max second harmonic value was calculated using a MATLAB code, and it was discovered that the relation has a max. peak and min. valley at current values of 78.95 mA and 81.31 mA, respectively, as shown in figure 3.26.

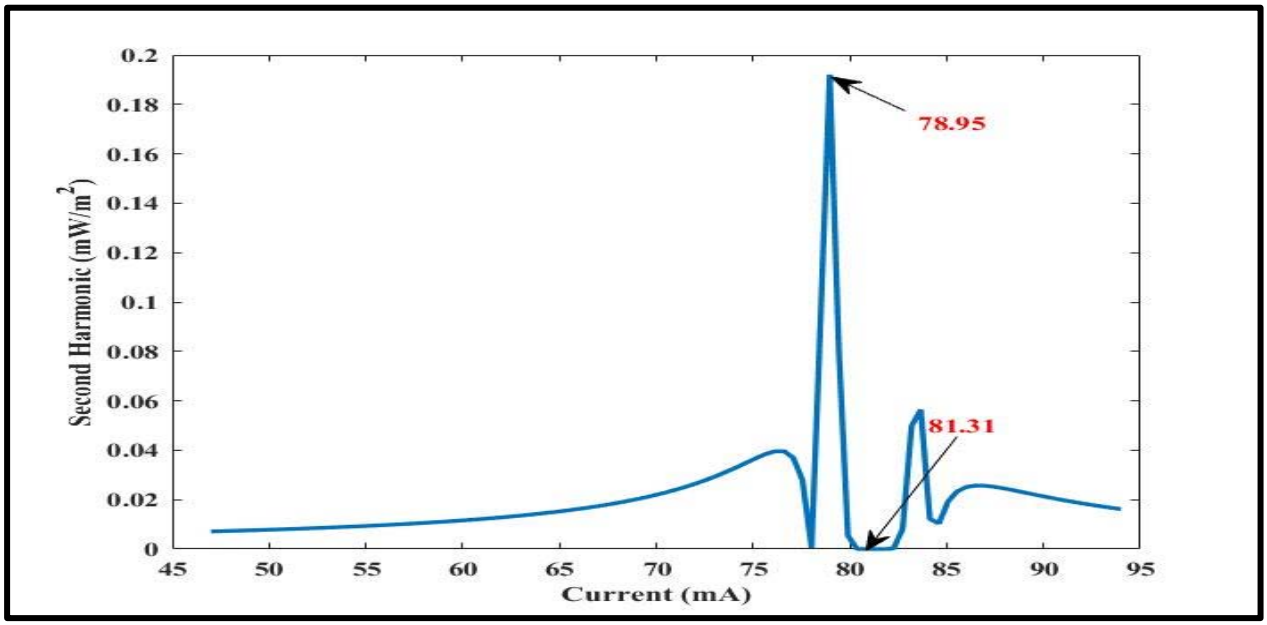

Figure 3.26: The variation of the second harmonic with the tuning current of ammonia gas in mid infrared region.

The spectrum wavelength was then set about 1nm in 0.02 nm steps to improve the tunable diode spectrometer's sensitivity (TDLS). And that was the primary purpose of this project. As seen in figure 3.27, the relation has a maximum peak and minimum valley at wavelength values of 2399.977 nm and 2400.001 nm in the mid infrared, respectively, as determined by MATLAB code.

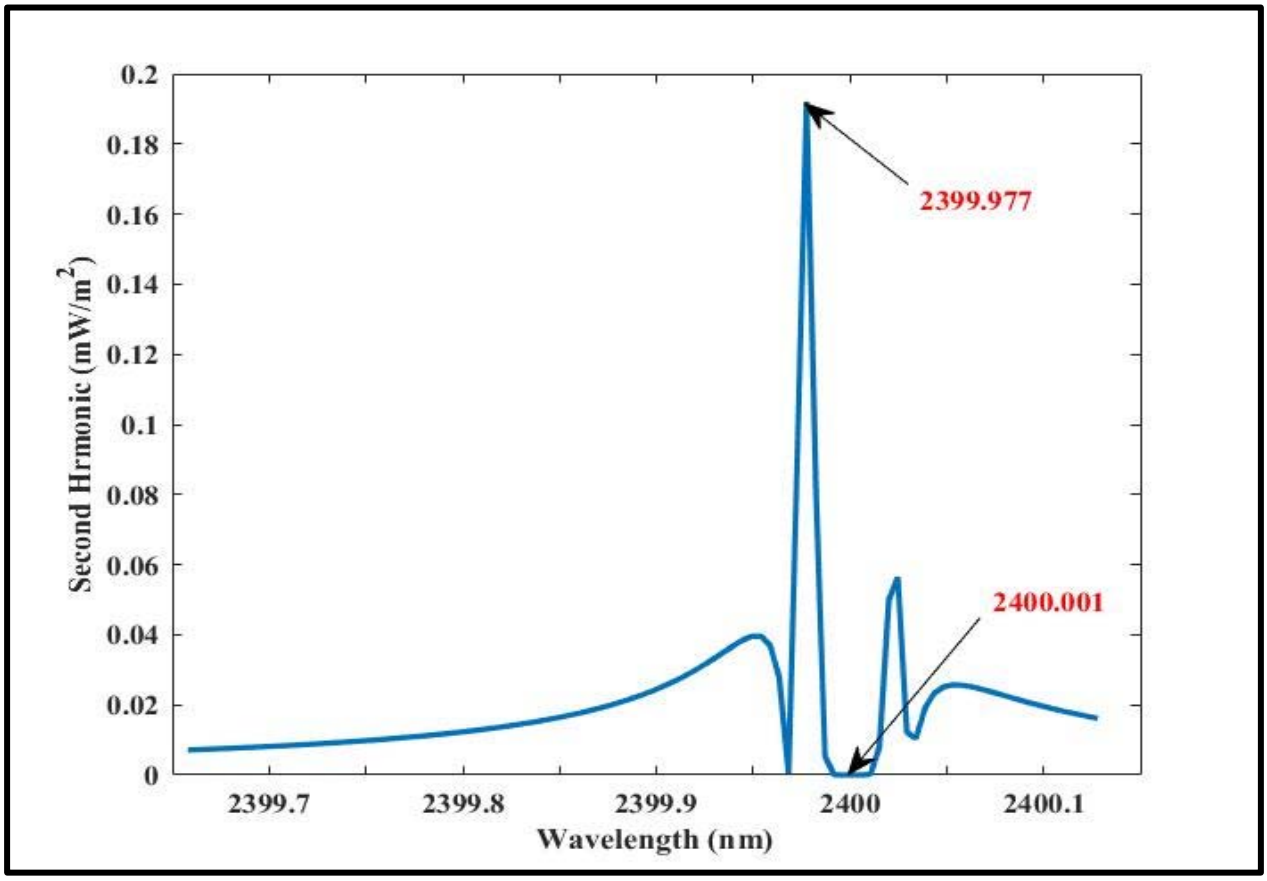

Figure 3.27: The wavelength spectrum of ammonia gas in mid infrared region has a one peak at (2399.977 nm).

Figure 3.28 depicts the relation between the second harmonic and gas concentration at the required value of the laser diodes driven current and at the correct wavelength 2399.977 nm. The relation seems to be linear, and the gas concentration's minimum value was 0.05 ppb.

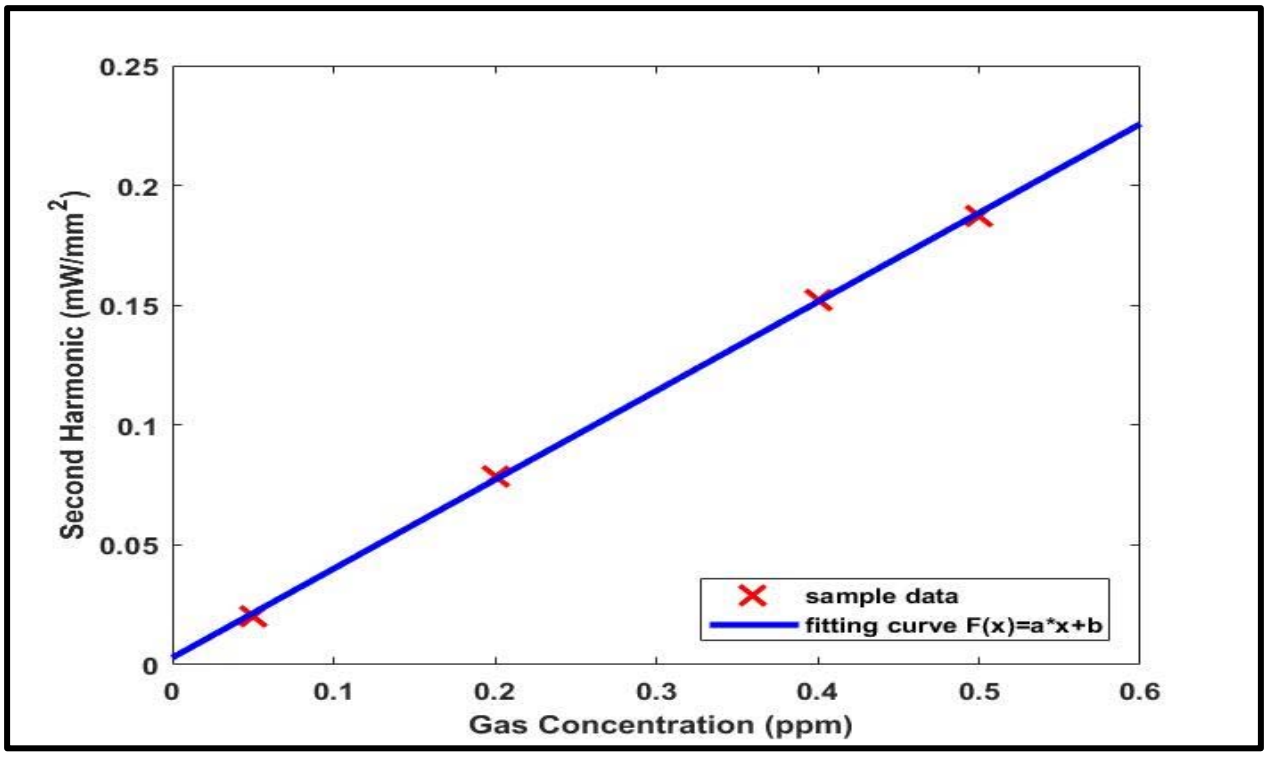

Figure 3.28: The relation between second harmonic and gas concentration of ammonia gas in mid infrared region.

3.6- Carbon Monoxide Gas Absorption Peak in The NIR Spectral Region

Finally, this study has been dealt with a common toxic gas (carbon monoxide CO). In terms of studying the absorption spectrum of this gas in the NIR region, appropriate drive current value at which the value of the second harmonic is as high as possible.

Figure 3.29 shows the absorption signal of the carbon monoxide gas at tuning current of laser diode 78.95 mA and the wavelength 1584.877 nm. The dip of the absorption peak locates exactly at the middle of the sine wave, and it is a slightly deep and sharp dip. That means there was a good sense of carbon monoxide gas for that specific wavelength 1584.877 nm, and the frequency of the laser light has been matching vibrational frequencies of the carbon monoxide gas at this wavelength. Note that the simulation measurements have been demonstrated at a constant

concentration value 0.5 ppb and the length of the open path spectrometer at 100 m. To complete the picture of the CO gas sense, the time domain data when the wavelength of the laser diode little further away from its desired value for gas absorption has been shown in Figure 3.30.

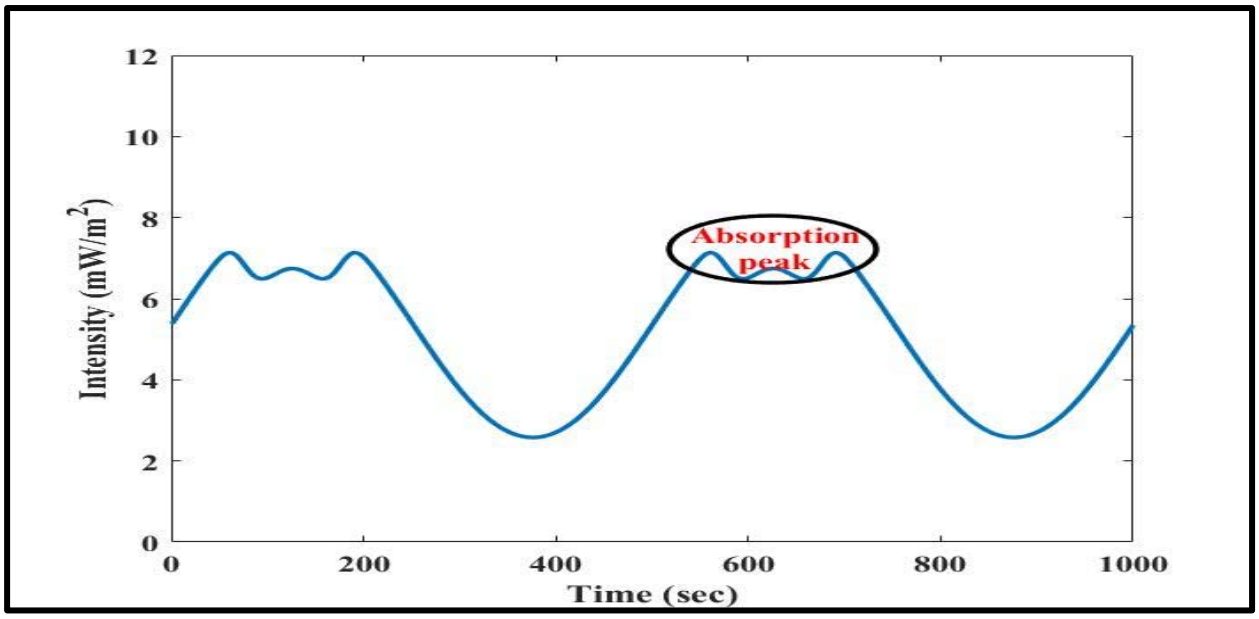

Figure 3.29: Carbon monoxide absorption peak in near infrared region at tuning current of laser diode (78.95 mA) and the wavelength (1584.877 nm).

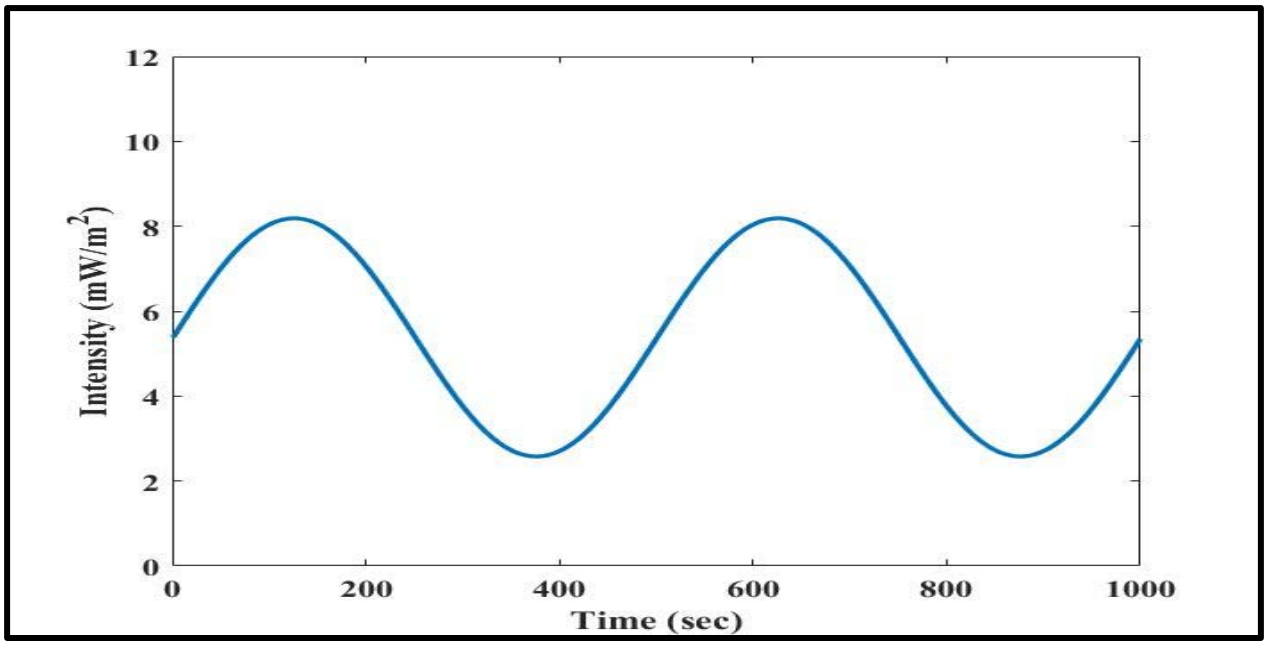

Figure 3.30: Absence of carbon monoxide absorption peak in near infrared region at tuning current of laser diode 81.31 mA and wave length 1584.901 nm.

A Fast Fourier transformation (FFT) have been adopted as in the gases studied above, that was done by written a MATLAB code to calculate the value of second harmonic as an indicator for the gas presence. Figure 3.31 shows the absorption spectrum in frequency domain. where the fundamental frequency located at 500 Hz and the second harmonic has been indeed in the 1000 Hz. Also, the value of the second harmonic seems to be significant 0. 23 mW/m^2 that mean the energy of light has been mostly absorb by the CO gas. As compare as the absorption spectrum in frequency domain with another Figure 3.32 exhibits the fundamental frequency and the value of second harmonic. It seems that the second harmonic has been diminished (there is no absorption peak).

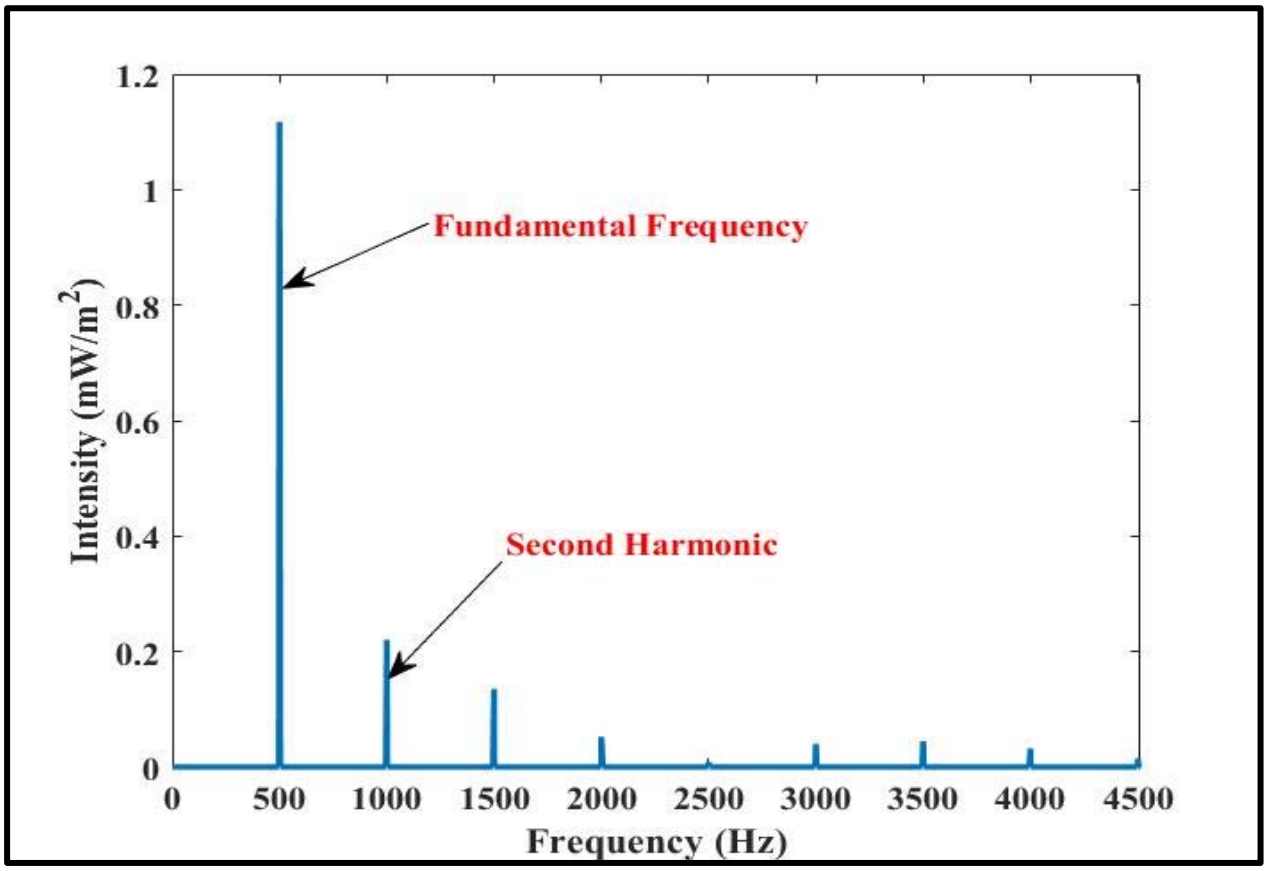

Figure 3.31: Fundamental frequency of carbon monoxide gas in near infrared region at 500 Hz and the absorption peak at 1000 Hz.

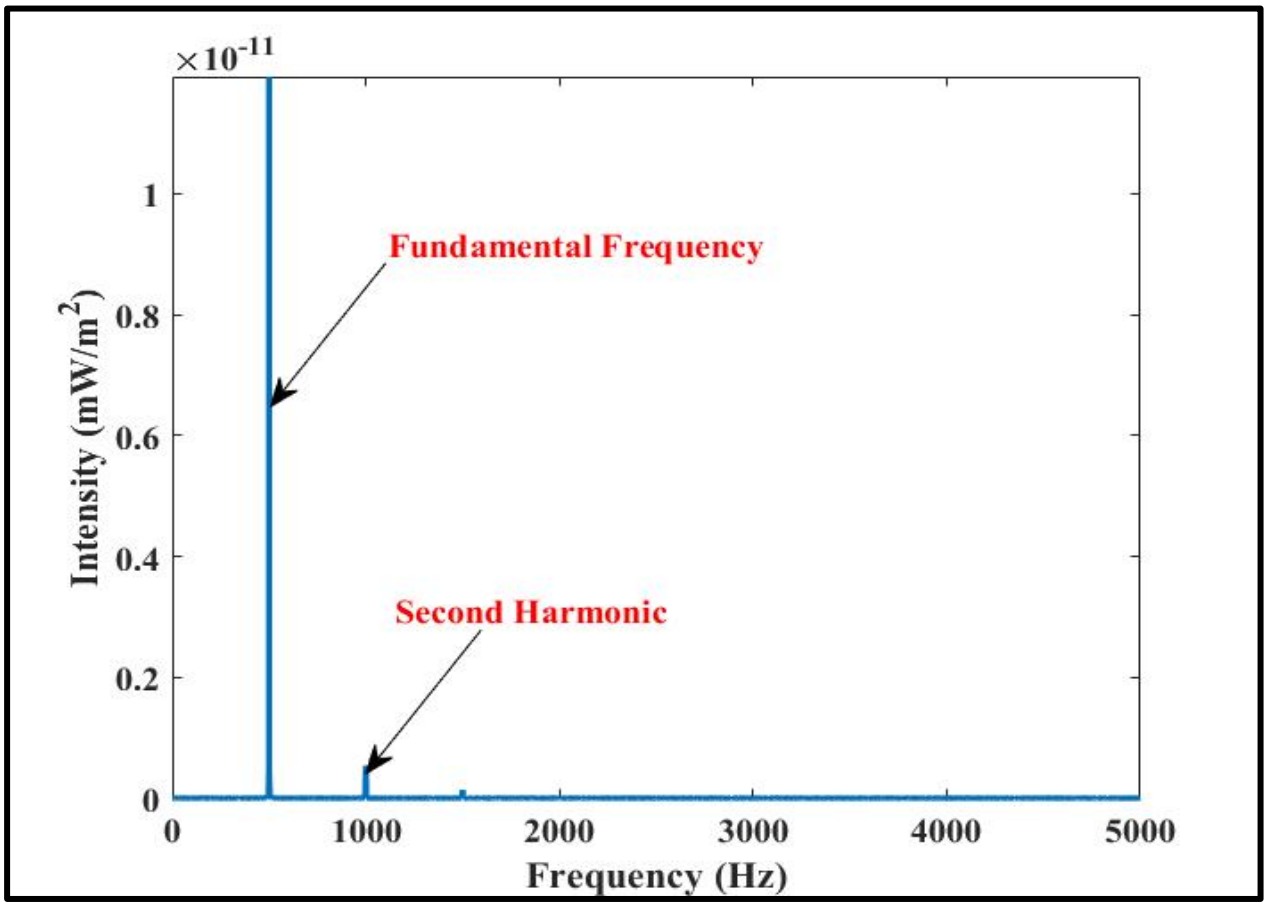

Figure 3.32.: Fundamental frequency of carbon monoxide gas in near infrared region at 500 Hz and the amount of the second harmonic reached about zero at1000 Hz.

A MATLAB code has been written to evaluate the amount at the operation current of laser diode (LD) that can be give a max second harmonic value and it was found that the relation has max. peak and min. valley at current values 78.95 mA, 81.31 mA respectively as shown in figure 3.33.

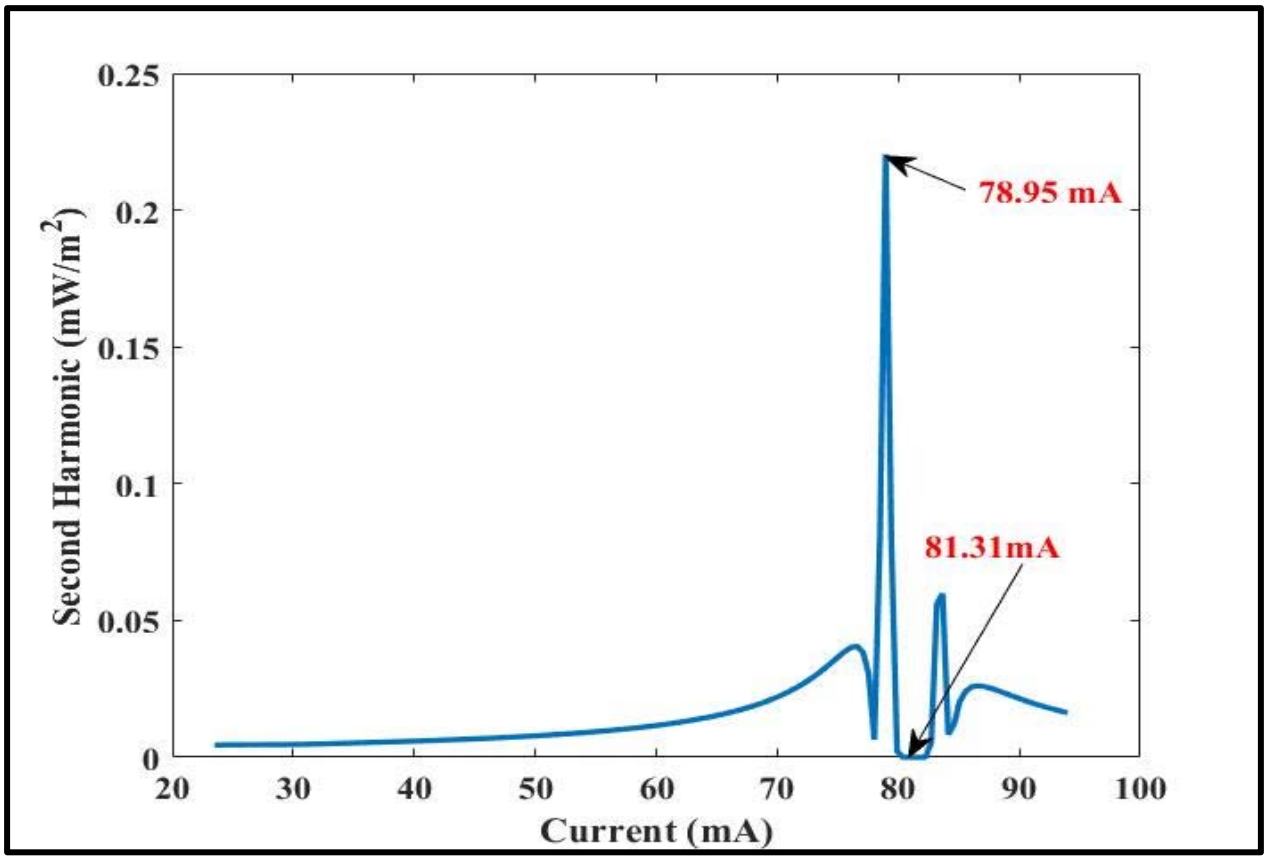

Figure 3.33: Variation of the second harmonic with the tuning current of carbon monoxide gas in near infrared region.

Then the spectrum wavelength has been tuned around 1nm in 0.02 nm steps to increase the sensitivity of the tunable diode spectrometer (TDLS). And it was the main goal of this work. as illustrate in figure 3.34 and it was found the relation has maximum peak and minimum valley at was wavelength values 1584.877 nm, 1584.901 nm, respectively in near infrared that was done by MATLAB code.

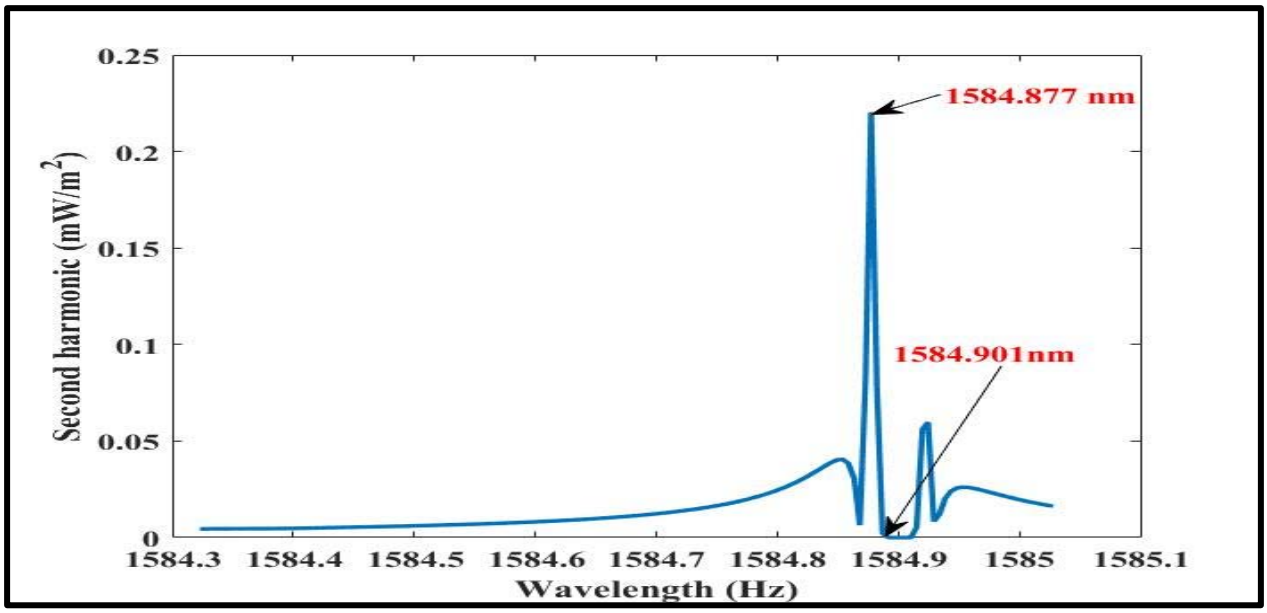

Figure 3.34: The wavelength spectrum of carbon monoxide gas in near infrared region has a one peak at (1584.877 nm).

Figure 3.35 shows the relation between the second harmonic and the gas concentration at desired value of the driven current of the laser diode and at exact wavelength the 1584.877 nm the relation seems to be linear and min value of the gas constrainer was 0.05 ppb.

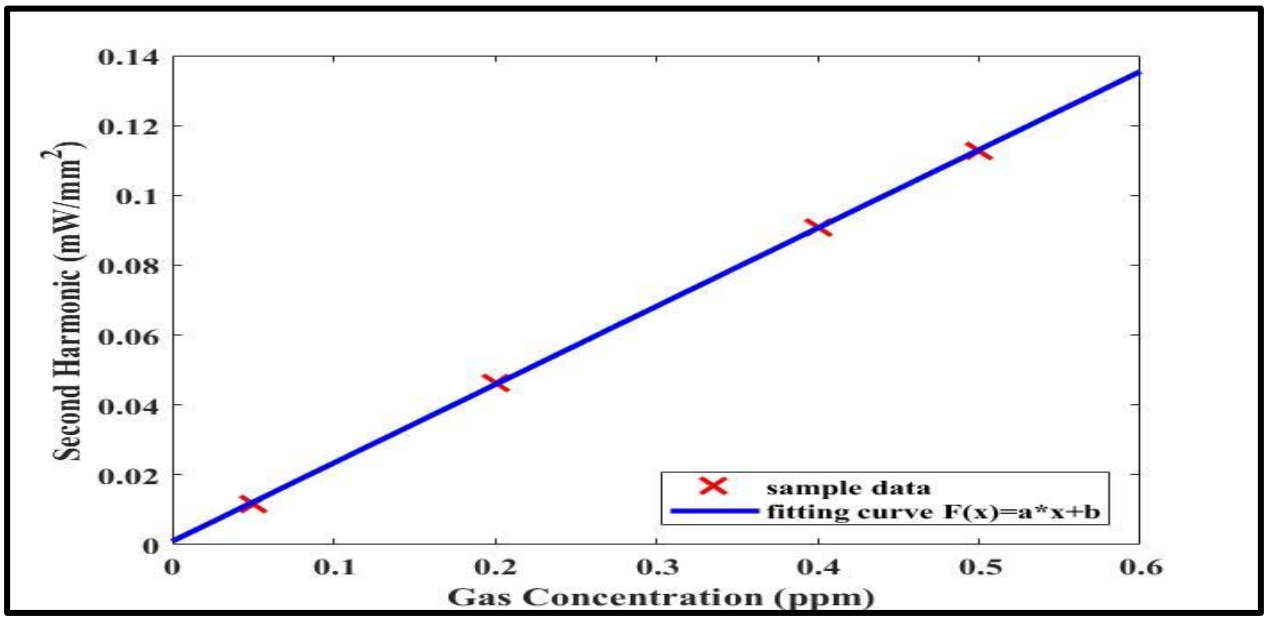

Figure 3.35: Relation between second harmonic and gas concentration of carbon monoxide gas in near infrared region.

3.7- Carbon Monoxide Gas Absorption Peak in The MIR Spectral Region

The absorption signal of carbon monoxide gas has been studied in MIR region under tuning current of laser diode 77.54 mA and wavelength 4650.463 nm. Figure 3.36 shows a dip of the absorption signal, this gives that the frequencies of the laser light in MIR region are favored by carbon monoxide gas. the absorption peak is located exactly in the center of the sine wave, implying that the gas has absorbed the whole energy of the sine wave.

Figure 3.37 shows the modulated sine signal in time domain and there is no dip of absorption signal as compare as with Figure 3.36. It is obvious the wavelength 4650.496 nm has no sense from CO gas. Because it does not touch the min. limits of the vibrational frequencies of carbon monoxide gas.

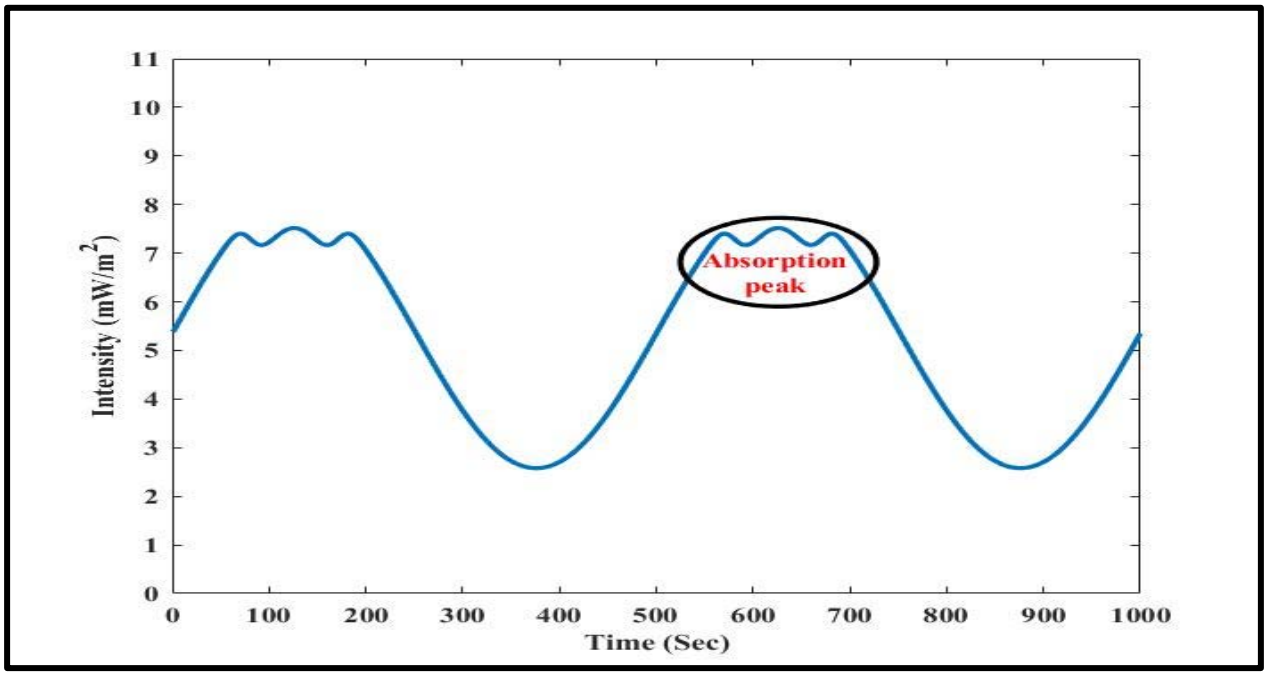

Figure 3.36: The absorption peak of carbon monoxide gas in mid infrared region at tuning current of laser diode (77.54 mA) and the wavelength (4650.463 nm).

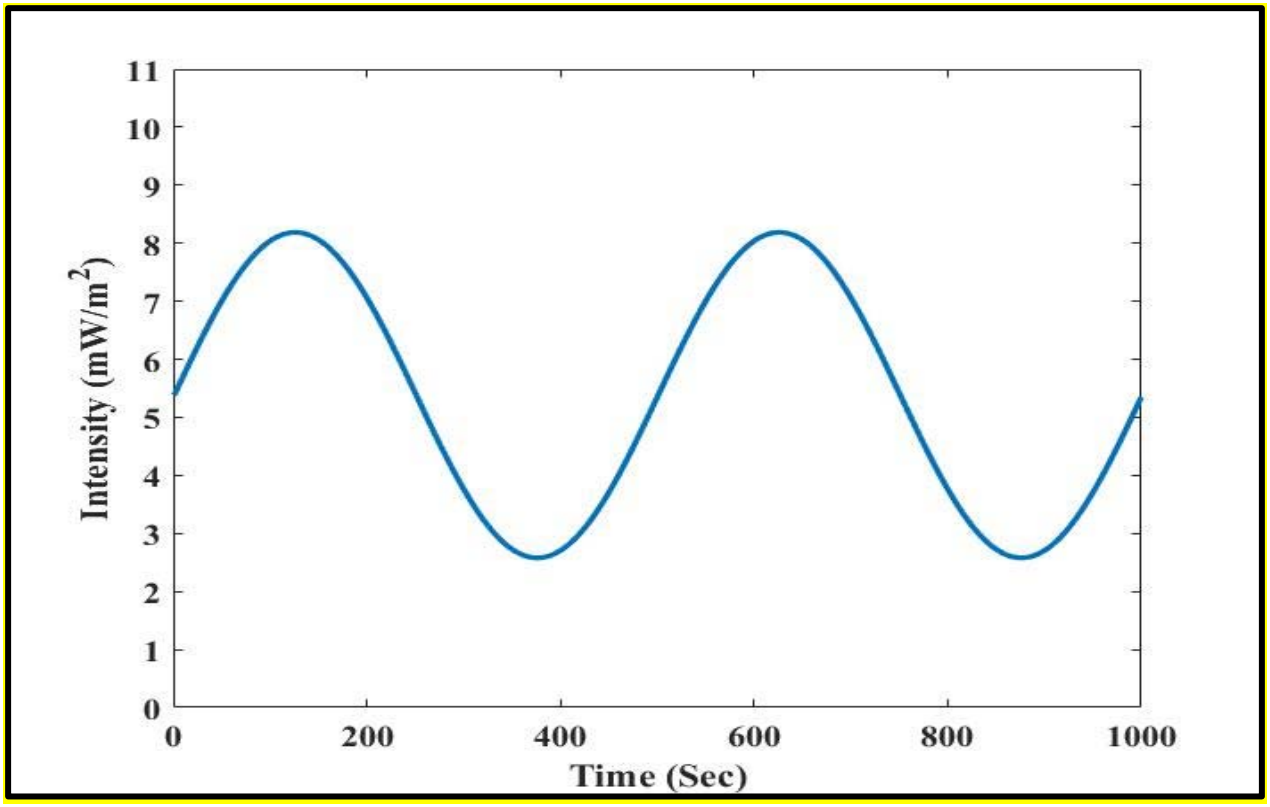

Figure 3.37: Absence of absorption peak of carbon monoxide gas in mid infrared region at tuning current of laser diode (80.84 mA) and wave length (4650.496 nm).

A signal processing in the frequency domain has been demonstrate using a Fast Fourier Transformation (FFT) to determine the second harmonic as a gas presence indication, that was done using MATLAB code. Figure 3.38 displays the frequency domain measurements of the time domain data shown in figure 3.36. Where the fundamental frequency is 500 Hz and the second harmonic is 1000 Hz, the value of the second harmonic appears to be an acceptable 0.18 mW/m^2. Figure 3.39 shows the fundamental frequency and the value of the second harmonic, the second harmonic have no readable value that can be announces the presence of gas when the value of wavelength a little far from the desired wavelength value.

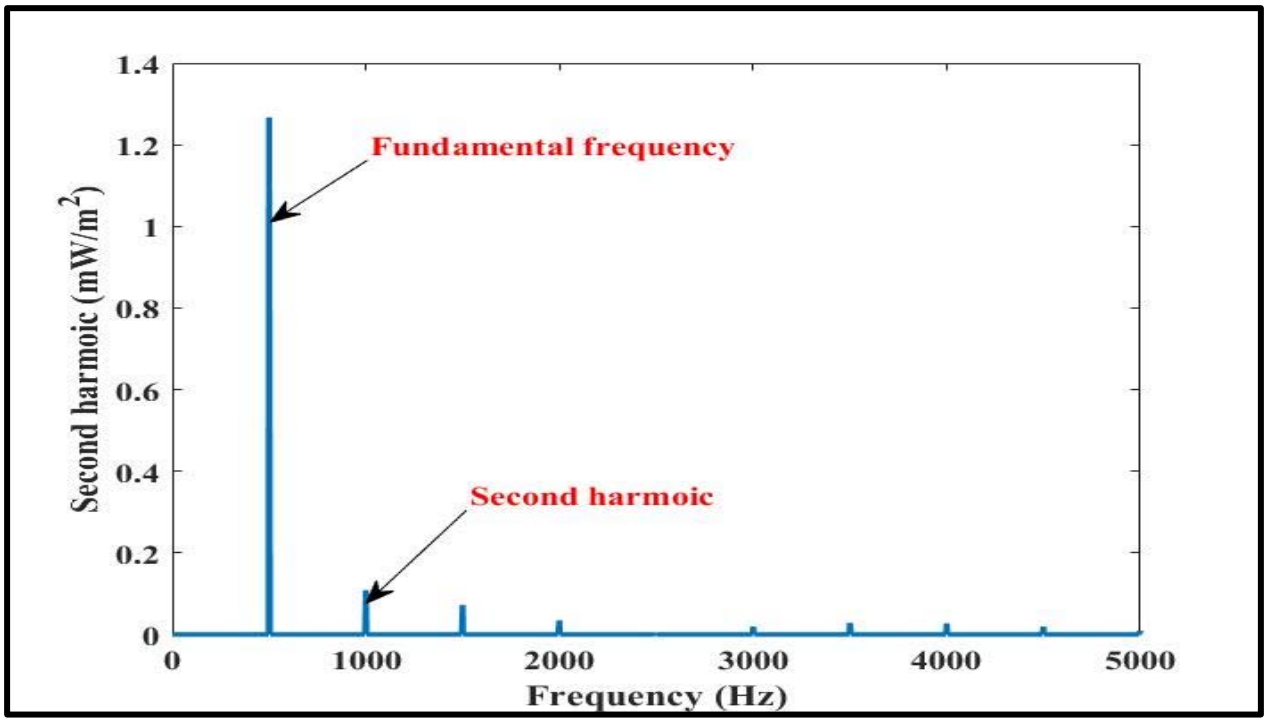

Figure 3.38: The fundamental frequency of carbon monoxide gas in mid infrared region at 500 Hz and the absorption peak at 1000 Hz.

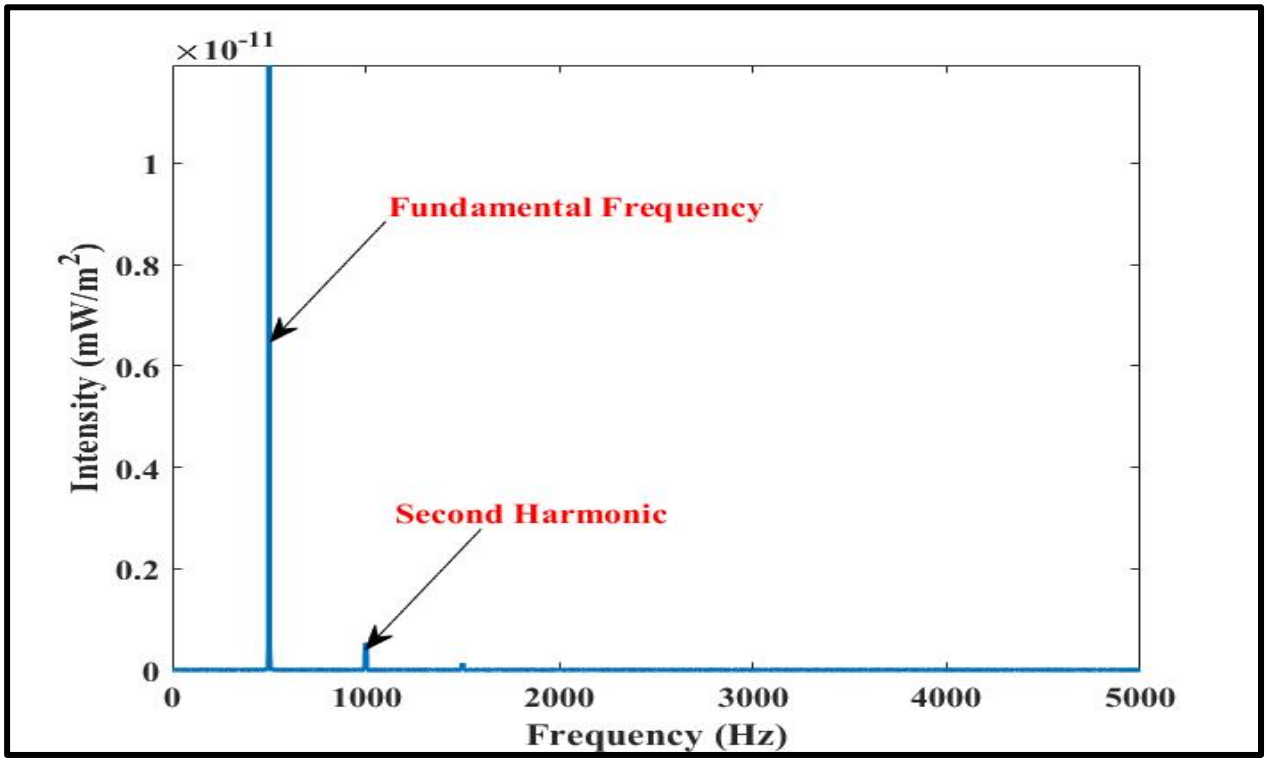

Figure 3.39: The fundamental frequency of carbon monoxide gas in mid infrared region at 500 Hz and the amount of the second harmonic reached about zero at 1000 Hz.

The amount of the operating current of a laser diode (LD) that may generate a max second harmonic value was calculated using a MATLAB code, and it was discovered that the relation has a max. peak and min. valley at current values of 77.54 mA and 80.84 mA, respectively, as shown in figure 3.40. The spectrum wavelength was then set about 1nm in 0.02 nm steps to improve the tunable diode spectrometer's sensitivity (TDLS). And that was the primary purpose of this project. As seen in figure 3.41, the relation has a maximum peak and minimum valley at wavelength values of 4650.463 nm and 4650.496 nm in the mid infrared, respectively, as determined by MATLAB code.

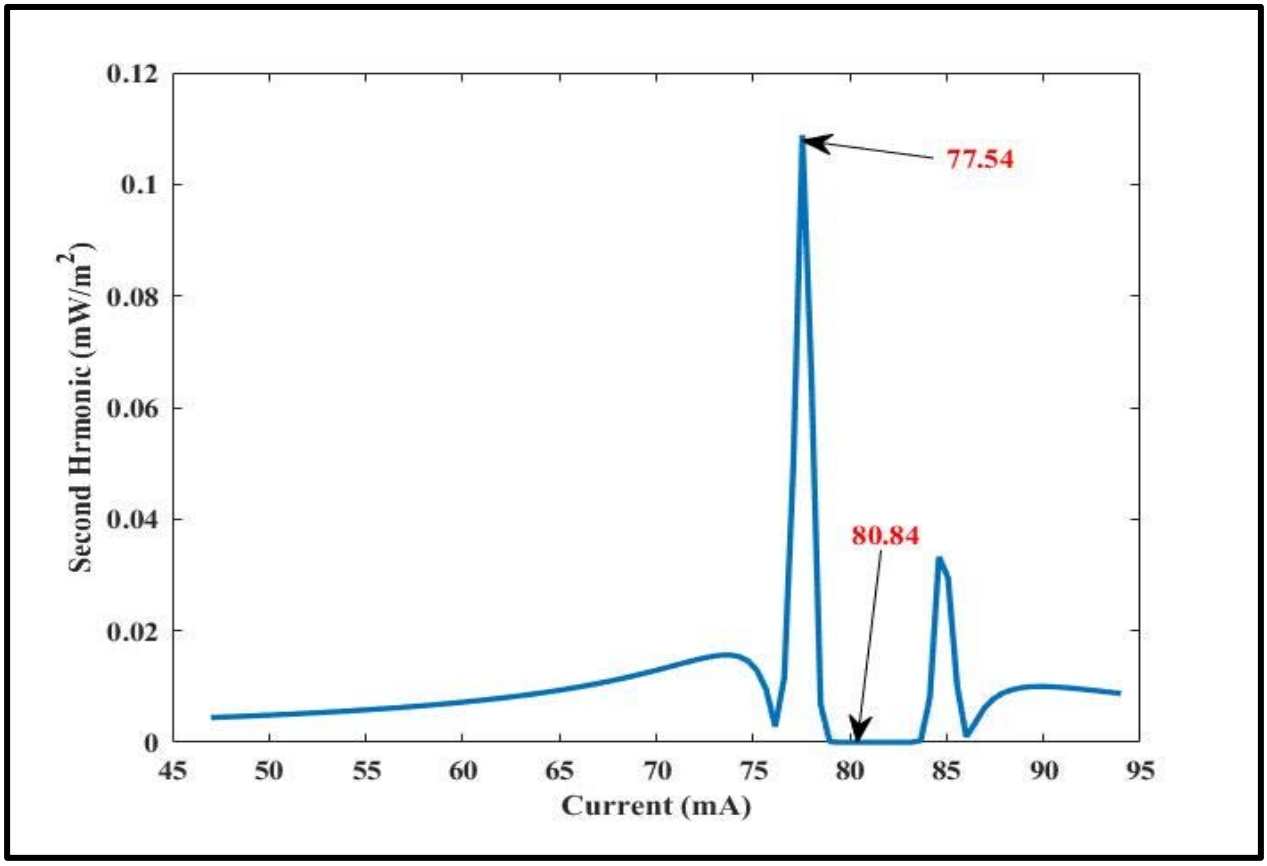

Figure 3.40: The variation of the second harmonic with the tuning current of carbon monoxide gas in mid infrared region.

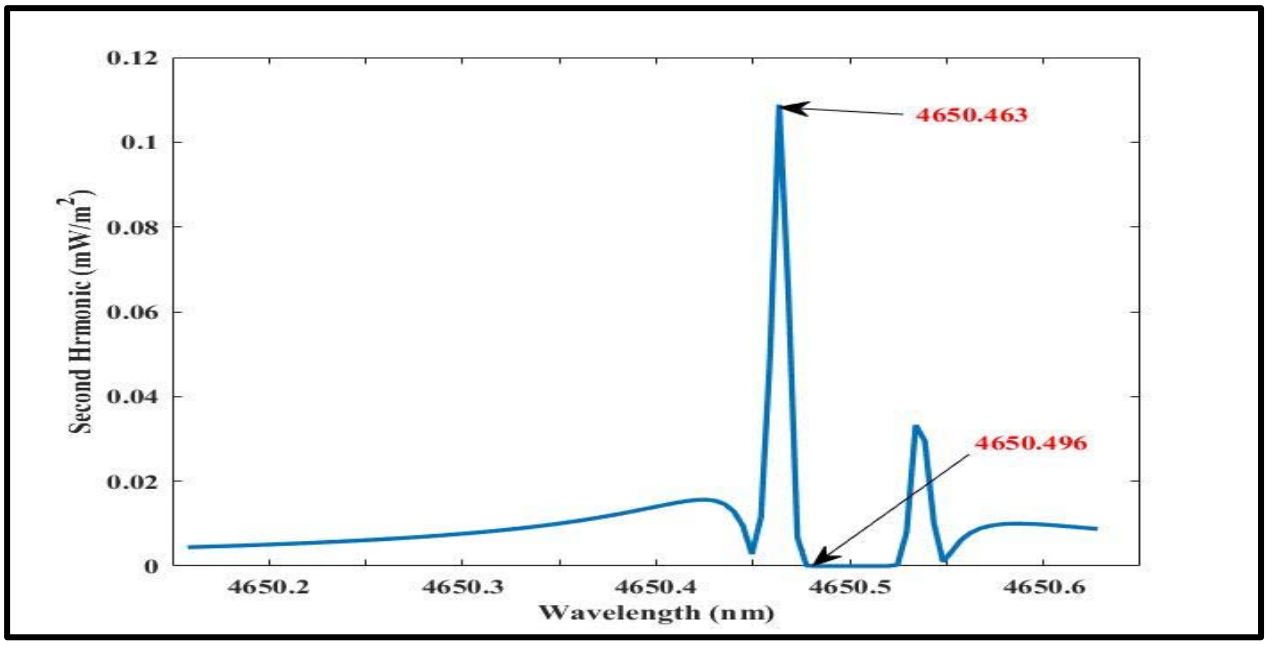

Figure 3.41: The wavelength spectrum of carbon monoxide gas in mid infrared region has a one peak at (4650.463 nm).

Figure 3.42 depicts the relation between the second harmonic and gas concentration at the required value of the laser diodes driven current and at the correct wavelength 4650.463 nm. The relation seems to be linear, and the gas concentration's minimum value was 0.05 ppb.

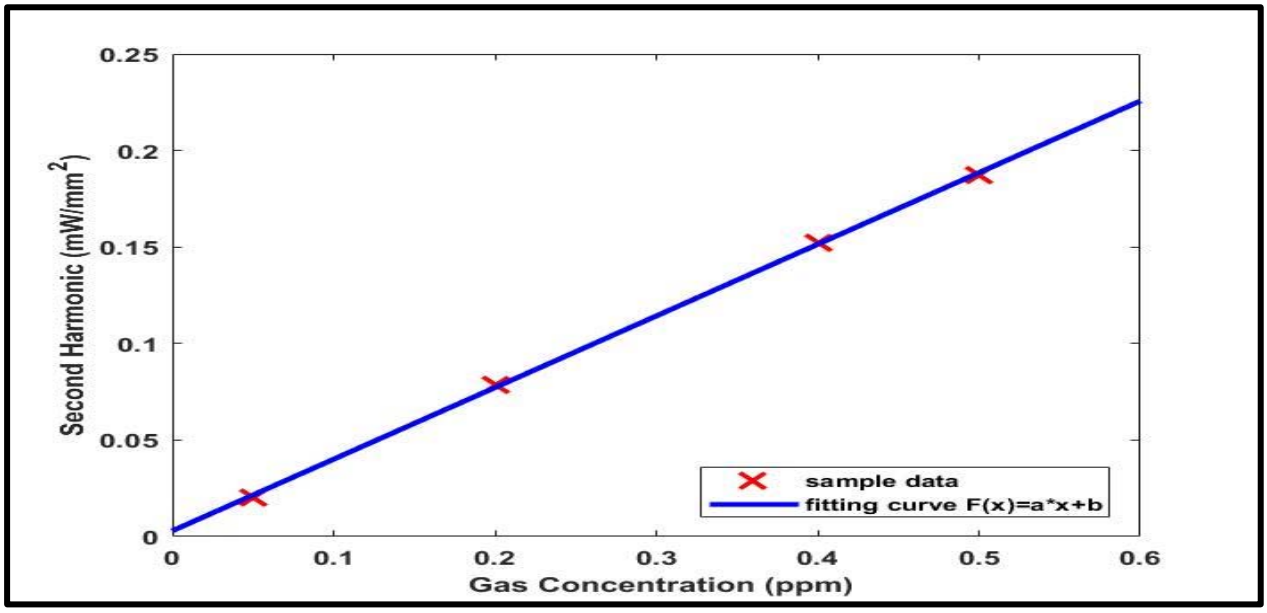

Figure 3.42: The relation between second harmonic and gas concentration of carbon monoxide gas in mid infrared region.

As shown in table (1) methane gas shows best wavelength and second harmonic at 1653.48 nm and 0.19 mW/m^2, respectively, in near infrared region, while in mid infrared region the wavelength and second harmonic at 3290.987 nm and 0.18 mW/m^2, respectively.

Ammonia gas displays greatest wavelength and second harmonic at 1543.027 nm and 0.33 mW/m^2, respectively, in near infrared region, whereas in mid infrared region the wavelength and second harmonic at 2399.977nm and 0.19 mW/m^2, respectively. In the near infrared area, carbon monoxide gas has the best wavelength and second harmonic at 1584.877nm and 0.23 mW/m^2, respectively, whereas the wavelength and second harmonic in the mid infrared area are 4560.463 nm and 0.18 mW/m^2, respectively.

Table 3.1: Shows best wavelength and second harmonic for methane, ammonia and monoxide gases in both near and mid infrared region.

Type of Gas	NIR		MIR	
	Favorite wavelength (nm)	**Value of second harmonic (mW/m^2)**	**Favorite wavelength (nm)**	**Value of second harmonic (mW/m^2)**
CH_4	1653.48	0.19	3290.987	**0.18**
NH_3	1543.027	0. 33	2399.977	**0.19**
CO	1584.877	0. 23	4560.463	**0.18**

3.8- Comparison

In this section a comparison between the value of the peak of the absorption spectrum in (nm) from the previous experimental work and the current work will be display in table 3.2.

Table 3. 2: Comparison between the value of the peak of the previous experimental work and the current work.

Gases used	w_p (nm) (Previous work)	w_p (nm) (Current work)
CH_4 (near)	1653.7 [35]	1653.48
CH_4 (mid)	3291.6 [36]	3290.987
NH_3(near)	1543.4 [31]	1543.027
NH_3(mid)	2399.9[32]	2399.977
CO (near)	1584.2 [33]	1584.877
CO (mid)	4650.8 [34]	4560.463

CHAPTER FOUR
CONCLUSIONS AND FUTURE WORK

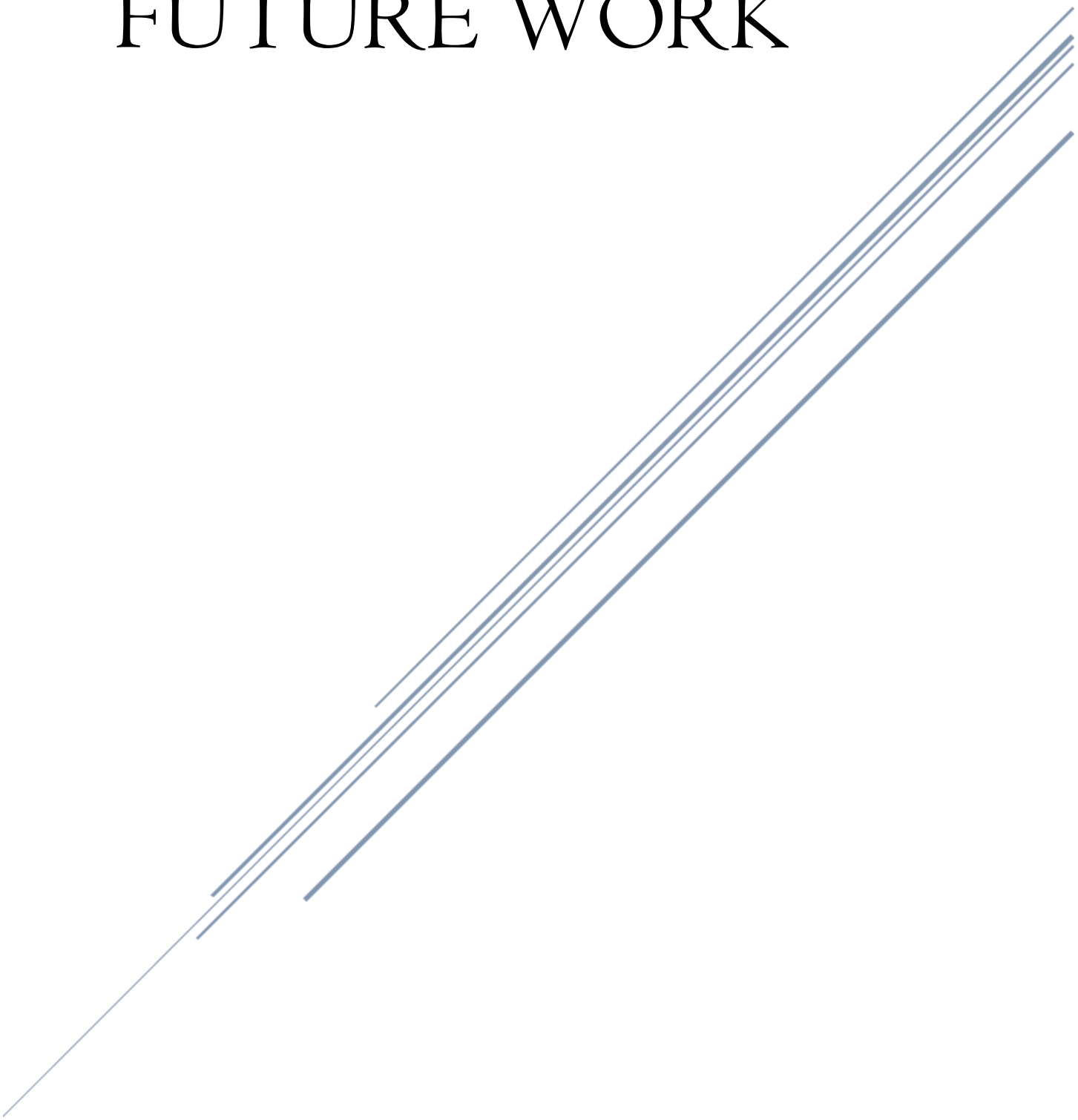

4.1- Conclusion

1- In this work the simulation process of TDLS has been implemented to enhance the sensitivity of the spectrometer by modulating the wavelength of a DFB tunable laser diode using a sinusoid signal.

2- The drive current of the laser has been tuned, therefore the wavelength of the laser diode will be change in tuning limits reach about 0.02 nm in NIR and MIR regions. That was done to evaluate the sensitivity of the TDLS spectrometer in these ranges of spectrum frequencies.

3- The simulation measurements show the min. limits of CH_4 gas concentration in NIR region at accurate wavelength 1653.48 nm were about 0.05 ppb, and in the MIR region at 3290.987 nm. Also, the drive current of the tunable diode laser has to be about 79.89 mA in NIR region, and about 79.90 mA in MIR region.

4- For the NH_3 gas the simulation measurements have been showed a same min. limits of the gas concentration but under different values of wavelength of DFB tunable laser diode. Where in NIR region the accurate wavelength was 1543.027 nm with drive was about 86.01 mA, and in MIR region the accurate wavelength h to be 2399.977 nm with drive current 78.95 mA.

5- The simulation measurements have been applied on the carbon monoxide CO gas in NIR and MIR region, the results show the sensitivity of the gas in NIR greater than in MIR. Where in NIR region the accurate wavelength was 1584.877 nm with drive was about 78.95 mA, and in MIR region the accurate wavelength to be 4650.463 nm with drive current 77.54 mA.

4.2- Future Work

1. Study other toxic gases that have a direct impact on human life and verify the sensitivity of these gases to open path tunable diode laser spectrometer.
2. Introducing noise on the studied gases and studying their effect.
3. The possibility of applying the study in practice and comparing the results**.**
4. Study the same gases in the study in addition to other toxic gases in far infrared region by open path tunable diode laser spectrometer.

REFERENCES

[1] Cassidy, D. T., & Reid, J. (1982). Atmospheric pressure monitoring of trace gases using tunable diode lasers. Applied Optics, 21(7), 1185-1190.

[2] Chen, C., Ren, Q., Piao, H., Wang, P., & Wang, Y. (2018). A trace carbon monoxide sensor based on differential absorption spectroscopy using mid-infrared quantum cascade laser. Micromachines, 9(12), 670.

[3] Nikodem, M., & Wysocki, G. (2012). Chirped laser dispersion spectroscopy for remote open-path trace-gas sensing. Sensors, 12(12), 16466-16481.

[4] Li, M., & Bai, F. (2018). Design of high sensitivity infrared methane detector based on TDLAS-WMS. Laser J, 39, 75-79.

[5Kluczynski, P., Jahjah, M., Nähle, L., Axner, O., Belahsene, S., Fischer, M., ... & Lundqvist, S. (2011). Detection of acetylene impurities in ethylene and polyethylene manufacturing processes using tunable diode laser spectroscopy in the 3-μm range. Applied Physics B, 105(2), 427-434.

[6] Zhang, L., & Cui, X. (2014). The design of carbon monoxide detector based on tunable diode lasers absorption spectroscope. Laser J, 35, 54-56.

[7] Werle, P. (1998). A review of recent advances in semiconductor laser based gas monitors. Spectrochimica Acta Part A: Molecular and Biomolecular Spectroscopy, 54(2), 197-236.

[8] Werle, P., Slemr, F., Maurer, K., Kormann, R., Mücke, R., & Jänker, B. (2002). Near-and mid-infrared laser-optical sensors for gas analysis. Optics and lasers in engineering, 37(2-3), 101-114.

[9] Werle, P., Slemr, F., Maurer, K., Kormann, R., Mücke, R., & Jänker, B. (2002). Near-and mid-infrared laser-optical sensors for gas analysis. Optics and lasers in engineering, 37(2-3), 101-114.

[10] Kurtz, J., Aizengendler, M., Krishna, Y., Walsh, P., & O'Byrne, S. B. (2015). Flight test of a rugged scramjet-inlet temperature and velocity sensor. In 53rd AIAA Aerospace Sciences Meeting (p. 0110).

[11] Wang, F., Wu, Q., Huang, Q., Zhang, H., Yan, J., & Cen, K. (2015). Simultaneous measurement of 2-dimensional H2O concentration and temperature distribution in premixed methane/air flame using TDLAS-based tomography technology. Optics Communications, 346, 53-63.

[12] Buchholz, B., Afchine, A., & Ebert, V. (2014). Rapid, optical measurement of the atmospheric pressure on a fast research aircraft using open-path TDLAS. Atmospheric measurement techniques, 7(11), 3653-3666.

[13] Lins, B., Zinn, P., Engelbrecht, R., & Schmauss, B. (2010). Simulation-based comparison of noise effects in wavelength modulation spectroscopy and direct absorption TDLAS. Applied Physics B, 100(2), 367-376.

[14] Chen, K., & Mei, M. (2014). Detection of gas concentrations based on wireless sensor and laser technology. Laser J, 35, 50-54.

[15] Mueller, H. G., Weber, J., & Hornsby, B. W. (2006). The effects of digital noise reduction on the acceptance of background noise. Trends in Amplification, 10(2), 83-93.

[16] Misiti, M., Misiti, Y., Oppenheim, G., & Poggi, J. M. (Eds.). (2013). Wavelets and their Applications. John Wiley & Sons..

[17] Li, J., Yu, B., Zhao, W., & Chen, W. (2014). A review of signal enhancement and noise reduction techniques for tunable diode laser absorption spectroscopy. Applied Spectroscopy Reviews, 49(8), 666-691.

[18] Zhang, K., Zhang, L., Zhao, Q., Liu, S., Chen, S., Wu, Y., ... & Yang, X. (2017,

October). Application of digital quadrature lock-in amplifier in TDLAS humidity detection. In AOPC 2017: Optical Spectroscopy and Imaging (Vol. 10461, p. 1046109). International Society for Optics and Photonics.

[19] Mohammad, I. L., Anderson, G. T., & Chen, Y. (2014, June). Noise estimation technique to reduce the effects of 1/f noise in Open Path Tunable Diode Laser Absorption Spectrometry (OP-TDLAS). In Sensors for Extreme Harsh Environments (Vol. 9113, p. 91130S). International Society for Optics and Photonics.

[20] Chighine, A., Fisher, E., Wilson, D., Lengden, M., Johnstone, W., & McCann, H. (2015, September). An FPGA-based lock-in detection system to enable chemical species tomography using TDLAS. In 2015 IEEE International Conference on Imaging Systems and Techniques (IST) (pp. 1-5). IEEE.

[21Tu, G., Dong, F., Wang, Y., Culshaw, B., Zhang, Z., Pang, T., ... & Wu, B. (2015). Analysis of random noise and long-term drift for tunable diode laser absorption spectroscopy system at atmospheric pressure. IEEE Sensors Journal, 15(6), 3535-3542.

[22] He, Q., Dang, P., Liu, Z., Zheng, C., & Wang, Y. (2017). TDLAS–WMS based near-infrared methane sensor system using hollow-core photonic crystal fiber as gas-chamber. Optical and Quantum Electronics, 49(3), 115.

[23] Frish, M. B., Wainner, R. T., Laderer, M. C., Parameswaran, K. R., Sonnenfroh, D. M., & Druy, M. A. (2011, May). Precision and accuracy of miniature tunable diode laser absorption spectrometers. In Next-Generation Spectroscopic Technologies IV (Vol. 8032, p. 803209). International Society for Optics and Photonics.

[24] Knight, J. C., Birks, T. A., Cregan, R. F., Russell, P. S. J., & De Sandro, P. D. (1998). Large mode area photonic crystal fibre. Electronics Letters, 34(13), 1347-1348.

[25] Dong, L., Tittel, F. K., Li, C., Sanchez, N. P., Wu, H., Zheng, C., ... & Griffin, R. J. (2016). Compact TDLAS based sensor design using interband cascade lasers for mid-IR trace gas sensing. Optics express, 24(6), A528-A535.

[26] Wang, F., Chang, J., Wang, Q., Wei, W., & Qin, Z. (2017). TDLAS gas sensing system utilizing fiber reflector based round-trip structure: Double absorption path-length, residual amplitude modulation removal. Sensors and Actuators A: Physical, 259, 152-159.

[27] Shao, L., Yan, R., Li, X., & Liu, Y. (2013). From heuristic optimization to dictionary learning: A review and comprehensive comparison of image denoising algorithms. IEEE transactions on cybernetics, 44(7), 1001-1013.

[28] Gupta, K., & Gupta, S. K. (2013). Image Denoising techniques-a review paper. IJITEE, 2, 6-9.

[29] Zhang, T., Kang, J., Meng, D., Wang, H., Mu, Z., Zhou, M., ... & Chen, C. (2018). Mathematical methods and algorithms for improving near-infrared tunable diode-laser absorption spectroscopy. Sensors, 18(12), 4295.

[30] Dhoore, S., Köninger, A., Meyer, R., Roelkens, G., & Morthier, G. (2019). Electronically tunable distributed feedback (DFB) laser on silicon. Laser & Photonics Reviews, 13(3), 1800287.

[31] Mahdi, S. A. (2013). An investigation of electro-optical 1/f noise reduction in an open-path tunable diode laser spectrometer (Doctoral dissertation, University of Arkansas at Little Rock).

[32] Popa, D., & Udrea, F. (2019). Towards integrated mid-infrared gas sensors. Sensors, 19(9), 2076.

[33] Gilbert, S. L., & Swann, W. C. (2002). Carbon Monoxide Absorption References for 1560 nm to 1630 nm Wavelength Calibration–SRM 2514 (12 C 16 O) and SRM 2515 (13 C 16 O). NIST special publication, 260, 146.

[34] Pal, S., Ozanyan, K. B., & McCann, H. (2007, October). A spectroscopic study for detection of carbon-monoxide using mid-infrared techniques for single-pass measurement. In Journal of Physics: Conference Series (Vol. 85, No. 1, p. 012020). IOP Publishing.

[35] Wang, W. Q., Zhang, L., & Zhang, W. H. (2013). Analysis of optical fiber methane gas detection system. Procedia Engineering, 52, 401-407.

[36] Seiter, M., & Sigrist, M. W. (1999). On-line multicomponent trace-gas analysis with a broadly tunable pulsed difference-frequency laser spectrometer. Applied optics, 38(21), 4691-4698.

[37] White, J. U. (1942). Long optical paths of large aperture. JOSA, 32(5), 285-288.

[38] White, J. U. (1976). Very long optical paths in air. JOSA, 66(5), 411-416.

[39] Chernin, S. M., & Barskaya, E. G. (1991). Optical multiphases matrix systems. Applied optics, 30(1), 51-58.

[40] Herriott, D., Kogelnik, H., & Kompfner, R. (1964). Off-axis paths in spherical mirror interferometers. Applied Optics, 3(4), 523-526.

[41] Richard, E. C., Kelly, K. K., Winkler, R. H., Wilson, R., Thompson, T. L.,

McLaughlin, R. J., ... & Tuck, A. F. (2002). A fast-response near-infrared tunable diode laser absorption spectrometer for in situ measurements of CH 4 in the upper troposphere and lower stratosphere. Applied Physics B, 75(2), 183-194.

[42] Brassington, D. J. (1995). Tunable diode laser absorption spectroscopy for the measurement of atmospheric species. ADVANCES IN SPECTROSCOPY-CHICHESTER-JOHN WILEY AND SONS-, 24, 85-85.

[43] Schiff, H. I., Mackay, G. I., & Bechara, J. (1994). The use of tunable diode laser absorption spectroscopy for atmospheric measurements. Research on chemical intermediates, 20(3), 525-556.

[44] Ku, R. T., Hinkley, E. D., & Sample, J. O. (1975). Long-path monitoring of atmospheric carbon monoxide with a tunable diode laser system. Applied optics, 14(4), 854-861.

[45] Hinkley, E. D. (1976). Laser spectroscopic instrumentation and techniques: long-path monitoring by resonance absorption. Optical and Quantum Electronics, 8(2), 155-167.

[46] Werle, P. (1998). A review of recent advances in semiconductor laser-based gas monitors. Spectrochimica Acta Part A: Molecular and Biomolecular Spectroscopy, 54(2), 197-236.

[47] Anderson, S. M., & Zahniser, M. S. (1991, May). Open-path tunable diode laser absorption for eddy correlation flux measurements of atmospheric trace gases. In Measurement of atmospheric gases (Vol. 1433, pp. 167-178). International Society for Optics and Photonics.

[48] Taslakov, M., Simeonov, V., Froidevaux, M., & Van Den Bergh, H. (2006).

Open-path ozone detection by quantum-cascade laser. Applied Physics B, 82(3), 501-506.

[49] Taslakov, M., Simeonov, V., Froidevaux, M., & Van Den Bergh, H. (2006). Open-path ozone detection by quantum-cascade laser. Applied Physics B, 82(3), 501-506.

[50] Nelson, D. D., Zahniser, M. S., McManus, J. B., Kolb, C. E., & Jimenez, J. L. (1998). A tunable diode laser system for the remote sensing of on-road vehicle emissions. Applied Physics B: Lasers & Optics, 67(4).

[51] Calvert, J. G., Heywood, J. B., Sawyer, R. F., & Seinfeld, J. H. (1993). Achieving acceptable air quality: some reflections on controlling vehicle emissions. Science, 261(5117), 37-45.

[52] Beaton, S. P., Bishop, G. A., Zhang, Y., Ashbaugh, L. L., Lawson, D. R., & Stedmam, D. H. (1995). On-road vehicle emissions: regulations, costs, and benefits. Science, 268(5213), 991-993.

[53] Adam, H., Bauer, J., Thornton, E., & Tulip, J. (2002, May). Greenhouse gas emissions and reduction studies using a portable TDL gas monitor. In Proceedings of the climate change and GHG technology conference and tradeshow, Calgary, AB, Canada (Vol. 2224).

[54] Xia, H., Liu, W., Zhang, Y., Kan, R., Wang, M., He, Y., ... & Geng, H. (2008). An approach of open-path gas sensor based on tunable diode laser absorption spectroscopy. Chinese Optics Letters, 6(6), 437-440.

[55] Anderson, G., Sheesley, C., Tolson, J., Wilson, E., & Tunstel, E. (2006, October). A mobile robot system for remote measurements of ammonia vapor in the atmosphere. In 2006 IEEE International Conference on Systems, Man and

Cybernetics (Vol. 1, pp. 241-246). IEEE.

[56] Bomse, D. S., Stanton, A. C., & Silver, J. A. (1992). Frequency modulation and wavelength modulation spectroscopies: comparison of experimental methods using a lead-salt diode laser. Applied optics, 31(6), 718-731.

[57] Carlisle, C. B., & Cooper, D. E. (1990). Tunable diode laser frequency modulation spectroscopy through an optical fiber: high-sensitivity detection of water vapor. Applied physics letters, 56(9), 805-807.

[58] Durry, G., Danguy, T., & Pouchet, I. (2002). Open multipass absorption cell for in situ monitoring of stratospheric trace gas with telecommunication laser diodes. Applied optics, 41(3), 424-433.

[59] C. Dyroff, "Performance assessment and design improvement of a Herriott-type multi- pass absorption cell for highly sensitive trace-gas measurements," Diploma thesis, University of Applied Sciences Oldenburg / Ostfriesland / Wilhelmshaven, Emden, Germany (2003).

[60] Goldstein, N., Adler-Golden, S., Lee, J., & Bien, F. (1992). Measurement of molecular concentrations and line parameters using line-locked second harmonic spectroscopy with an AlGaAs diode laser. Applied optics, 31(18), 3409-3415.

[61] Kerstel, E. T., Gagliardi, G., Gianfrani, L., Meijer, H. A. J., Van Trigt, R., & Ramaker, R. (2002). Determination of the 2H/1H, 17O/16O, and 18O/16O isotope ratios in water by means of tunable diode laser spectroscopy at 1.39 μm. Spectrochimica Acta Part A: Molecular and Biomolecular Spectroscopy, 58(11), 2389-2396.

[62] Kormann, R., Königstedt, R., Parchatka, U., Lelieveld, J., & Fischer, H. (2005).

QUALITAS: A mid-infrared spectrometer for sensitive trace gas measurements based on quantum cascade lasers in CW operation. Review of scientific instruments, 76(7), 075102.

[63] Lübken, F. J., Dingler, F., von Lucke, H., Anders, J., Riedel, W. J., & Wolf, H. (1999). MASERATI: a rocketborne tunable diode laser absorption spectrometer. Applied optics, 38(25), 5338-5349.

[64] Webster, C. R., May, R. D., Trimble, C. A., Chave, R. G., & Kendall, J. (1994). Aircraft (ER-2) laser infrared absorption spectrometer (ALIAS) for in-situ stratospheric measurements of HCl, N 2 O, CH 4, NO 2, and HNO 3. Applied Optics, 33(3), 454-472.

[65] Wert, B. P., Fried, A., Rauenbuehler, S., Walega, J., & Henry, B. (2003). Design and performance of a tunable diode laser absorption spectrometer for airborne formaldehyde measurements. Journal of Geophysical Research: Atmospheres, 108(D12).

[65] Wienhold, F. G., Fischer, H., Hoor, P., Wagner, V., Königstedt, R., Harris, G. W., ... & Schilling, T. (1998). TRISTAR-A tracer in-situ TDLAS for atmospheric research.

[66] Weibring, P., Richter, D., Fried, A., Walega, J. G., & Dyroff, C. (2006). Ultra-high-precision mid-IR spectrometer II: system description and spectroscopic performance. Applied Physics B, 85(2), 207-218.

[67] Kluczynski, P., & Axner, O. (1999). Theoretical description based on Fourier analysis of wavelength-modulation spectrometry in terms of analytical and background signals. Applied optics, 38(27), 5803-5815.

[68] Arslanov, D. D., Spunei, M., Ngai, A. K. Y., Cristescu, S. M., Lindsay, I. D.,

Persijn, S. T., ... & Harren, F. J. M. (2011). Rapid and sensitive trace gas detection with continuous wave Optical Parametric Oscillator-based Wavelength Modulation Spectroscopy. Applied Physics B, 103(1), 223-228.

[69] Reid, J., & Labrie, D. (1981). Second-harmonic detection with tunable diode lasers—comparison of experiment and theory. Applied Physics B, 26(3), 203-210.

[70] Cao, J., Zhang, K., Yang, R., & Wang, Z. (2010, July). Modulation coefficient analysis in optical fiber methane gas sensor based on wavelength modulation spectroscopy. In 2010 8th World Congress on Intelligent Control and Automation (pp. 7021-7025).

[71] Wang, X. M., Zhang, Y. J., Xia, H., Fang, X., Kan, R. F., Wang, T. D., ... & Liu, J. (2007). Measurement of CO2 concentration in flame based on tunable diode laser absorption spectroscopy. J. Atmos. Environ. Opt., 2(4), 290-295.

[72] Kluczynski, P., Gustafsson, J., Lindberg, Å. M., & Axner, O. (2001). Wavelength modulation absorption spectrometry—an extensive scrutiny of the generation of signals. Spectrochimica Acta Part B: Atomic Spectroscopy, 56(8), 1277-1354.

[73] Reid, J., & Labrie, D. (1981). Second-harmonic detection with tunable diode lasers—comparison of experiment and theory. Applied Physics B, 26(3), 203-210.

[74] Demtröder, W. (2013). Laser spectroscopy: basic concepts and instrumentation. Springer Science & Business Media.

[75] Peng, B., Zhang, Q., Liu, X., Ji, Y., Demir, H. V., Huan, C. H. A., ... & Xiong, Q. (2012). Fluorophore-doped core–multishell spherical plasmonic

nanocavities: resonant energy transfer toward a loss compensation. ACS nano, 6(7), 6250-6259.”.

[76] Andrade, E. D. C. (1959). Doppler and the Doppler effect.

[77] Lundsbergnielsen, L., Hegelund, F., & Nicolaisen, F. M. (1993). Analysis of the high-resolution spectrum of ammonia (14NH3) in the near-infrared region, 6400-6900 cm− 1. Journal of molecular spectroscopy, 162(1), 230-245.

[78] Webber, M. E., Baer, D. S., & Hanson, R. K. (2001). Ammonia monitoring near 1.5 μm with diode-laser absorption sensors. Applied optics, 40(12), 2031-2042.

[79] Ohtsu, M., Kotani, H., & Tagawa, H. (1983). Spectral Measurements of NH3 and H2O for Pollutant Gas Monitoring by 1.5 μm InGaAsP/InP Lasers. Japanese journal of applied physics, 22(10R), 1553.

[80] Fehér, M., Martin, P. A., Rohrbacher, A., Soliva, A. M., & Maier, J. P. (1993). Inexpensive near-infrared diode-laser-based detection system for ammonia. Applied optics, 32(12), 2028-2030.

[81] Mihalcea, R. M., Webber, M. E., Baer, D. S., Hanson, R. K., Feller, G. S., & Chapman, W. B. (1998). Diode-laser absorption measurements of CO2, H2O, N2O, and NH3 near 2.0 μm. Applied Physics B, 67(3), 283-288.

[82] Linnerud, I., Kaspersen, P., & Jaeger, T. (1998). Gas monitoring in the process industry using diode laser spectroscopy. Applied Physics B: Lasers & Optics, 67(3).

[83] Modugno, G., & Corsi, C. (1999). Water vapour and carbon dioxide interference in the high sensitivity detection of NH3 with semiconductor diode lasers at 1.5 μm. Infrared physics & technology, 40(2), 93-99.

[84] Webber, M. E., Baer, D. S., & Hanson, R. K. (2001). Ammonia monitoring near

1.5 μm with diode-laser absorption sensors. Applied optics, 40(12), 2031-2042.

[85] Czajkowski, A., Alcock, A. J., Bernard, J. E., Madej, A. A., Corrigan, M., & Chepurov, S. (2009). Studies of saturated absorption and measurements of optical frequency for lines in the ν 1+ ν 3 and ν 1+ 2ν 4 bands of ammonia at 1.5 μm. Optics express, 17(11), 9258-9269.

[86] Guelachvili, G., Abdullah, A. H., Tu, N., Rao, K. N., Urban, Š., & Papoušek, D. (1989). Analysis of high-resolution Fourier transform spectra of 14NH3 at 3.0 μm. Journal of Molecular Spectroscopy, 133(2), 345-364.

[87] Martin, N. A., Ferracci, V., Cassidy, N., & Hoffnagle, J. A. (2016). The application of a cavity ring-down spectrometer to measurements of ambient ammonia using traceable primary standard gas mixtures. Applied Physics B, 122(8), 1-11.

[88] Schilt, S., Thévenaz, L., Niklès, M., Emmenegger, L., & Hüglin, C. (2004). Ammonia monitoring at trace level using photoacoustic spectroscopy in industrial and environmental applications. Spectrochimica Acta Part A: Molecular and Biomolecular Spectroscopy, 60(14), 3259-3268..

[89] Manne, J., Sukhorukov, O., Jäger, W., & Tulip, J. (2006). Pulsed quantum cascade laser-based cavity ring-down spectroscopy for ammonia detection in breath. Applied optics, 45(36), 9230-9237..

[90] Shadman, S., Rose, C., & Yalin, A. P. (2016). Open-path cavity ring-down spectroscopy sensor for atmospheric ammonia. Applied Physics B, 122(7), 1-9.

[91] von Bobrutzki, K., Braban, C. F., Famulari, D., Jones, S. K., Blackall, T., Smith, T. E. L., ... & Nemitz, E. (2010). Field inter-comparison of eleven atmospheric ammonia measurement techniques. Atmospheric Measurement Techniques, 3,

91-112.

[92] Miller, D. J., Sun, K., Tao, L., Khan, M. A., & Zondlo, M. A. (2014). Open-path, quantum cascade-laser-based sensor for high-resolution atmospheric ammonia measurements. Atmospheric Measurement Techniques, 7(1), 81-93.

[93] Maithani, S., Mandal, S., Maity, A., Pal, M., & Pradhan, M. (2018). High-resolution spectral analysis of ammonia near 6.2 μm using a cw EC-QCL coupled with cavity ring-down spectroscopy. Analyst, 143(9), 2109-2114.

[94] Gordon, I. E., Rothman, L. S., Hill, C., Kochanov, R. V., Tan, Y., Bernath, P. F., ... & Zak, E. J. (2017). The HITRAN2016 molecular spectroscopic database. Journal of Quantitative Spectroscopy and Radiative Transfer, 203, 3-69.

[95] Owen, K., Es-sebbar, E. T., & Farooq, A. (2013). Measurements of NH3 linestrengths and collisional broadening coefficients in N2, O2, CO2, and H2O near 1103.46 cm− 1. Journal of Quantitative Spectroscopy and Radiative Transfer, 121, 56-68.

[96] Nadezhdinskii, A., Berezin, A., Chernin, S., Ershov, O., & Kutnyak, V. (1999). High sensitivity methane analyzer based on tuned near infrared diode laser. Spectrochimica Acta Part A: Molecular and Biomolecular Spectroscopy, 55(10), 2083-2089.

[97] D'amato, F., Mazzinghi, P., & Castagnoli, F. (2002). Methane analyzer based on TDL's for measurements in the lower stratosphere: design and laboratory tests. Applied Physics B, 75(2), 195-202.

[98] Chan, K., Ito, H., & Inaba, H. (1983). Optical remote monitoring of CH4 gas using low-loss optical fiber link and InGaAsP light-emitting diode in 1.33-μm

region. Applied physics letters, 43(7), 634-636.

[99] Schilt, S., Besson, J. P., & Thévenaz, L. (2006). Near-infrared laser photoacoustic detection of methane: the impact of molecular relaxation. Applied Physics B, 82(2), 319-328.

[100] Shemshad, J., Aminossadati, S. M., & Kizil, M. S. (2012). A review of developments in near infrared methane detection based on tunable diode laser. Sensors and Actuators B: Chemical, 171, 77-92.

[101] Tran, H., Hartmann, J. M., Toon, G., Brown, L. R., Frankenberg, C., Warneke, T., ... & Hase, F. (2010). The 2ν3 band of CH4 revisited with line mixing: Consequences for spectroscopy and atmospheric retrievals at 1.67 μm. Journal of Quantitative Spectroscopy and Radiative Transfer, 111(10), 1344-1356.

[102] Gagliardi, G., & Gianfrani, L. (2002). Trace-gas analysis using diode lasers in the near-IR and long-path techniques. Optics and lasers in engineering, 37(5), 509-520.

[103] Chan, K., Ito, H., & Inaba, H. (1983). Optical remote monitoring of CH4 gas using low-loss optical fiber link and InGaAsP light-emitting diode in 1.33-μm region. Applied physics letters, 43(7), 634-636.

[104] Chan, K., Ito, H., Inaba, H., & Furuya, T. (1985). 10 km-long fibre-optic remote sensing of CH 4 gas by near infrared absorption. Applied Physics B, 38(1), 11-15.

[105] Washenfelder, R. A., Wennberg, P. O., & Toon, G. C. (2003). Tropospheric methane retrieved from ground-based near-IR solar absorption spectra. Geophysical research letters, 30(23).

[106] Gordon, I. E., Rothman, L. S., Hill, C., Kochanov, R. V., Tan, Y., Bernath, P.

F., ... & Zak, E. J. (2017). The HITRAN2016 molecular spectroscopic database. Journal of Quantitative Spectroscopy and Radiative Transfer, 203, 3-69.

[107] Gharavi, M., & Buckley, S. G. (2005). Diode laser absorption spectroscopy measurement of linestrengths and pressure broadening coefficients of the methane 2ν3 band at elevated temperatures. Journal of molecular spectroscopy, 229(1), 78-88.

[108] Frankenberg, C., Warneke, T., Butz, A., Aben, I., Hase, F., Spietz, P., & Brown, L. R. (2008). Pressure broadening in the 2ν 3 band of methane and its implication on atmospheric retrievals. Atmospheric chemistry and physics, 8(17), 5061-5075.

[109] Wang, F., Jia, S., Wang, Y., & Tang, Z. (2019). Recent developments in modulation spectroscopy for methane detection based on tunable diode laser. Applied sciences, 9(14), 2816.

[110] Pine, A. S. (1992). Self-, N2, O2, H2, Ar, and He broadening in the ν3 band Q branch of CH4. The Journal of chemical physics, 97(2), 773-785.

[111] Tran, H., Flaud, P. M., Gabard, T., Hase, F., Von Clarmann, T., Camy-Peyret, C., ... & Hartmann, J. M. (2006). Model, software and database for line-mixing effects in the ν3 and ν4 bands of CH4 and tests using laboratory and planetary measurements—I: N2 (and air) broadenings and the earth atmosphere. Journal of Quantitative Spectroscopy and Radiative Transfer, 101(2), 284-305.

[112] Sun, K., Chao, X., Sur, R., Goldenstein, C. S., Jeffries, J. B., & Hanson, R. K. (2013). Analysis of calibration-free wavelength-scanned wavelength modulation spectroscopy for practical gas sensing using tunable diode lasers. Measurement Science and Technology, 24(12), 125203.

[113] Upschulte, B. L., Sonnenfroh, D. M., & Allen, M. G. (1999). Measurements of CO, CO 2, OH, and H 2 O in room-temperature and combustion gases by use of a broadly current-tuned multisection InGaAsP diode laser. Applied Optics, 38(9), 1506-1512.

[114] Nguyen, Q. V., Edgar, B. L., Dibble, R. W., & Gulati, A. (1995). Experimental and numerical comparison of extractive and in situ laser measurements of non-equilibrium carbon monoxide in lean-premixed natural gas combustion. Combustion and Flame, 100(3), 395-406.

[115] Upschulte, B. L., Sonnenfroh, D. M., & Allen, M. G. (1999). Measurements of CO, CO 2, OH, and H 2 O in room-temperature and combustion gases by use of a broadly current-tuned multisection InGaAsP diode laser. Applied Optics, 38(9), 1506-1512.

[116] Duffin, K., McGettrick, A., Johnstone, W., & Stewart, G. (2007, July). Tunable diode laser spectroscopy for industrial process applications. In Third European Workshop on Optical Fibre Sensors (Vol. 6619, p. 661927). International Society for Optics and Photonics.

[117] Chao, X., Jeffries, J. B., & Hanson, R. K. (2013). Real-time, in situ, continuous monitoring of CO in a pulverized-coal-fired power plant with a 2.3 μm laser absorption sensor. Applied Physics B, 110(3), 359-365.

[118] Sur, R., Sun, K., Jeffries, J. B., Hanson, R. K., Pummill, R. J., Waind, T., ... & Whitty, K. J. (2014). TDLAS-based sensors for in situ measurement of syngas composition in a pressurized, oxygen-blown, entrained flow coal gasifier. Applied Physics B, 116(1), 33-42.

[119] Wang, J., Maiorov, M., Baer, D. S., Garbuzov, D. Z., Connolly, J. C., & Hanson, R. K. (2000). In situ combustion measurements of CO with diode-laser

absorption near 2.3 μm. Applied Optics, 39(30), 5579-5589.

[120] Lu, H., Zheng, C., Zhang, L., Liu, Z., Song, F., Li, X., ... & Wang, Y. (2021). A Remote Sensor System Based on TDLAS Technique for Ammonia Leakage Monitoring. Sensors, 21(7), 2448.

[121] So, S., Park, J., Song, A., Hwang, J., Yoo, M., & Lee, C. (2020). Detection Limit of CO Concentration Measurement in LPG/Air Flame Flue Gas Using Tunable Diode Laser Absorption Spectroscopy. Energies, 13(16), 4234.

[122] Xiao, C., & Hu, S. (2020, March). Optimization of the optical path of the methane telemetry system based on TDLAS technology. In 2019 International Conference on Optical Instruments and Technology: Optical Systems and Modern Optoelectronic Instruments (Vol. 11434, p. 114341B). International Society for Optics and Photonics.

[123] Wang, F., Jia, S., Wang, Y., & Tang, Z. (2019). Recent developments in modulation spectroscopy for methane detection based on tunable diode laser. Applied sciences, 9(14), 2816.

[124] Zhu, X., Yao, S., Ren, W., Lu, Z., & Li, Z. (2019). TDLAS monitoring of carbon dioxide with temperature compensation in power plant exhausts. Applied Sciences, 9(3), 442.

[125] Mumma, M. J., Villanueva, G. L., Novak, R. E., Hewagama, T., Bonev, B. P., DiSanti, M. A., ... & Smith, M. D. (2009). Strong release of methane on Mars in northern summer 2003. Science, 323(5917), 1041-1045.

[126] Zhang, T., Kang, J., Meng, D., Wang, H., Mu, Z., Zhou, M., ... & Chen, C. (2018). Mathematical methods and algorithms for improving near-infrared tunable diode-laser absorption spectroscopy. Sensors, 18(12), 4295.

[127] Li, B., Zhang, S. C., & Chi, Y. D. (2018). Development and integration of a CO detection system based on wavelength modulation spectroscopy using near-infrared DFB laser. Journal of Spectroscopy, 2018.

[128] Cui, X., Dong, F., Zhang, Z., Xia, H., Pang, T., Sun, P., ... & Yu, R. (2017). Environmental Application of High Sensitive Gas Sensors with Tunable Diode Laser Absorption Spectroscopy. Green Electronics.

[129] Cai, T., Gao, G., & Wang, M. (2016). Simultaneous detection of atmospheric CH 4 and CO using a single tunable multi-mode diode laser at 2.33 μm. Optics express, 24(2), 859-873.

[130] Behera, A., & Wang, A. (2016). Calibration-free wavelength modulation spectroscopy: symmetry approach and residual amplitude modulation normalization. Applied optics, 55(16), 4446-4455.

[131] Huang, J. Q., Zheng, C. T., Gao, Z. L., Ye, W. L., & Wang, Y. D. (2014). Near-infrared methane detection device using wavelength-modulated distributed feedback diode laser around 1.654 μm. Spectroscopy Letters, 47(3), 197-205.

[132] Houghton, J. (2002). The physics of atmospheres. Cambridge University Press.

[133] Rothman, L. S., Gordon, I. E., Barbe, A., Benner, D. C., Bernath, P. F., Birk, M., ... & Vander Auwera, J. (2009). The HITRAN 2008 molecular spectroscopic database. Journal of Quantitative Spectroscopy and Radiative Transfer, 110(9-10), 533-572.

[134] Milton Filho, B., da Silva, M. G., Sthel, M. S., Schramm, D. U., Vargas, H., Miklós, A., & Hess, P. (2006). Ammonia detection by using quantum-cascade

laser photoacoustic spectroscopy. Applied optics, 45(20), 4966-4971.

[135] Oppenheim, A. V., Buck, J. R., & Schafer, R. W. (2001). Discrete-time signal processing. Vol. 2. Upper Saddle River, NJ: Prentice Hall.

[136] Nyquist, H. (1928). Certain topics in telegraph transmission theory. Transactions of the American Institute of Electrical Engineers, 47(2), 617-644.

[137] Shannon, C. E. (1949). Communication in the presence of noise. Proceedings of the IRE, 37(1), 10-21.

[138] Reid, J., & Labrie, D. (1981). Second-harmonic detection with tunable diode lasers—comparison of experiment and theory. Applied Physics B, 26(3), 203-210.

[139] Philippe, L. C., & Hanson, R. K. (1993). Laser diode wavelength-modulation spectroscopy for simultaneous measurement of temperature, pressure, and velocity in shock-heated oxygen flows. Applied optics, 32(30), 6090-6103.

[140] Kluczynski, P., & Axner, O. (1999). Theoretical description based on Fourier analysis of wavelength-modulation spectrometry in terms of analytical and background signals. Applied optics, 38(27), 5803-5815.

[141] Schilt, S., Thevenaz, L., & Robert, P. (2003). Wavelength modulation spectroscopy: combined frequency and intensity laser modulation. Applied optics, 42(33), 6728-6738.

[142] Tiwari, S., Vasa, N. J., & Srinivasan, B. (2016, April). Fiber Bragg grating-based wavelength modulation spectroscopy technique for trace gas sensing. In Optical Sensing and Detection IV (Vol. 9899, p. 98992E). International Society for Optics and Photonics.

[143] Walker, J. S. (1996). Fast fourier transforms (Vol. 24). CRC press.

[144] Werle, P. (1998). A review of recent advances in semiconductor laser-based gas monitors. Spectrochimica Acta Part A: Molecular and Biomolecular Spectroscopy, 54(2), 197-236.

[145] Reid, J., & Labrie, D. (1981). Second-harmonic detection with tunable diode lasers—comparison of experiment and theory. Applied Physics B, 26(3), 203-210.

[146] Wang, W. Q., Zhang, L., & Zhang, W. H. (2013). Analysis of optical fiber methane gas detection system. Procedia Engineering, 52, 401-407.

في هذه الدراسة، تم إثبات أن عملية محاكاة TDLS تعزز حساسية مقياس الطيف من خلال تعديل الطول الموجي لصمام الليزر الثنائيDFB القابل للضبط باستخدام إشارة جيبية. وتم ضبط تيار تشغيل الليزر، وبالتالي سيتغير الطول الموجي للدايود الليزري في حدود ضبط تصل إلى حوالي 0.02 نانومتر في منطقة الأشعة تحت الحمراء القريبة (NIR) ومنطقة الأشعة تحت الحمراء المتوسطة(MIR) . وتم ذلك باستخدام ثلاثة أنواع من الغازات السامه وهي: الميثان CH_4 والأمونيا NH_3 وأول أكسيد الكاربون CO.

تم إجراء تقييم حساسية المطياف الليزري القابل للضبط TDLS عند قيمة تركيز ثابتة 0.5 جزء لكل بليون (ppb) وطول ثابت للمسار المفتوح (البعيد بين مصدر الليزر والعاكس الخلفي) 100 متر. تمت كتابة كود برنامج MATLAB لضبط الطول الموجي الدقيق في منطقة NIR وMIR، ثم تم إجراء قياسات مجال التردد لاستخراج التوافقي الثاني (second harmonic) كمؤشر على وجود الغاز. أظهرت النتائج أن القيمة الدقيقة لطول الموجة لغاز الميثان في منطقة NIR هي 1653.48 نانومتر وطول الموجة الدقيق لغاز الميثان في منطقة MIR هو (3290.987 نانومتر). بينما غاز الأمونيا تظهر النتيجة أن الطول الموجي الدقيق في منطقة NIR هو 1543.027 نانومتر والطول الموجي الدقيق لغاز الأمونيا في منطقة MIR هو 2399.977 نانومتر. بينما غاز أول أكسيد الكربون تظهر النتيجة أن الطول الموجي الدقيق في منطقة NIR هو 1584.877 نانومتر والطول الموجي الدقيق لغاز الأمونيا في منطقة MIR هو 4650.463 نانومتر. لاحظ أنه تم إثبات القياسات عند L = 100 متر، وكان تركيز الغاز N = 0.05 إلى 0.5 جزء في البليون في 0.2 خطوة لجميع أنواع قياس الغاز.

جمهورية العراق
وزارة التعليم العالي والبحث العلمي
جامعة بابل ـ كلية العلوم
قسم الفيزياء

عملية محاكاة لمطياف ليزر المسار المفتوح القابل للضبط لقياس تركيز الغازات

رسالة ماجستير في الفيزياء مقدمة الى قسم الفيزياء، كلية العلوم، جامعة بابل

كجزء من متطلبات نيل شهادة الماجستير في الفيزياء

من قبل

رؤى قحطان محمود مظلوم

بكالوريوس في علوم فيزياء / ٢٠١١

بإشراف

أ.م. د. سميرة عدنان مهدي

١٤٤٢ هـ ٢٠٢١ م